THE UNIVERSITY OF ADELAIDE

DEPARTMENT OF CIVIL AND ENVIRONMENTAL ENGINEERING

EARTHQUAKE RESPONSE OF REINFORCED CONCRETE FRAMES WITH MASONRY INFILL PANELS

By Rouska Gueorguieva Malinova

December 1996

CONTENTS

ABSTRACT

Infill walls substantially influence the strength and stiffness characteristics of framed structures, their energy dissipating capacity and considerably reduce the period of oscillation. If frames are designed taking into account the presence of infill walls, the walls might have a beneficial effect on their performance during earthquakes. This research is a theoretical investigation into the lateral response of reinforced concrete frames with brick masonry infill panels. A review of the literature describes the main trends in the solution of the problem of infilled frames. This research made use of the two main approaches: the finite element method for static analysis and the diagonal strut analogy for dynamic analysis. Eight models were investigated to qualitatively assess the influence of the relative stiffness of the frame and the wall, the length to height ratio and the presence of a construction gap on the overall response of the frame-wall system.

The static analysis was performed using the finite element program "Images - 3D" to investigate the behaviour of the frame-wall system in the elastic range of the masonry material. However, non-linear spring elements modelled the frame-wall interface. Strength and stiffness values of the wall panel at yield were derived from the results of the static analysis and were later used in the non-linear dynamic analysis.

The dynamic analysis was carried out using the non-linear analysis program "Ruaumoko". A model of a reinforced concrete frame braced with one diagonal was developed. The frame elements and the diagonal elements were able to develop non-linear deformations thanks to the variety of non-linear hysteresis rules available in "Ruaumoko". Two generalised types of models were developed: one for the case of perfect fit (which was assumed to correspond to the realistic situation of a gap equal to or less than 5mm) and one for the case of presence of a construction gap (which was assumed to correspond to any gap size more than 5mm). The response of these models under cyclic loading was verified by comparison with experimental results by other researchers.

This work contains no material which has been accepted for the award of any other degree or diploma in any university or other tertiary institution and, to the best of my knowledge and belief, contains no material previously published or written by another person, except where due references have been made in the text.

I give consent to this copy of my thesis, when deposited in the University Library, being available for loan or photocopying.

DATE: 29.08.97

ACKNOWLEDGMENTS

The author would like to thank Dr. Michael Griffith, Senior Lecturer and Head of the Department of Civil and Environmental Engineering for supervising this research; Anthony Wong and Greg Klopp for their help and advice; S. Carr, Computer Officer at the Department of Civil and Environmental Engineering, for the assistance in problems with the computer.

CHAPTER 1 - INTRODUCTION

Framed structures infilled with walls are a common form of construction. Usually the design of the frame does not account for the presence of the infill walls and treats them as non-structural elements. Besides their self-supporting and architectural function, the infill panels change dramatically the lateral resistance of the frame. Therefore, many researchers have tried to solve the complex statically indeterminate problem of infilled frames and evaluate the overall response to earthquake loading of the frame-wall system. It has been known that the infill walls have strengthening and stiffening effect on the surrounding frame but their failure might cause unexpected frame behaviour which should be taken into account.

Provided out-of-plane wall failure does not occur first, the frame confines the wall and the wall acts in a manner similar to a diagonal bracing for the frame. The mode of failure of the infill wall governs the mode of failure of the frame. Different mechanical models have been suggested to describe the complex mechanisms of failure in the wall which cause different types of failure in the frame. Most of the models are based to a different extent on the diagonal strut concept which approximates the role of the infill wall as diagonal bracing. The confinement provided by the frame depends on many factors. The major factors are: (1) the relative stiffness of the frame and the wall, (2) the length of the wall and (3) the presence of initial gap between them.

This research is a theoretical investigation on the influence of the above mentioned factors on the lateral response of reinforced concrete frames with brick masonry infill panels. The investigation is divided in two stages: static analysis and dynamic analysis. The static analysis evaluates the performance of infilled frames in the elastic range of the materials and derives the properties which are used in the development of the dynamic model. The dynamic model investigates the behaviour of the infilled frames in the inelastic range and evaluates the overall performance under cyclic loading.

The model for the static analysis is based on the finite element method. Brick masonry is a two phase material with oriented planes of weakness. Research in the past has proved that masonry can be treated as a homogeneous orthotropic material. The finite element mesh for the infill wall encorporated bricks and mortar joints. Failure in the wall was assumed to occur when the shear stress in a plate element reached 0.3 MPa.

The changes introduced in the behaviour of infilled frames by lack of initial fit of the wall into the frame are of main concern in the analyses of infilled frames with different relative stiffness and length configurations.

The remainder of the thesis consists of the following main chapters:

- Chapter 2 - A review of the literature which shows the major trends in research of infilled frames is presented in chapter 2.
- Chapter 3 - This chapter shows the aims of this research and defines the geometry, material properties and the initial assumptions for the eight theoretical models of reinforced concrete frames with brick masonry infill panels.
- Chapter 4 - This chapter investigates the behaviour of the infilled frames in the elastic range of the materials. Partial non-linearity was introduced by non-linear springs which connect the frame and the wall. This part of the analysis determines the influence of the relative stiffness of the frame and the wall, the length of the wall and the initial gap on the strength and stiffness of the wall panel under static loading.
- Chapter 5 - In this chapter a dynamic model based on a single diagonal strut analogy is developed. Results obtained with the help of the dynamic theoretical model are compared with experimental results.
- Chapter 6 - The results from the investigation of the overall response of the eight theoretical models under cyclic loading is presented in this chapter.

The thesis concludes with evaluation of the influence of the relative stiffness of the frame and the wall, the length to height ratio of the wall panel and presence of a construction gap on the overall response of infilled frames under lateral loading. The adequacy of the presented dynamic model is also discussed.

CHAPTER 2 - LITERATURE REVIEW

2.1. General review

The composite behaviour of infilled frames with walls was investigated theoretically and experimentally by many researchers during the last decades. The earliest attempts to solve the complex problem of infilled frames were made by Polyakov in 1948. Since then two main trends were developed for solution of the problem: diagonal strut analogy which developed a number of variations and the finite element method employing different degrees of detailing of the system. Very often these two trends were followed simultaneously by using the results from a finite element method analysis to define the properties of the diagonal struts. Numerous experimental results were analysed to cope with the versatility of the materials of the infill and the frame, with the different types of design of the two components of the system and the various boundary interface and support conditions.

2.2. The diagonal strut concept

2.2.1. Simple one diagonal strut analogy

The diagonal strut model was originally suggested by Polyakov [1,2]. He carried out experiments on a multi-storey multi-bay infilled frame and concluded that the infilled frames behaved as a braced system and also suggested approximate values of the loads in the infill using theory of elasticity. A simple strength of materials method to evaluate the ultimate load and deflections of an infilled frame using the diagonal strut analogy was suggested by Holmes [3]. The width of the diagonal which he used was 1/3 of the infill diagonal length.

Smith [4,5,6,7] further developed the diagonal strut concept in the 1960s by suggesting that the contact length between the frame and the wall was analogous to the contact

length of a beam on an elastic foundation. Using this principle he derived the values of the contact length between the frame and the wall which was governed by the relative stiffness of the frame and the wall. He also suggested a parameter λh, which related the stiffness of the frame to the wall stiffness and could be used as a convenient measure for evaluating the resistance of an infilled frame. For diagonally loaded frames he related the mode of failure of the infill with certain values of λh: for λh>9.5 corner crushing was the initial mode of failure with the infill still resisting considerable part of the load, for values smaller than 9.5 the diagonal cracking was the failure mode of the infill and for values around 9.5 the mode of failure was a combination of both. These results were obtained for steel frames and mortar infill. The parameter was initially defined by equation (2.1) and it was concerning square infilled frames.

$$\lambda l = \sqrt[4]{\frac{E_c t}{4EIl'}}\, l \tag{2.1}$$

In the above equation E_c, t, l' are the Young's modulus, thickness and length of the wall panel and E, I, l are the Young's modulus, moment of inertia and length of the frame. This parameter was later improved to account for the length to height ratio l/h [6] (the investigation was for ratios of 1:1 to 2.5:1). Benjamin and Williams [8] had earlier found that the length to height ratio of the panel had important influence on the lateral response of infilled frames. The influence was included in equation (2.1) through the angle θ which the diagonal forms with the base of the wall and it was modified to equation (2.2):

$$\lambda l = \sqrt[4]{\frac{E_c t \sin 2\theta}{4EIl'}}\, l \tag{2.2}.$$

2.2.2. Types of loading - diagonal and lateral

Both diagonal and lateral loading were used in theoretical and experimental investigations. Most of Smith's investigation was of diagonally loaded frames, which according to other researchers [9], was a different situation from the laterally loaded infilled frames since rotation or slip could occur in a laterally loaded frame and the forces and deflections should account for such condition. Recent tests carried out by Dukuze et al. [10] revealed that the in-plane distortion of individual unreinforced masonry panels in a three storey three bay reinforced concrete frame was similar to the one in a one storey one bay diagonally loaded frame.

2.2.3. Investigations on factors determining the response of infilled frames

Mainstone [11], who investigated infilled frames adopting the diagonal strut concept, pointed out the importance of the following factors in the lateral response of infilled frames:

- flexural stiffness of beams and columns;
- external restraints on the frame (such as neighbouring infills);
- rotational stiffness of the joints of the frame;
- the extent to which the joints open under loading; and
- initial fit of the wall panel into the frame.

Another important factor in the lateral resistance of infilled frames, investigated by Liauw and Kwan, was the presence of shear connectors at the frame-wall interface. They developed plastic theories for these two separate cases which were interpreted as non-integral infilled frames where the contribution of friction had been neglected and regarded as strength reserve and infilled frames with finite shear strength of the interface [12,13]. An intermediate case was also investigated which was defined as semi-integral frames [14]. For the development of the above theories the stress distribution in the wall panel under collapse had been investigated in advance using a non-linear finite element analysis [15].

2.2.4. The diagonal strut analogy at high load

At different stages of loading the response of the system is completely different. At high loads the infill would develop the so called double arching effect (fig. 2.1) (Smolira [16]). The central region of the infill is cracked and the infill resists the lateral action by an arching action of the neighbouring segments.

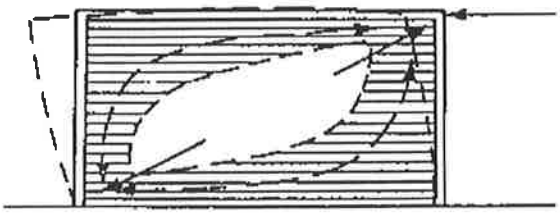

Fig. 2.1. Double arching effect of the infill at high loads
(after Smolira [16])

The analytical procedure for evaluation of the behaviour of steel frames developed by Islam et al. [17] was based on the following typical stages from the lateral response (fig. 2.2):

- monolithic shear wall - at very low lateral loads the wall acts as a whole cantilever until cracks appear at the boundary interface;
- diagonal compression strut - after separation at the frame/wall interface the wall acts as a diagonal strut for the frame;
- separation of individual segments of the infill and mechanism at failure - after separation of the segments the behaviour is changed drastically and the braced length of the column is different from the original one;

The short column effect which developed in such cases led to hinging of the unbraced portion of the columns in steel frames and usually shear failure in reinforced concrete frames.

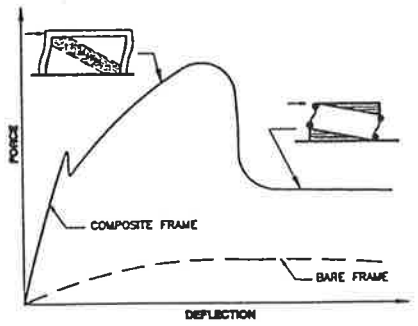

Fig. 2.2. Force/displacement diagram for solid URM infilled steel frame (after Islam et al. [17])

Zarnich and Tomazevic [18] considered the infilled frame behaviour in two stages: response in the small deformation range and response in the large deformation range. For behaviour in the large deformation range they suggested use of the model in fig. 2.3 which could account for the short column effect and the possible shear failure in columns after the separation of the infill.

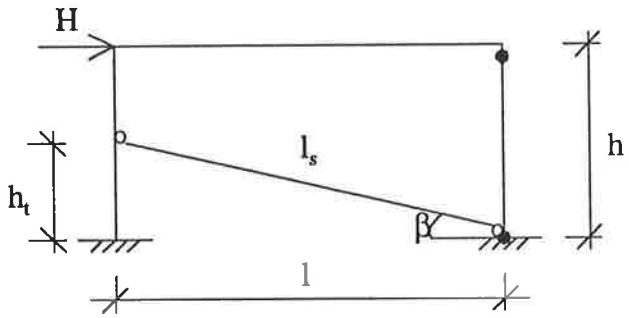

Fig. 2.3. Mechanism of the infilled frame behaviour
(after Zarnic and Tomazevic [18])

Leuchars and Scrivener [19] carried out tests which were in close agreement with the so called "knee braced frame" concept suggested by Fiarato et al. (fig. 2.4). This concept went away from the original diagonal strut and coped with the failure at the centre of the panel and locking of the two segments in the corner regions. As a result shear failure in the columns as well as flexural failure can be interpreted by the model.

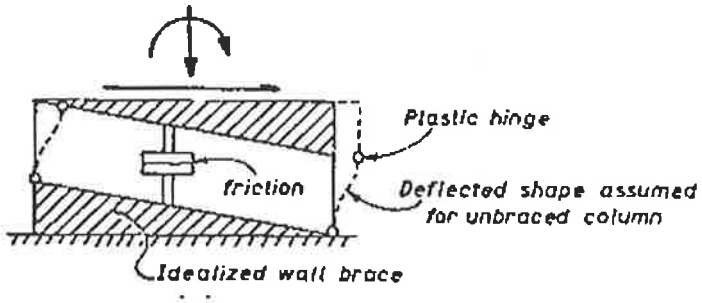

Fig. 2.4. Knee braced frame model
(after Fiarato et al.)

The formation of a secondary mechanism within the panel after cracking along a diagonal is an important stage of the behaviour of infilled frames at high load since the infill still resists a considerable part of the lateral load but in a different manner from the initial mechanism. A model which accounts for cracking and separation in the panel confined by a steel frame was suggested by Mander et al. [20]. Secondary struts (C_2) were introduced in the frame (fig. 2.5) to account for the loss of strength at the centre of the panel followed by stress redistribution.

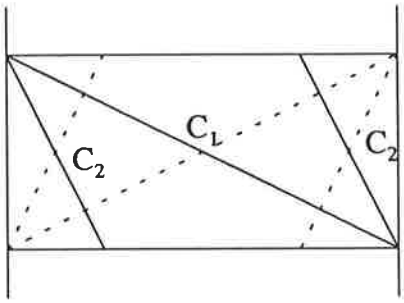

Fig. 2.5. Secondary bracing of the frame
(after Mander et al. [20])

Thiruvengadam [21] suggested using multiple struts which came in contact with half of the beam and αh contact length along the column where α was in the range from 0.2 to 0.8 (fig. 2.6). This multiple strut model gave results which compared well with the experimental results except for very short frames. The calculated frequencies using this model were in good agreement with Finite Element Method (FEM) results.

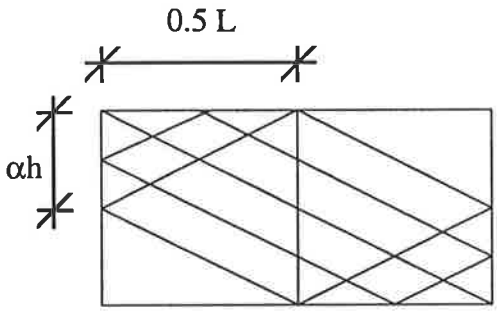

Fig. 2.6. Multiple strut model for separating infill
(after Thiruvengadam [21])

Substitution of the traditional one diagonal bracing with three or more diagonals was an improvement in the diagonal strut concept. One of these models (fig. 2.7) developed by Chrysostomou et al. [22] and also used by other researchers [23,24] was for the dynamic non-linear analysis of infilled frames with three diagonal struts in each direction with degrading stiffness and strength.

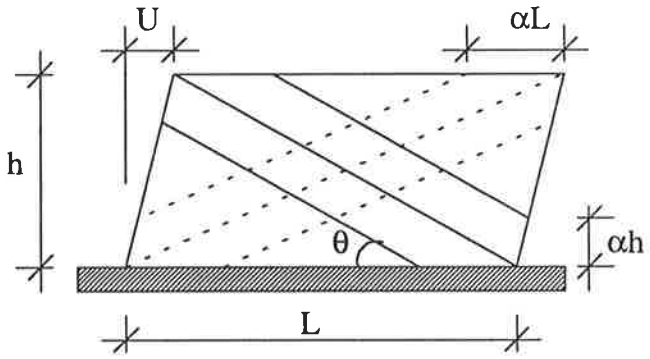

Fig. 2.7. Three diagonals in each direction with degrading strength and stiffness (after Crysostomou et al. [22])

2.2.5. Effective diagonal area

A very important characteristic of the diagonal strut was its effective cross-sectional area. Researchers in the past have proposed different values for the width of the diagonal. Holmes [3] suggested diagonal width equal to 1/3 of the length of the diagonal. Hamburger [25] suggested diagonal width no greater than twice the thickness of the masonry wall. Originally Smith [4,5,6] suggested the contact length between the frame and the wall ,hence, the effective diagonal width, to depend on the relative stiffness of the frame and the wall and the length to height ratio of the infill panel. Durrani et al.[26] compared their results with formulae suggested by Mainstone. Mainstone's formulae were for rectangular frames and the effective width was defined differently for different stages: for effective secant stiffness, for ultimate strength and for first cracking strength of the infill. Durrani et al. [26] found that the formula in the version for initial stiffness gave different results from their finite element investigation because it was based on an empirical approach which neglected the stiffness of the beam. However, their research found that the effective width was more sensitive to the column stiffness than the beam stiffness. The formula for the effective width for initial stiffness of the infill suggested by Durrani et al. [26] (2.3) was based on the finite element analysis and also included the stiffness of the frame and the wall and the angle of the diagonal with the horizontal θ:

$$\gamma = \frac{w_e}{w_d} = 0.32\sqrt{\sin 2\theta}\left(\frac{H^4 E_i t}{m E_c I_c b}\right)^{-0.1} \qquad (2.3)$$

In the above equation w_e is the effective width of the diagonal, w_d is the diagonal length, H is the storey height, E_i and t are the elastic modulus and the thickness of the infill, E_c and I_c are the elastic modulus and the moment of inertia of the column and b is the infill height. The parameter m depends on the relative stiffness of the beam and the column.

As mentioned above the stiffness of the beam was not of primary importance to the formation of the diagonal and its effective width (also[9]) and many researchers (including Thiruvengadam [21]) adopted a contact length along the beam equal to half the length of the beam.

2.3. Finite element method simulations

The FEM was very often used to compare theoretical results with experimental and for evaluation of the performance of existing buildings with infilled frames.

2.3.1. Type of elements used for the infill wall

Masonry is a two phase material with planes of weakness oriented along the bed joints. Because of this peculiarity the strength and failure mechanisms of masonry are usually predicted adopting techniques from rock mechanics or soil mechanics. Two major trends have developed for the representation of the infill walls by finite elements as distinguished by Lourenco et al. [27]: the micro-modelling and macro-modelling techniques.

Micro-modelling The micro-modelling technique concentrates on detailed precision of presenting the individual components of the masonry wall and the cracking or crushing phenomena which occur at their interfaces or within the materials. One material model for brick masonry was developed by Page [28], where the elastic bricks were set in an inelastic mortar matrix. The joint elements had very high compressive strength, low tensile strength and shear strength depending on the normal stresses on the bed joint.

The micro-modelling technique was usually preferred when the properties of the brickwork have to be derived [29] or for investigating wall panels with large openings

where the precision of the solution would be greatly influenced by both the choice of type and number of elements. A detailed mesh finite element analysis was carried out by Crisafulli [30] to verify a theory for the strength envelope of masonry. Zhuge et al. [29] used this type of masonry modelling to obtain the behaviour of the brickwork under static and dynamic loading.

Macro-modelling The macro-modelling technique incorporates bricks and mortar joints into larger elements and introduces the cracking and separation phenomena at the nodal points of the elements. Rectangular or triangular plate elements were used in those models and the number of the degrees of freedom (DOF) were different for different models depending on the initial assumption. Most often rectangular elements with two degrees of freedom at each node were used [31,32,33,24] however rectangular or triangular elements with more degrees of freedom were also used (3 DOF at each node [34,35,15] or 4 generalised DOF at each node used by Kost et al.[36]). In most of the cases the brickwork was considered to be a linear-elastic homogeneous material. Rivero et al. [37] introduced joint elements at the nodes of the wall to approximately represent the cracking of the wall. A similar mechanical model was used by Shing et al. [38] where interface elements were inserted at critical locations to present the sliding failure of the mortar joints.

The macro-modelling technique is very convenient when analysing larger infilled frame models (especially in multi-storey frames). It allows similar accuracy of the solution with much less computational effort. This method has often been used for evaluation of the deformation characteristics of the wall subassemblage and to define the parameters of diagonal strut models. Many researchers have followed this methodology [24,31,39,26].

2.3.2. Type of elements used for the frame members

In one of the earliest solutions of the problem with the help of the finite element method (Karamanski [40,41]) the frame was modelled using elements which carried only axial forces. As a result the lateral forces on the frame were carried to the infill wall unchanged, an assumption which is adequate only for very weak frames. Most often the frame consisted of standard six DOF (two translational and one rotational at each node)

elements. However, El Haddad [33] included the frame non-linearity and the effect of shear deformations due to crack presence by cracked beam elements. Rivero et al. [37] included non-linearity of the frame by possible hinging at the nodes of the frame elements. Youssef [42] carried out investigations to study the influence of the finite element modelling assumptions concerning frame members, beam-column connections, frame-infill interface and vertical restraints on top of the wall.

2.3.3. Modelling of the frame-wall interface

There were various solutions for representing the frame wall interface depending on the various boundary conditions between the frame and wall. The transfer of forces at the frame-wall interface is affected by the following factors:

- presence of shear connectors at the interface;
- existence of slip; and
- lack of initial fit of the wall into the frame.

Most often the interface was represented by link or joint elements which had very big compressive stiffness and very low tensile stiffness. Riddington and Smith [32] were the first to introduce the short stiff linking element. This type of element usually introduced friction at an interface without shear connectors [32,34,35,15] or it was a simpler representation of the compression and tension regimes at the interface [31,36]. Interface elements which had shear and normal stiffness were used by King et al. [43] around the four edges of the infill wall panel including the boundary interface at the base of the wall. Another method, used by El Haddad [33], was based on introducing additional nodes after the appearance of a crack at the boundary and using a link element to connect the two nodes. The contact length between the frame and the wall still shared common nodes. Gergely et al. [24] used higher order finite elements which provided rigidity between the frame and the wall by three spring stiffnesses - two translational and one rotational.

2.3.4. Lack of initial fit between the frame and the wall

It has been proven by test result, observations of actual earthquake damage and theoretical investigation that lack of initial fit between the frame and the wall changes

dramatically the lateral resistance of infilled frames. Dawson and Ward [31] found after experiments of infilled frames with initial gap that there was no compression on the top edge of the wall. To investigate the behaviour of such a frame they used for the interface gap-link elements which were essentially pin jointed struts which take into account the gap. Kost et al. [36] introduced the influence of the gap by keeping track of the horizontal (vertical) displacements of the peripheral nodes of the wall and the nodes of the column (respectively beam). The gap closed when the difference of those displacements became bigger than the initial gap size. Horizontal or vertical gap elements were introduced at the frame-wall interface by Rivero et al. [37] which had low stiffness in compression until the initial gap was closed and high stiffness in compression after that.

The simultaneous use of a coarse mesh of wall elements and detailed modelling of local behaviour such as the crack appearance at the interface and the cracked regions of the wall requires the simultaneous application of two approaches: the smeared crack approach and the discrete crack approach. Different levels of non-linearity in the frame wall system are possible. Most often the frame and the wall elements were elastic while the modelling of the boundary interface provided the overall non-linear response of the system. The model suggested by Rivero et al. [37] is one of the most precise models in terms of representing the non-linear behaviour of the system and at the same time it did not concentrate on each component of the frame wall assemblage. This model was able to simulate the non-linearity of the frame members, the wall cracking and separation phenomena and the non-linearity of the frame-wall interface. The model developed by Shing et al. [38,44] also used the smeared-crack approach and the discrete-crack approach. Smeared crack elements were used for the tension and compression behaviour of the masonry units while interface elements modelled the fracture of mortar joints, the separation of the frame-panel interface and the shear in the concrete columns. This precision in the finite element idealisation was necessary because of "the sensitivity of the lateral resistance of infilled frames to the shear strength of the masonry infill wall". This type of model had excellent correlation with experimental results [44]. Jankulovski et al. [45] also adopted similar approach for evaluation of the lateral resistance of masonry walls using a combination of the Finite element method and Discrete element methods.

2.4. Dynamic simulations and dynamic behaviour

Researches in the past have pointed out the importance of dynamic testing of infilled frames compared to static. Scaletti et al. [46], after comparing the results from static, shaking table tests and pseudodynamic tests, found that the behaviour of the infilled frames was highly non-linear and the results from the static tests showed lower strength which was probably due to the stress relaxation. Both the finite element method [47,21,48,39] and the diagonal strut model [39,21] have been used to simulate and evaluate the behaviour of infilled frames under dynamic loading. Both methods were usually used in two dimensional analyses. However, Manos et al. [49] pointed out that the diagonal strut model is not able to cope with the stiffening effect in torsion of the infill wall on a structure which is of considerable importance for torsionally flexible structures.

2.4.1. Hysteresis rule for masonry infilled frames

The hysteresis behaviour of infilled frames modelled with the help of diagonal struts could be characterised by the Three Parameter Model which was used by Zarnic [50]. The Three Parameter Model was also used by El-Gazairly [51] to evaluate the resistance of an existing structure. The Three Parameter Model was originally proposed by Park, Reinhorn and Kunnath and used three parameters α, β and γ, to define the stiffness degradation, the strength deterioration and the pinching of the hysteresis. The program used by Zarnic [50] in the theoretical analysis was "DRAIN-2D". Frame members were modelled by flexural longitudinal springs. The skeleton curves for the frame members and the diagonal members and the composite hysteresis rule are shown in fig. 2.8.

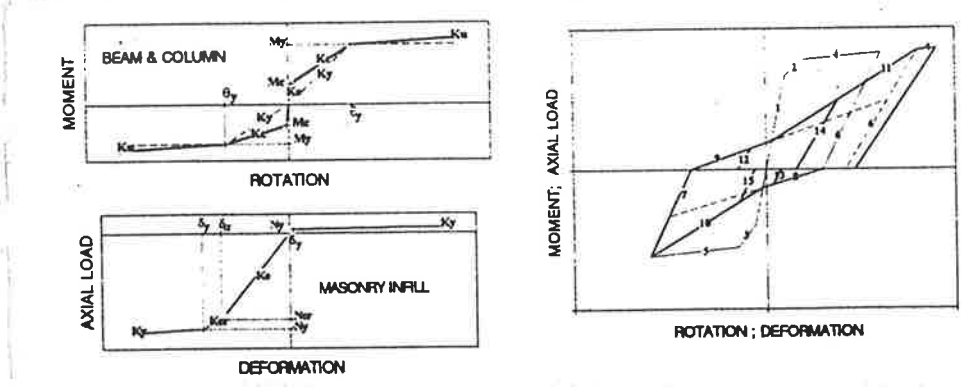

Fig. 2.8. Skeleton curves and hysteretic model (after Zarnic [50])

The envelope of an idealised hysteresis looked like the one on fig. 2.9. The three slopes correspond to different stages of cracking and lateral resistance of the infilled frame: H_s was the shear resistance at separation of the infill and H_u was the ultimate shear resistance of the infilled frame. K_i was the initial stiffness of the infilled frame, K_e was the effective stiffness and K_c was the stiffness at attained ultimate shear resistance.

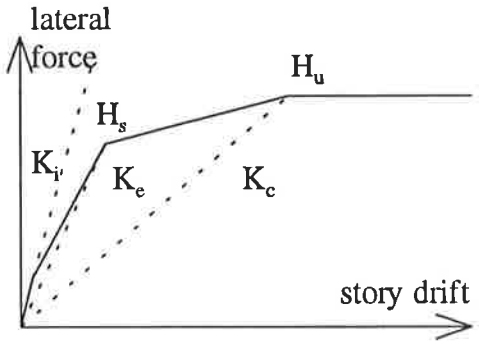

Fig. 2.9. Linear idealisation of the hysteresis envelope
(after Zarnic [50])

The stiffness and strength of the infill wall influences the shape of the hysteresis envelope. Schuller et al. [52] carried out tests to establish the influence of the relative strength of the infill and the length to height ratio on the load resistance and the energy dissipation capacity of infilled reinforced concrete frames. Two designs for the frame were considered in the investigation: "weak" frame design which was only for wind pressure and "strong" frame design which was only for equivalent static forces for zone 4 from the UBC (1991). Two infill cases were also considered: "weak" infill which was hollow concrete blocks and "strong" infill which was solid concrete blocks. Some of the envelopes from the result of the cyclic test are shown on fig. 2.10. The stronger panel increased both the lateral stiffness and strength of a "weak" frame more than the weaker panel. However after the ultimate load the drop in the lateral resistance was more rapid in the strong infill than in the weak infill which was attributed partly to the shear failure in the column and to the compression failure of the infill. The stronger infill also had better energy dissipation. For strong frame and strong infill combination the strength was even higher and it gave better results that any other combination because the frame confined the wall more effectively with a longer contact length causing diagonal action

and shear failure in the column was more unlikely to happen. From the results shown on fig. 2.10 it can be seen that the length to height ratio had little importance on the strength and ductility of the specimens. It should be noted that the total vertical loads were the same in all tests.

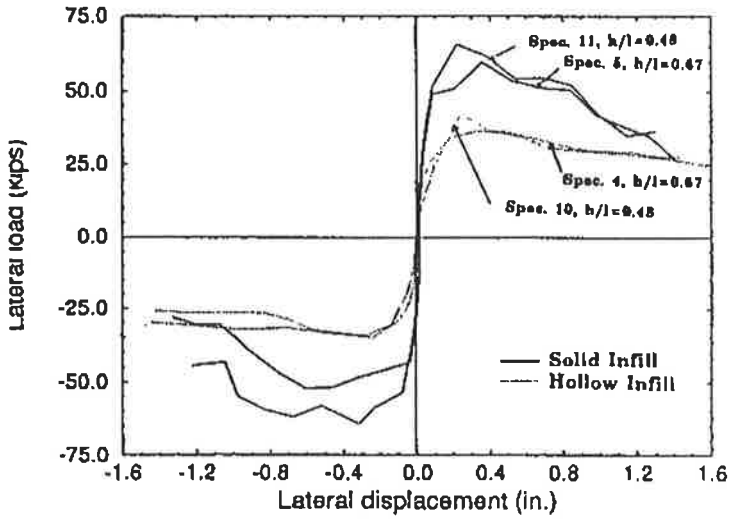

Fig. 2.10. Load/displacement envelopes from cyclic loading (weak frame) (after Schuller et al. [52])

2.4.2. Damping and natural frequencies

According to Mallick and Severn [53] there are four factors causing damping in infilled frames: material damping (internal friction), friction between the infill wall and the bounding frame, friction between the cracked surfaces of the infill and loss of energy due to impact (when the panel rocks inside the frame under vibrations of high amplitude). In view of the above mentioned factors a comparison [53] between infilled frame with shear connectors and without shear connectors at the boundary interface showed that the infilled frame without shear connectors had a smaller stiffness but greater damping capacity.

The presence of infill walls reduces the period of vibration and ductility of the frames and introduces changes to the mode shapes. For example, El-Gazairly [51] found that the presence of infill walls in a case study building reduced the period of the building by a

maximum of 61.5%. Dawson and Ward [31], after investigating the behaviour of a four storey frame, found that the presence of infill walls removed the peaks in the displacement/frequency diagram which are from the second and third mode of vibration. Removing of the bottom wall reintroduced the second mode of vibration in the response spectrum (fig. 2.11).

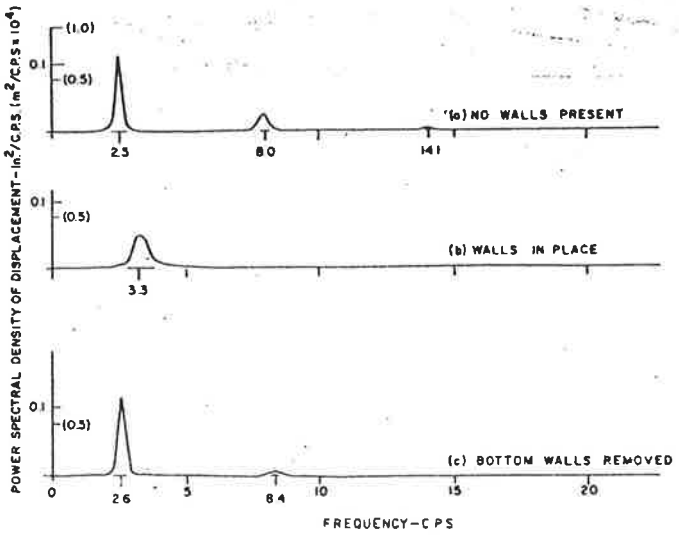

Fig. 2.11. Power spectral density of displacement for a four storey frame (after Dawson and Ward [31])

2.5. Clay brick masonry properties

The wall panel material in infilled frames investigated by other researchers varied from mortar infill to brick and concrete masonry walls which in some cases were reinforced. The effect of the reinforcement on the lateral resistance has also been previously investigated. The present research concentrated on the influence of unreinforced clay brick masonry infill. Here, the properties of masonry panels was required to be defined *a priori*.

2.5.1. Young's modulus of masonry

It has been found through the years that Young's modulus of masonry varies within a very large range of values. For example, Base and Barker [54] cited a value of 22 546

MPa for Young's modulus of solid brick masonry running horizontally (the theoretically predicted value was 21 235 MPa). In research by Page [28] and Dhanakesar [55,56] the reported value was 5800 MPa for solid brick masonry. However, in another paper [57] the value which was assumed was 7000 MPa and Poisson's ratio ν=0.2. It had been found that those values depend on the orientation of applied load to the bed joint. Zhuge et al. [29] suggested a formula for calculation of the Young' modulus based on results from finite element method analysis for dynamic and static loading conditions. The formula included the values of the Young's modulus of the brick and the mortar in a specific ratio:

$$E_0 = cE_b + (1-c)E_m \tag{2.4}$$

In the above equation:

E_b=14700 MPa - Young's modulus for brick;

E_m=7400 MPa - Young's modulus for mortar;

c=0.8 - coefficient for static loading, hence E_o=13240 MPa; and

c=0.5 - coefficient for static loading, hence E_o=11050 MPa.

The value obtained from theoretical and test results by Klopp [58] was 1065 MPa and is the suggested value for solid brick masonry for South Australia. Calvi [46] obtained a similar number of 1000 MPa from static in-plane shear tests (ν=0.25).

2.5.2. Failure modes and failure surfaces of brick masonry

Masonry walls confined in frames can suffer the following modes of failure: shear failure at a horizontal bed joint or a series of bed joints; tensile failure of the brick; and crushing of the brick and the mortar. These modes of failure depend on the relative stiffness of the frame and the wall and the length to height ratio of the infill wall panel.

Depending on the detailing of the masonry theoretical models, several failure surfaces have been suggested. Coulomb failure criterion was used most often to represent the shear strength of masonry. Mann Mullers's theory which is based on equilibrium conditions was modified by Crisafulli et al. [30] to represent the strength envelope of masonry.

For macro-modelling approaches where a relatively coarse mesh was used for the masonry, the failure surface was defined in two ways. Some failure surfaces were based on the principal stresses and their orientation to the bed joint, others on the stresses parallel and perpendicular to the bed joint and the shear stress on the bed joint. A failure surface consisting of three elliptic cones and derived for the stresses parallel and perpendicular to the bed joint and the shear stress on the bed joint was suggested by Dhanakesar et al. [55,56]. Von Mises failure criterion is usually used for crushing failure. Shing et al. [23,44] used Von Mises failure criterion and Rankin type cut-off surface for the smeared crack elements. Lourenco et al. [27] suggested for micro-modelling the failure surface of the interface elements to consist of a combination of tension cut-off, Coulomb and elliptical cap regimes. For macro-modelling the failure surface consisted of Hill and Rankine type yield surfaces.

2.6. Behaviour of the frame members

Priestly [60] identified that some of the possible types of failure of infilled reinforced concrete frames include:

- tension failure of columns;
- diagonal failure of the infill wall; and
- shear or bending failure of the column or beam-column joint following sliding failure of the infill.

Conclusions concerning the strength of infilled frames may be drawn by these modes of failure concerning the forces in the frame. Firstly, that the presence of the infill may increase considerably the axial forces in the columns. This was also observed by Hamburger et al. [25]. Second, measures should be taken against flexural or shear failure of the column, especially against shear failure which is the more undesirable type of failure. Kato et al. [61] carried out cyclic tests on four infilled frames with different ratio of the shear and axial reinforcement of the columns. One frame had heavy axial and shear reinforcement, another had heavy axial and poor shear reinforcement, the third had heavy shear and poor axial reinforcement and the fourth had poor axial and poor shear reinforcement. The test results showed that the overall hysteresis rules and the modes of

failure were different and were highly dependant on the percentage reinforcement of the column. The results from their investigation can be summarised as follows: increased axial reinforcement of the column can improve the load carrying capacity of the masonry wall and adequate shear reinforcement can avoid shear failure in columns. Kato et al. [61] also defined an important goal for the investigation of infilled frames design: "adequate reinforcements in confined frames are indispensable to improve the earthquake resistant capacity of confined masonry building, the subjects in seismic design are to find better combinations of two factors, ie. the ratio of axial reinforcement and that of shear reinforcement".

2.7. Retrofit

The research investigations of infilled frames are very important for the evaluation of the seismic resistance of infilled frame buildings and their retrofit. The evaluation of framed buildings should take into account the presence of the infill since it changes the demand on column axial loads as compared to those for the frame without infill [25]. Proper evaluation of the damping characteristics of infilled frame buildings is also important when their retrofit includes introducing viscous dampers in the infilled frames to improve the damping of the system [62]. Theoretical techniques are a powerful tool when improving the performance of the infill panel by coating of the wall [18,20]or grouting of the damaged regions [18]. A seismic rehabilitation study was carried out by Comartin et al. [63] on unreinforced masonry buildings which included an infilled frame structure. The proposed procedure included replacement of the masonry infill above or above and below windows with concrete. The diagonal strut model was shown to be a powerful methodology to present and evaluate the dynamic performance of existing infilled frame structures.

2.8 Conclusion

To investigate the complex statically indeterminate problem of infilled frames, two main concepts have been developed: the diagonal strut concept and various models employing finite element methods. The accuracy of the models and the solutions of the problem

usually depend on the initial assumptions and simplifications input in the philosophy of each model. The finite element method gives a precise methodology to cope with the problem. It is able to model with great complexity the stress distribution and the modes of failure of the models under different levels of loading. In contrast, diagonal strut models are an approximation of the problem which usually give reasonably accurate solutions of the problem. These two types of methods are very often used together. It has often been discussed which one gives better results in terms of the efforts involved in the development of the model and final precision of the solution. The problem of infilled frames is complex and highly dependant on the initial conditions and assumptions. Therefore, Homes [3], who proposed a relatively simple solution, agreed with Benjamin and Williams who stated that: "Numerous studies were made involving exact mathematical procedures. The results were in no way better or more reliable than the most elementary procedures of strength of materials."

This research adopted the diagonal strut model for the overall evaluation of the response of infilled frames. The composite behaviour for the case of perfect fit and lack of initial fit between the frame and the wall was considered to be dramatically different. Although the use of one diagonal for the case of a construction gap is questionable, for the sake of simplicity of the solution, the diagonal strut model with a single brace was used in this analysis. The single diagonal strut analogy appears to have many disadvantages, however, its main advantage is the simple and in most practical cases satisfactory performance in basic analyses. As other researchers have stated: "The complexity and uncertainty of the infill materials justifies the use of approximate material modeling"[23]. The finite element method will be used to derive the properties of the diagonal struts.

CHAPTER 3 - AIMS AND BASIC DEFINITIONS

3.1. Aims of this research

The main purpose of this research was to study the influence of the masonry wall on the overall dynamic response of reinforced concrete frames with brick masonry infill panels. In particular, the analysis attempted to establish the importance of the following factors on the behaviour of the frame-wall system:

- the relative stiffness of the frame and the wall, initially estimated by the parameter λh;
- the length to height ratio of the wall panel l/h; and
- the presence of a construction gap between the frame and the wall and the size of this gap.

The changes introduced by presence of a construction gap will be of main consideration.

Other factors which influence the lateral resistance of infilled frames are: beam and column relative stiffness, the detailing of the reinforced concrete frame joint, reinforcing of the masonry wall and strengthening and repair of the infill, method of construction (building the wall before the frame or subsequently after the frame) and openings in the wall. The influence of these factors was not investigated in this research. The masonry infill walls considered were unreinforced and without openings. All models used the same cross-sectional area for the beams and the columns. The infill walls were considered to be built after the frame, thereby, introducing a gap between the frame and the wall.

3.2. Definitions of the geometry and design of the infilled frames

The parameter of relative stiffness, as suggested by other researchers [6], was used for the initial evaluation of the wall to frame stiffness and is given below in equation (3.1):

$$\lambda h' = \sqrt[4]{\frac{E_w t \sin 2\theta}{4 E_c I_g h}}\, h' \tag{3.1}$$

In the above equation (see also fig. 3.1):

E_w - Young's modulus of the clay brick wall;

t - thickness of the clay brick wall;

θ - angle between the diagonal of the wall and the horizontal;

h' - height of the column;

h - height of the wall;

E_c - Young's modulus of the reinforced concrete frame; and

I_g - moment of inertia of the column cross-section.

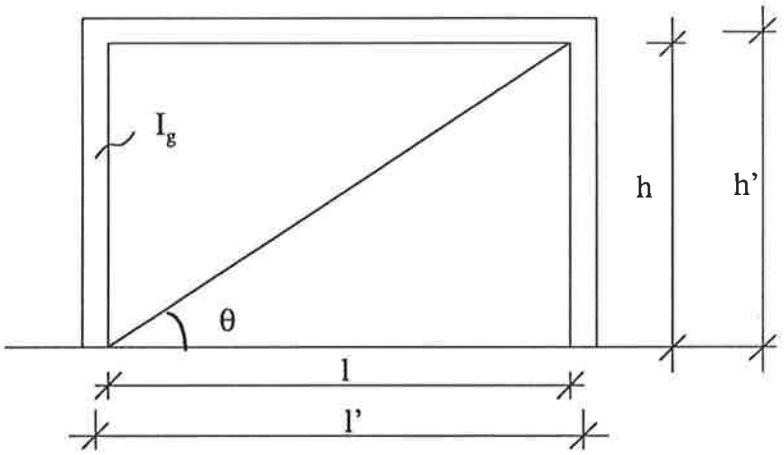

Fig. 3.1. Basic definitions

Obviously, formula (3.1) accounts not only for the stiffness of both the frame and the wall but also takes into account the length to height ratio of the infill panel. Therefore, these parameters will be altered separately in the models' geometry in order to study separately their effect on the overall response.

Eight models were investigated. The geometry of these models is summarised in Table 3.1. The geometry of the models was chosen so that maximum possible variations of the relative stiffness parameter λh and the length to height ratio (*l*/h) were achieved. Models M2, M3, M6 and M7 held the frame moment of inertia constant and λh varied from 4.63

to 3.86 (due to changing length to height ratio l/h from 1.33 to 2.66). Models M3, M4 and M5 had constant l/h =1.5 and variable relative stiffness values (from 4.20 to 2.52) due to changes in the moment of inertia of the frame. All calculations for the relative stiffness parameter λh used the gross moment of inertia I_g.

Model M1 was a square infilled frame. The reinforced concrete frame had a very small stiffness by itself. The columns of the frame were slender and the frame, by itself, did not comply with design code requirements. Therefore, the interest in this model was only for investigation of extreme case of a very "weak" frame with a very "strong" infill wall (λh=6.36).

Model M8 was a full size model of a reinforced concrete frame investigated by Wong [64] with respect to the joint detailing. The response to lateral loading of the frame when infilled with brick masonry wall was investigated in this research.

Table 3.1. Geometry of the models

model	Frame				Infill				λh
	h' (m)	l' (m)	I_g x10^8, mm^4	cross-section, mm	h (m)	l (m)	l/h	sin 2θ	
M1	3.100	3.20	1.33	200/200	3.0	3.0	1.0	1.000	6.36
M2	3.165	4.33	9.88	330/330	3.0	4.0	1.33	0.960	4.63
M3	3.165	4.83	9.88	330/330	3.0	4.5	1.5	0.923	4.20
M4	3.225	5.00	26.58	450/350	3.0	4.5	1.5	0.923	3.34
M5	3.300	5.10	90.00	600/500	3.0	4.5	1.5	0.923	2.52
M6	3.165	6.33	9.88	330/330	3.0	6.0	2.0	0.800	4.05
M7	3.165	8.33	9.88	330/330	3.0	8.0	2.66	0.660	3.86
M8	3.150	6.00	21.3	400/400	2.8	5.6	2.0	0.800	3.36

Note: The cross-sectional area is equal for the columns and the beams for all models except for model M8. For model M8 the table shows the column properties, the beam moment of inertia is I_g=114.3 x10^8 mm^4 and the cross-section is 700mm/400mm.

The material properties of the brick wall were modelled by treating the brick masonry as an isotropic material. Based on results from Page et al. [65] the properties were taken as follows: Young's modulus of masonry E_w=5800 MPa and Poisson's ratio ν=0.23. The thickness of the wall was 110 mm for model M1 and 220 mm for all other models.

The detailing of the reinforced concrete cross-section and material properties of the frame are summarised in Table 3.2. The table shows the assumed percentage reinforcement which was used later for calculating the strength line of the beams and columns of the frame. Due to insufficient design data the area of reinforcement was chosen from average values of steel proportion for the beams and the columns, as required by AS 3600 [66].

Table 3.2. Concrete material properties and reinforcement percentage

model	E_c , MPa	f_c' , MPa	beam		column	
			$p=A_s/A_g$ (%)	A_s , mm^2	$p=A_s/A_g$ (%)	A_s , mm^2
M1	25000	20	1.65	660	3.10	1240
M2	25000	20	1.71	1860	2.94	3200
M3	34500	40	1.71	1860	2.94	3200
M4	34500	40	1.71	2700	3.18	5000
M5	34500	40	1.60	4800	2.50	7500
M6	34500	40	1.71	1860	2.94	3200
M7	34500	40	1.71	1860	2.94	3200
M8	34500	40	1.71	4800	3.10	5000

The influence of the slab on the beam cross-sectional properties was ignored. In the calculations for the static (linear with partial nonlinearity) analyses, a value of 50%I_g was used for the beams and the columns of the infilled frames. For the dynamic (nonlinear) analyses, 25%I_g and 30%I_g for the beams and the columns were used for the bare frame and for the infilled frame, respectively, to account for the stiffening effect of the wall on the frame characteristics.

CHAPTER 4 - STATIC ANALYSIS

4.1. Introduction

It has previously been shown by researchers that the finite element method can be used to give accurate results for evaluating the behaviour of infilled frames even with relatively simple finite element configurations. The static finite element analysis performed in this research used orthotropic material properties for the infill wall and a linear elastic constitutive law for the materials to evaluate the strength and stiffness of the infill wall as a function of the relative stiffness parameter ,λh, the length to height ratio of the panel ,l/h, and the gap size between the frame and the wall. The results of the static analysis reported here are used in chapter 5 for the development of a non-linear dynamic model.

In this chapter the minimum number and type of elements for the wall are established first and then an improved finite element model is developed. With the help of the improved model the stress distributions in the panels, the contact lengths between the frames and the walls and the properties of the diagonal struts are found. Finally, the yield strengths and the stiffness for the elastic range of the infill walls are found for the investigated models.

4.2. Development of the models for static analysis based on the finite element method

The program used to analyse the infilled frames under static loading was "Images - 3D" - Finite Element Analysis Program [67]. The program is able to perform static and dynamic analyses assuming linear elastic material properties. Partial non-linearity can be represented through the use of non-linear spring elements.

The models were developed as shown in fig. 4.1. Standard rectangular plate elements (element type 1) were used to model the wall and standard beam elements (element type 2) were used to model the frame. Non-linear spring elements (element type 3) were used to model the frame-wall interface and linear springs represent the friction in the crack which first appeared at the base of the wall.

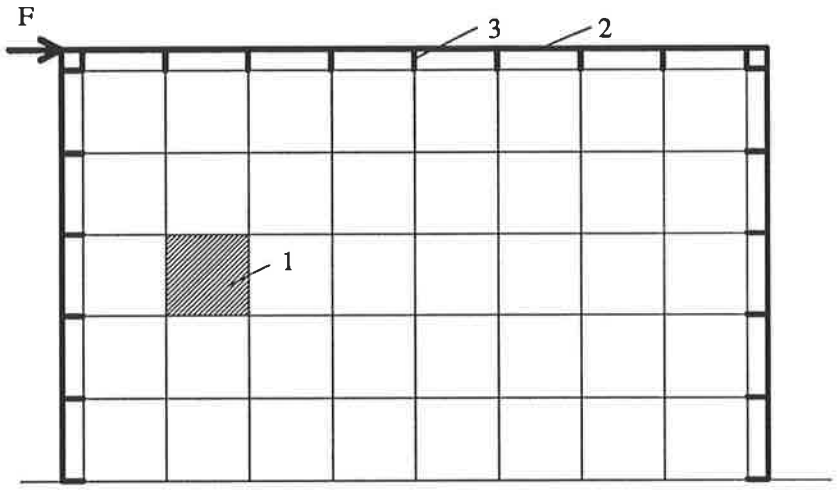

Fig. 4.1. Finite element model

4.2.1. The wall elements - minimum number and type

Model M1 was investigated for the minimum number of plate elements required for accurate solution. The results showed that the height or length of each element should be 2 to 2.5 times the thickness.

Model 4 was investigated to find out the sensitivity of the results to the element pattern. Keeping the dimensions of the wall and the frame constant the following cases were investigated:

- model M4 - standard rectangular plate elements;
- model M44 - standard rectangular plate elements with increased number of elements in the loaded and diagonally opposite corners;
- model M44a - triangular plate elements forming a grid as shown in fig. 4.2 with the same number of nodal points as for model M4 but double the number of elements; and

- model M44b - triangular plate elements which differ from model M44a only in the way they are arranged into a grid (fig. 4.2).

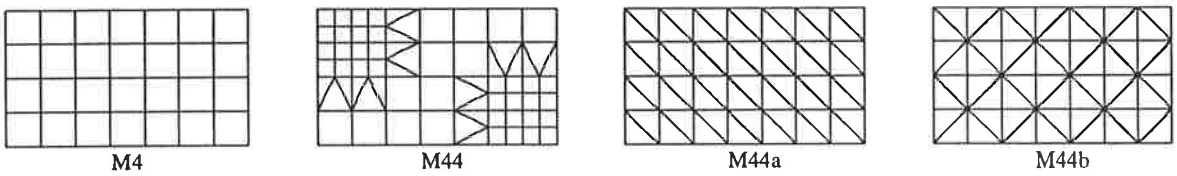

Fig. 4.2. Influence of the type of grid for the wall

The following results, summarised in Table 4.1, were obtained from these analyses:

1. The shear stresses in the wall were considerably higher in the models with triangular elements (the maximum difference was about 50%).
2. The stiffness of the wall was the same irrespective of the type of elements.
3. The forces in the left hand (directly loaded) column drop about 3 times for the models with triangular elements.

Table 4.1. Comparison of the results for different types of elements

model	applied force,kN	max τ, MPa	$F_{left\ col}$, kN	$F_{right\ col}$, kN	F_{wall}, kN	Δ_{wall}, mm	k_{wall},x10^7 N/m
M4	94	0.2563	-1.922	4.301	91.612	0.2019	45.38
M44	94	0.2989	-1.895	4.084	91.811	0.2010	45.68
M44a	94	0.3913	-0.648	4.041	90.607	0.1978	45.69
M44b	94	0.3648	-0.733	4.026	90.707	0.1952	46.47

For applied force at the top of the left hand column of the frame the terms used in the table above are defined as follows: $F_{left\ col}$ - force in the left column below the contact region; $F_{right\ col}$ - force in the right column above the contact region; F_{wall} - force in the wall equal to the difference of the applied force minus the forces in the columns; Δ_{wall} - displacement at the top right hand corner of the wall; and $k_{wall} = F_{wall}/\Delta_{wall}$.

The finite element method in plane analysis is "finding the stresses and displacements in continua by dividing it into finite number of elements connected only at their nodal points"[68]. Consequently, the displacement function used for determining the displacements within the element which better fulfils the continuity requirement along the edges of the element will give more accurate results. The displacement function for triangular elements results in constant strain distribution throughout an element while rectangular elements assume linear strain distribution over an element. The program uses standard finite elements and it was expected the results obtained from the models with rectangular elements to be more accurate for a mesh with the same number of nodes.

One of the models was solved for solids used for the wall. It was found that the use of solids did not improve considerably the accuracy of the results. For such a plane model, the use of solids and the associated increase in computational time were found to be unjustified.

4.2.2. The beam elements

The beam elements were defined using the properties from Table 3.1 and Table 3.2. The constitutive law for the material used in the program had a linear stress-strain distribution. Appearance of cracks in concrete members reduces their gross moment of inertia. Therefore, a moment of inertia equal to 50% I_g was used in the analysis.

4.2.3. The non-linear spring elements

The spring elements at the frame-wall interface were required to model the appearance and progress of cracks between the frame and the wall and adequately model the load transfer mechanism between them in the contact areas. The stiffness of the spring elements in tension was 0 (actually, 10e-8 due to requirements of the program) and more than 10e6 times the stiffness of the nodes in the required direction. The stiffness of the non-linear elements in compression provided deformation compatibility of corresponding nodes from the frame and the wall (fig. 4.3). The stiffness of the nodes from the frame was calculated from the flexural stiffness of a beam element, which is given by:

$$k_f = 12\frac{E_f I}{l^3} \qquad (4.1).$$

The stiffness of a node from the wall in x-direction is given by the following equation (4.2):

$$k_w = \frac{t}{12}\left(4d_{11}p^{-1} + 4d_{33}p\right) \qquad (4.2),$$

where the values of d_{11} and d_{33} were calculated by:

$$d_{11} = \frac{E}{1-\nu^2} \text{ and } d_{33} = \frac{E}{2(1+\nu)} \qquad (4.3)$$

and $p = \frac{a}{b}$ (a-horizontal, b-vertical dimension of an element).

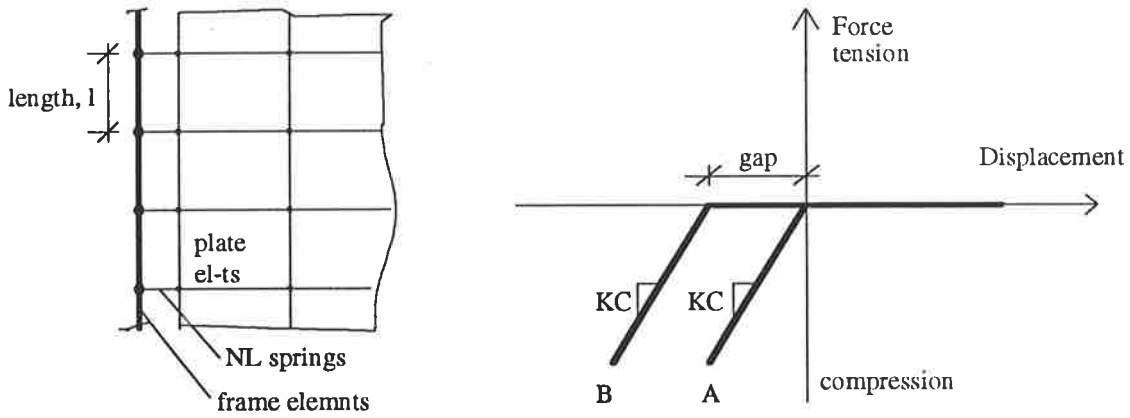

Fig. 4.3. Stiffness of the non-linear springs

(A-perfect fit between the frame and the wall, B-gap between the frame and the wall)

4.2.4. Linear spring elements

The interface between the base of the wall and the supporting beam or foundation was modelled using linear springs and the friction was assumed to be constant along the whole length of the wall. Therefore, the stiffness of the springs was linear and corresponded to a mean shear bond strength of 0.3 MPa in the brickwork. Each node at the base of the wall was rigidly connected to the foundation in vertical direction and restrained by the linear springs in horizontal direction.

The results from the stiffness calculations of the linear and non-linear springs for all frames are summarised in Table 4.2. In this table the stiffness for the nodes from the

frame was calculated using the gross moment of inertia I_g, KC is the stiffness in compression of the non-linear spring elements and K is the stiffness of the linear springs.

Table 4.2. Node and spring stiffness (all numbers in N/mm)

model	M1	M2	M3	M4	M5	M6	M7	M8
$k_{frame\ node} \times 10^8$	0.50	0.87	1.22	2.07	7.00	1.22	1.22	11.04
$k_{wall\ node} \times 10^5$	6.20	11.74	11.74	11.74	11.74	11.74	11.74	11.74
KC(NL springs)	10^{14}	10^{14}	10^{14}	10^{14}	3.5×10^{14}	10^{14}	10^{14}	1.1×10^{15}
K (L springs)	9000	33000	33000	33000	33000	33000	33000	33000

4.2.5. Further improvement of the model - increasing the number of elements in the loaded corner and diagonally opposite corner

The number of elements in the loaded and diagonally opposite corners was increased as shown in fig. 4.4. This provided more detailed information in the regions of stress concentration. For the cases when gaps were introduced between the frame and the wall this model was more sensitive to the deformations of the frame and better defined the contact length between the two components of the composite system.

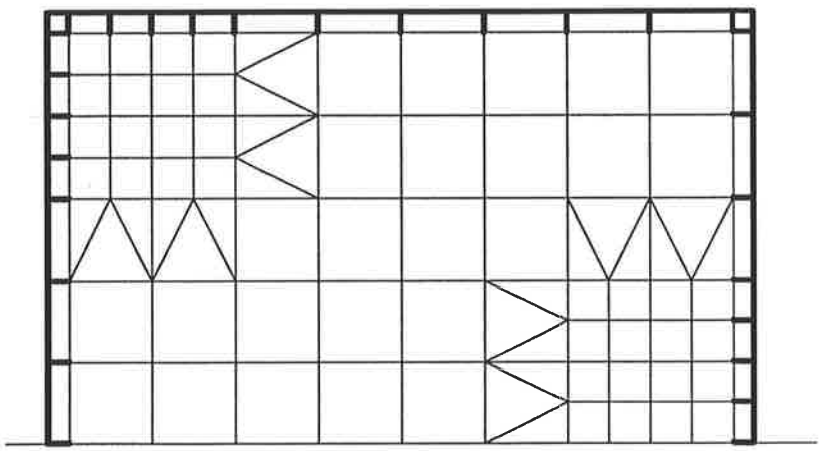

Fig. 4.4. Improved model with more elements at the loaded and diagonally opposite corners

4.2.6. Assumptions and restrictions of the finite element model

The accuracy of the results depend on the assumptions made while creating the finite element model. The assumptions and restrictions of the program were as follows:

- The constitutive law for the materials was assumed to be linear. Hence, the tensile cracks which appear in the masonry panel were ignored and only the stresses along the diagonal were subjected to analysis. Redistribution of stresses within the panel was not considered in these analyses. Consequently, the strength and stiffness of the infill wall were slightly overestimated.
- Non-linear effects were modelled with the help of non-linear spring elements. The equations at each iteration were not solved for deformed configuration of the system. When deformed configuration was used, the solution did not reach convergence which was probably because a solution for the deformed configuration turned the system into a mechanism.
- In the cases where a gap was modelled, the distance between the frame centre line and the wall remained constant as in the case of no gap (where it was equal to half the depth of the column cross section). Moving the frame out at a distance half column cross section height plus the gap size slightly increased the forces in the frame but the stiffness and the strength of the infill wall were essentially the same.
- Loads were applied only as a single concentrated force at the upper corner of the frame. Distributing the forces in a series of nodes along the beam did not substantially improve the accuracy of the results and for static analysis the applied load configuration was clearly adequate.
- Due to insufficient design data, it was assumed that no vertical loads acted in the plane of the frame coming from upper storeys or self weight. If vertical loads were imposed, they would confine additionally the infill panel and increase its strength and stiffness. Thus, the results from these analyses give lower bound estimates of the strength and stiffness of the infill wall.

The finite element model without the additional elements in the corners was used for preliminary analysis and development of the model. All final results and conclusions are based on the improved model which used more elements at the loaded and diagonally opposite corners.

4.3. Results from the static analysis

The purpose of this analysis was to find the value of the applied horizontal load which induced shear stresses in the panel equal to 0.3 MPa. This value was assumed to be the shear strength of the panel and was equal to the mean shear bond strength determined by Dhanasekar et al. [56]. The use of this value was even more relevant for the walls with gaps since no vertical forces were transferred from the beam and the wall panel was actually unconfined under this condition.

4.3.1. Stress distribution within the panel

Typical stress distributions in the panel are shown in fig. 4.6. Fig. 4.5 shows the positive directions of the in-plane stresses acting on an element. The highest vertical and horizontal stresses are concentrated in the loaded and the diagonally opposite corners of the masonry wall. The maximum shear stresses occur along the diagonal from the loaded corner to the opposite corner at the base of the wall. The stress distribution confirms the diagonal bracing action of the masonry wall. The distribution of normal stresses was essentially the same for all models, irrespective of the different values of λh or l/h.

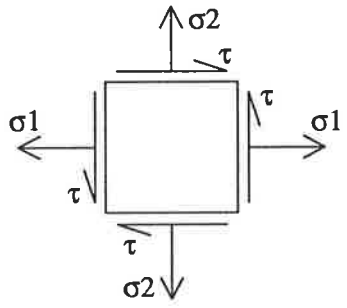

Fig. 4.5. Stresses on a plate element - positive directions

It was also found that the shear stress contours did not vary much with changes of λh due to increased frame stiffness. The shear stresses distribution, however, changed significantly with increases in the l/h ratio. For comparison, fig. 4.7 shows the shear stress contours for model M4 and model M7. For model M4, the angle between the diagonal and the base was closer to 45 degrees than the diagonal of model M7. Hence

σ1 stress contours
1 - -0.130 MPa
2 - -0.304 MPa
3 - -0.478 MPa
4 - -0.652 MPa
5 - -0.826 MPa
6 - -1.000 MPa
7 - -1.170 MPa
8 - -1.350 MPa
9 - -1.520 MPa
10 - -1.700 MPa

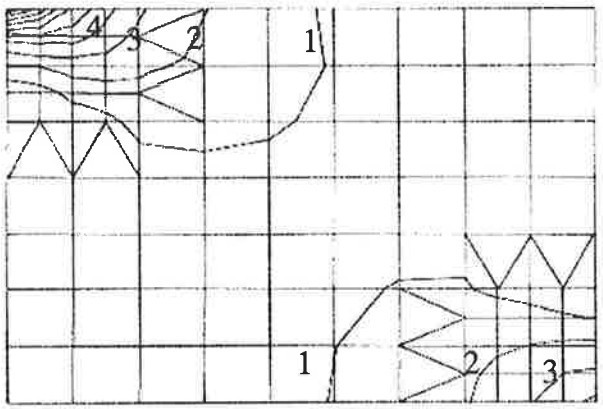

σ2 stress contours
1 - +0.0496 MPa
2 - -0.056 MPa
3 - -0.161 MPa
4 - -0.267 MPa
5 - -0.372 MPa
6 - -0.478 MPa
7 - -0.583 MPa
8 - -0.688 MPa
9 - -0.794 MPa
10 - -0.899 MPa

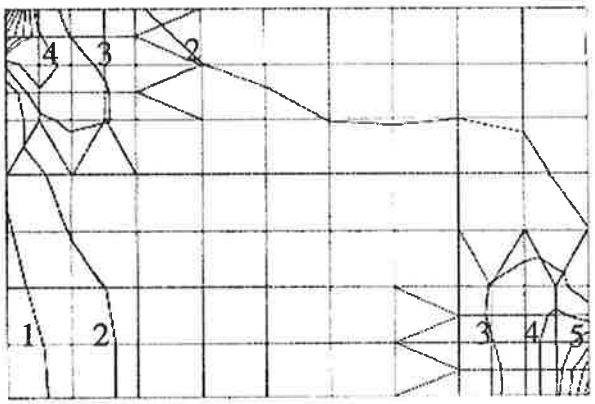

shear stress contours
1 - 0.235 MPa
2 - 0.211 MPa
3 - 0.187 MPa
4 - 0.163 MPa
5 - 0.140 MPa
6 - 0.116 MPa
7 - 0.092 MPa
8 - 0.069 MPa
9 - 0.045 MPa
10 - 0.021 MPa

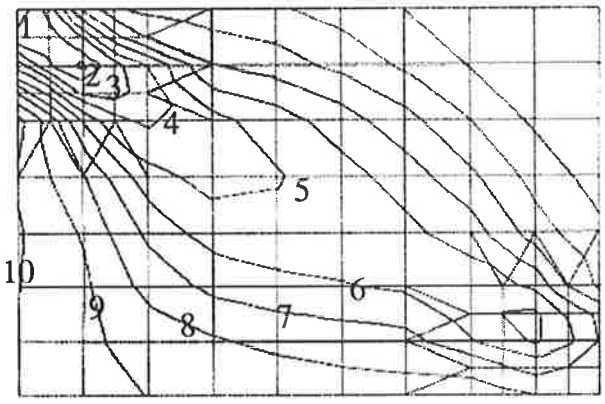

Fig. 4.6. Stress contours in the wall panel for model M4

the stress contours followed strictly this diagonal and were relatively symmetrical about it. In contrast, the stress contours for model M7 followed a 45 degree line down from the loaded corner and were obviously unsymmetrical in regard of the main diagonal. The higher shear stresses towards the loaded corner, even in the case without a gap, were a consequence of the linear material properties used by the program. The fine cracks due to tensile normal stresses which in practice appear in the region below the loaded diagonal were not introduced in the model. In practice, these cracks would cause stress redistribution within the masonry wall resulting in better defined diagonal action and less frequent changes in magnitude of the shear stresses along the main diagonal.

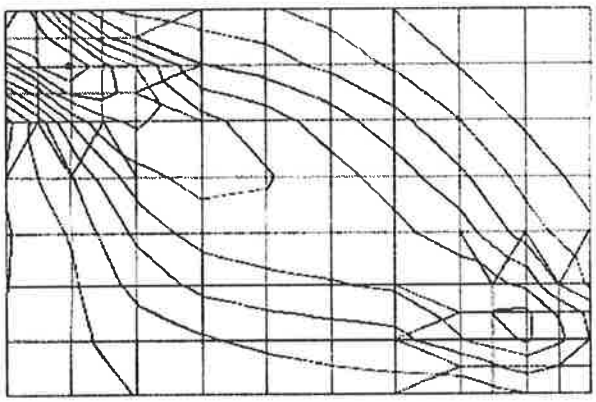

shear stress contours for model M4

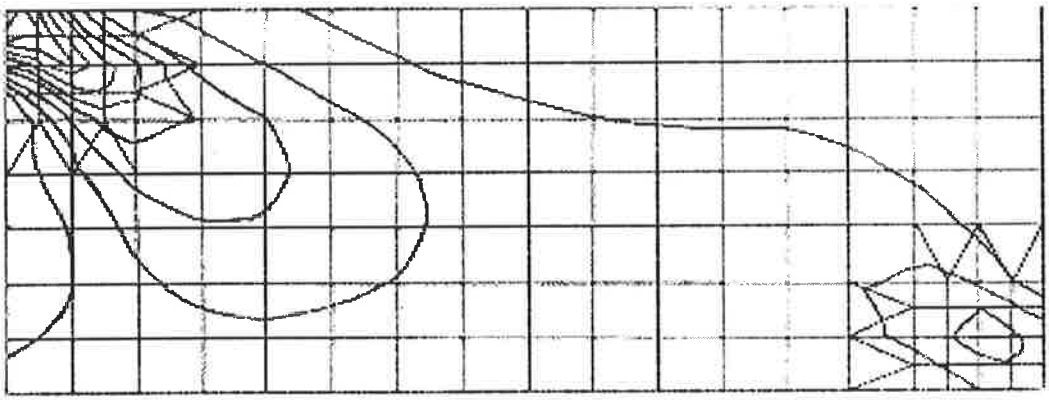

shear stress contours for model M7

Fig. 4.7. Changes in the shear stress contours depending on the *l*/h ratio

4.3.2. Analysis of the loaded springs

It was possible to estimate the contact length and the magnitude of the force transfer between the frame and the infill panel through the forces in the non-linear springs. The mechanism is illustrated in fig. 4.8. The deflections in the frame cause compression in some of the springs and tension in others. The negligibly small tensile spring forces (due to the very small almost zero stiffness in tension) indicate crack opening while the compressive spring forces correspond to the panel forming an effective diagonal strut which transfers a considerable part of the load in the manner of a diagonally braced frame.

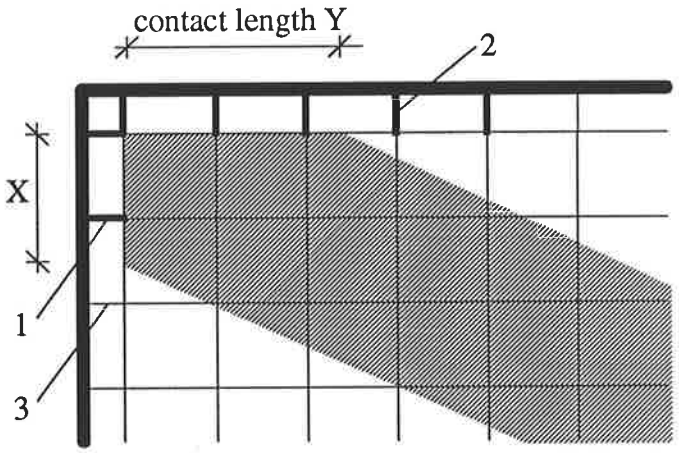

1 - loaded springs along the column, forming contact length X

2 - loaded springs along the beam, forming contact length Y

3 - springs with no load

Fig. 4.8. Formation of the diagonal strut

After analysing the forces in the springs for each model, the values of the contact length and the corresponding effective cross-sectional area for the diagonal strut were found. Fig. 4.9 gives a summary of the results for the case of no gap in all models. The numbers on the diagrams are the maximum values of the forces in the springs for the load which caused 0.3 MPa maximum shear stress in the wall panel, at which point local cracking was assumed to occur. When calculating the contact length Y (fig. 4.8) the small values of the spring loads along the beam were ignored (springs far from the loaded corner and

M1

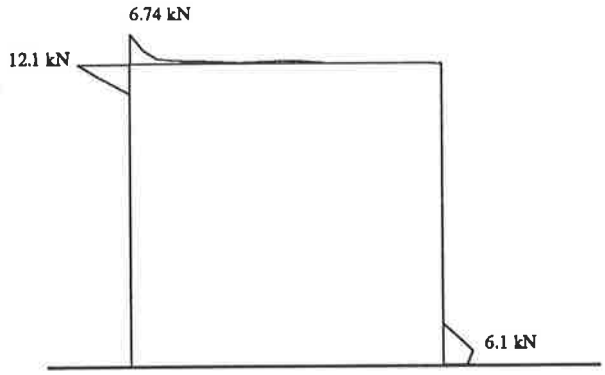

M2

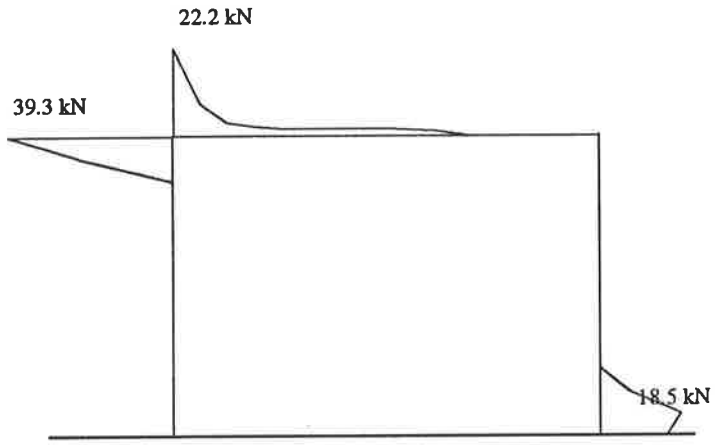

M3

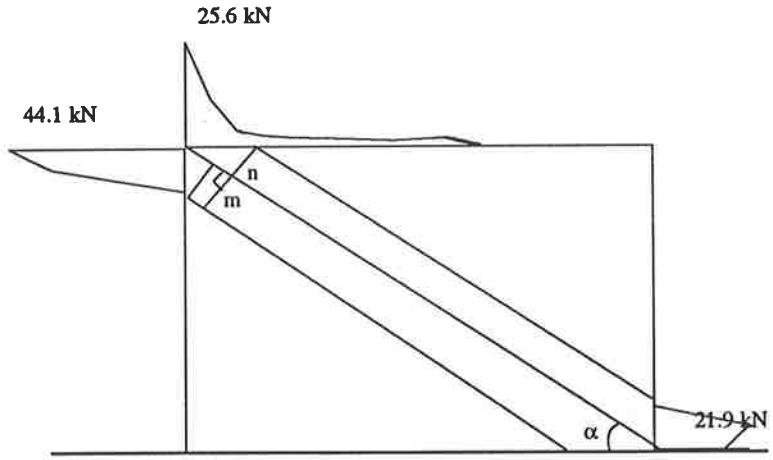

Fig 4.9. Forces in the compression springs - no gap

M4

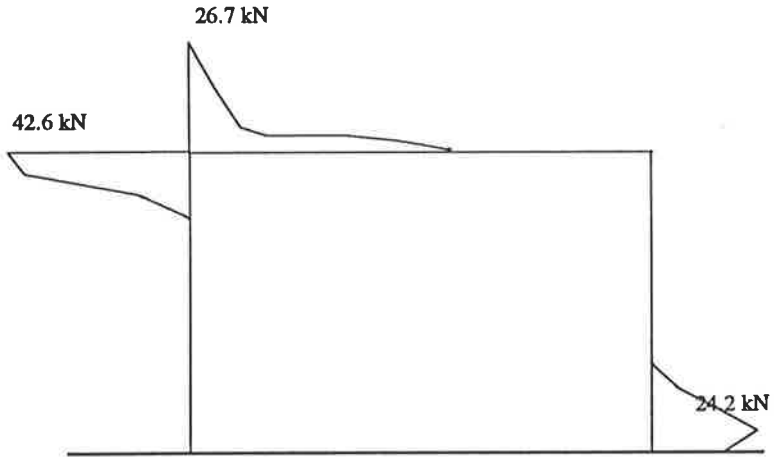

M5

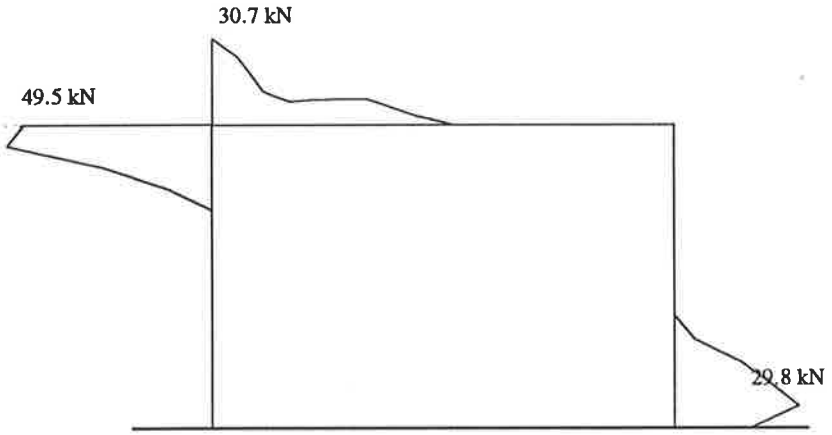

M6

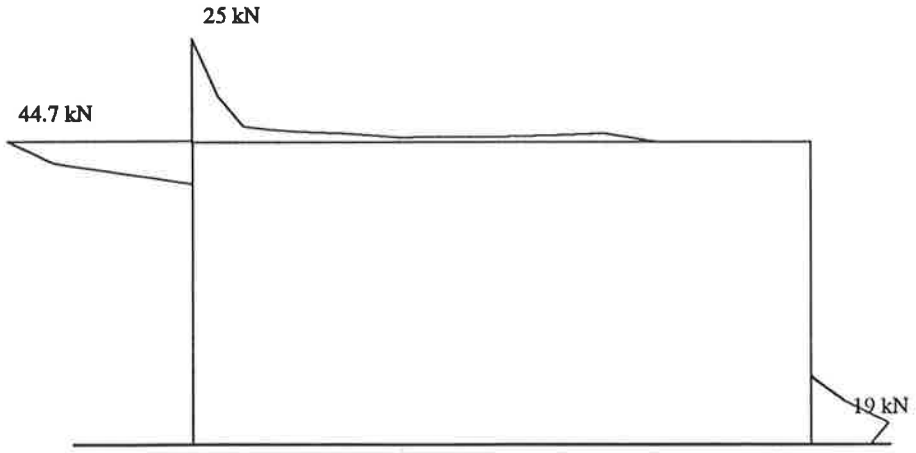

Fig 4.9. Forces in the compression springs - no gap

(continued)

M7

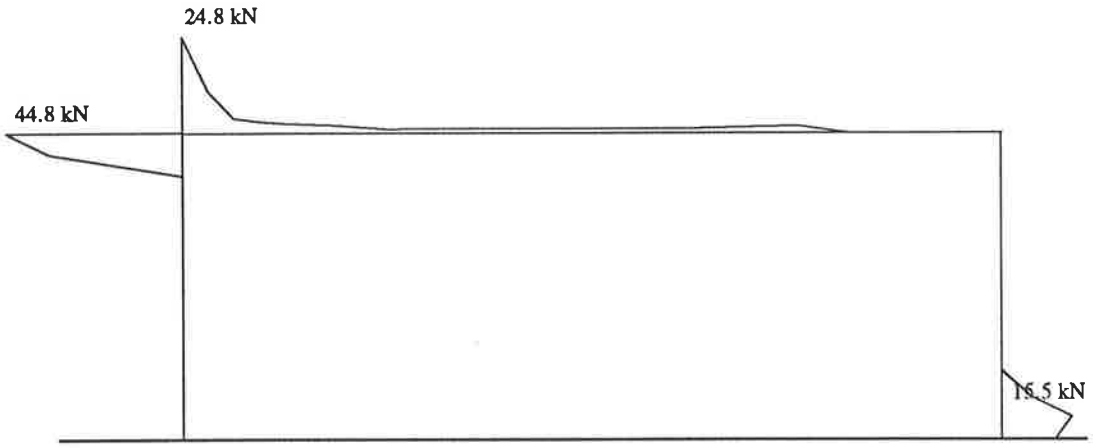

M8

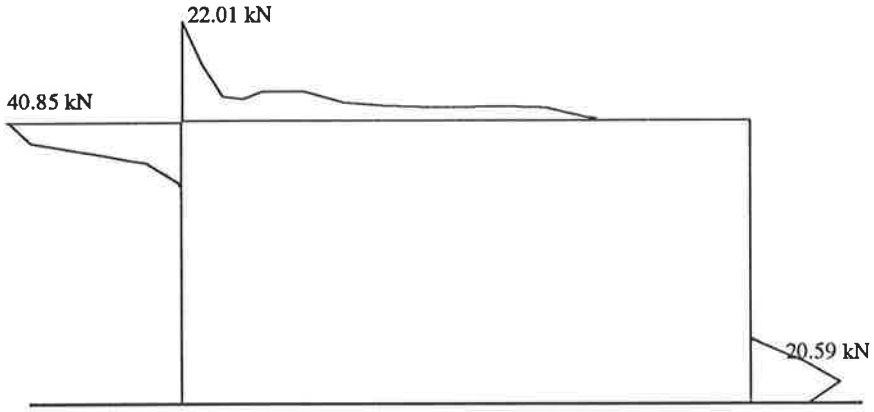

Fig 4.9. Forces in the compression springs - no gap

(continued)

with small compressive force) since their effect in comparison to the large loads transferred by the compressed springs near the corner was negligible.

4.3.3. Effective diagonal area

On the basis of the above results, the column-wall (X) and the beam-wall (Y) contact lengths were calculated. It was found that the contact length along the beam was 1.2 to 2.33 times the column-wall contact length. Table 4.3 gives a summary of the results for the beam-wall and column-wall contact lengths. The effective diagonal cross-sectional area was calculated directly from the contact lengths for all models for the case of no gap

between the frame and the infill wall. As shown on model M3 fig. 4.9, the width of the diagonal was taken to be equal to A=m+n from the right angle triangles.

Table 4.3. Contact length and effective diagonal area for perfect fit between the frame and the wall (see also fig. 4.8 and fig. 4.9)

model	X, mm	Y, mm	Y/X	A=m+n, $x10^3$ mm^2	l_{diag}, m	EA/l_{diag}, $x10^6$ N/m
M1	136	273	2.00	31.79	4.243	43.46
M2	214	500	2.33	103.62	5.000	120.20
M3	429	500	1.17	139.48	5.408	149.59
M4	429	750	1.75	170.06	5.408	182.39
M5	643	750	1.17	209.22	5.408	224.39
M6	429	500	1.17	133.54	6.708	115.46
M7	429	500	1.17	126.94	8.544	86.17
M8	400	600	1.50	137.72	6.261	127.58

It should be noted that the stiffer frames had a larger effective cross-sectional area for the diagonal strut. For example, the model M5 strut was 1.5 times bigger in cross-section than the M3 strut.

The axial diagonal stiffness (Table 4.3) is much smaller than the stiffness calculated for the infill wall in Table 4.4 (page 44) for the case of no gap. This is a result of one or a combination of the following reasons: (1) the effect of springs with small compressive loads along the beam-wall interface was ignored, (2) for the longer models the effective diagonal formed an angle closer to 45 degrees, hence, the length of the diagonal should be smaller and the cross-sectional area bigger and (3) widening of diagonal at the center of the panel which would result in a bigger value of A. The value of the cross sectional area calculated in Table 4.3 is the minimum value.

4.3.4. Moment and shear force distribution in the columns

The presence of the infill wall changes the moment and shear force distribution in the frame. Typical moment diagrams for the columns of the infilled frames are shown on fig. 4.10. The moment diagram for the directly loaded column resembles the moment diagram of a beam on an elastic foundation loaded with a point load, especially in the contact region. This is consistent with the analogy used in previous research [5,6] for calculation of the contact length using beam on an elastic foundation methodology. The maximum and minimum values of the moments in the columns varied from model to model with the variation of column stiffness but the shape of the diagrams was essentially the same for all models.

The shear force distribution in the columns was strongly influenced by the relative stiffness of the frame and the wall. In comparison to the shear force distribution for a frame without infill where the shear forces have the same direction in both columns and do not change over the height of the columns, the shear force in the left hand column below the contact region was in the opposite direction to that in the right hand column for all the infilled frames. Model M5 was the only exception where the shear forces in both columns had one and the same direction over the height of the columns due to the very large stiffness of the frame.

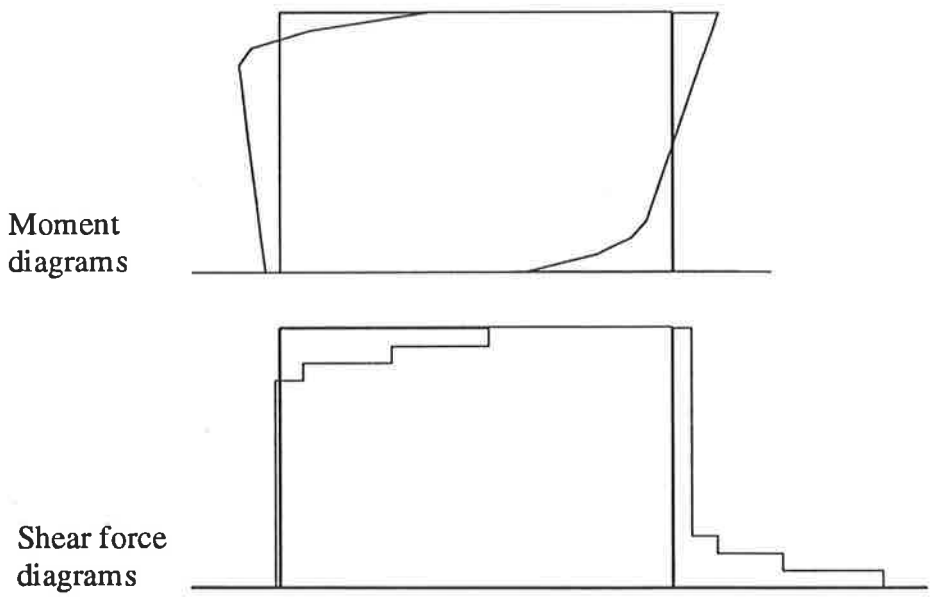

Fig. 4.10. Moment and shear force diagrams for the columns of an infilled frame (no gap between the frame and the wall)

4.4. Behaviour of the infilled frame in the case of an existing construction gap

When a gap was introduced between the frame and the infill wall, the loads in the non-linear springs changed dramatically from those for the case of no gap. Irrespective of the gap size, only one spring was active in transferring force into the wall (the gap was empty - no shear connectors or elastomers in the gap). There were no loaded springs along the beam wall interface and as such there were no normal forces to confine the wall. Therefore, the behaviour of the wall was expected to be similar to that of a free standing wall loaded with a horizontal point load. The failure mechanism for this type of load would follow the mortar joints which are the planes of weakness in the masonry wall and the failure load would be the one which causes shear stress in the panel equal to 0.3 MPa.

The resulting stress contours (fig. 4.11) confirmed the above result. The maximum stresses were mainly concentrated in the loaded corner and the shear stress contours showed initial formation of a diagonal only at the loaded corner. Fig. 4.11 shows the stress contours for model M4 with a 12 mm gap. The difference between the stress contour diagrams in fig. 4.11 and the previous diagrams (fig. 4.6) highlights the benefits of wall confinement.

The moment and shear force distribution along the columns was very similar to the pattern seen for a frame without infill. Since the wall was not significantly confined, it did not greatly influence the frame.

σ1 stress contours
1 - +0.007 MPa
2 - -0.212 MPa
3 - -0.431 MPa
4 - -0.650 MPa
5 - -0.869 MPa
6 - -1.090 MPa
7 - -1.310 MPa
8 - -1.530 MPa
9 - -1.740 MPa
10 - -1.960 MPa

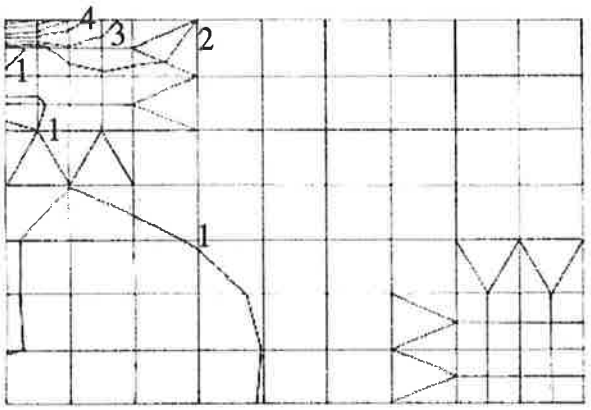

σ2 stress contours
1 - +0.529 MPa
2 - +0.443 MPa
3 - +0.357 MPa
4 - +0.271 MPa
5 - +0.185 MPa
6 - +0.099 MPa
7 - +0.013 MPa
8 - -0.073 MPa
9 - -0.159 MPa
10 - -0.245 MPa

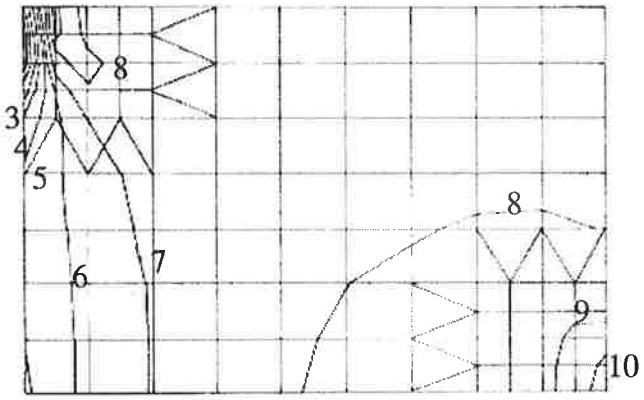

shear stress contours
1 - 0.267 MPa
2 - 0.234 MPa
3 - 0.201 MPa
4 - 0.168 MPa
5 - 0.136 MPa
6 - 0.103 MPa
7 - 0.070 MPa
8 - 0.037 MPa
9 - 0.0045 MPa
10 - -0.028 MPa

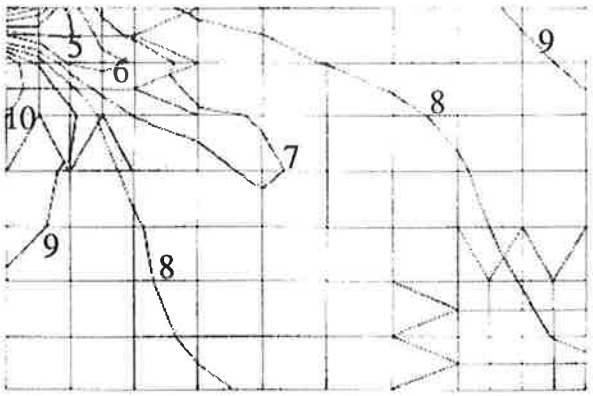

Fig. 4.11. Stress contours for the wall panel for model M4 - 12 mm empty gap

4.5. Stiffness and strength of the masonry infill wall

The main aim of the static analysis was to determine the stiffness and strength of the infill wall in relation to: (1) relative stiffness of the frame and the wall (λh), (2) the length/height ratio of the infill (l/h) and (3) the gap size. The results of these analyses were subsequently used in the development of a non-linear diagonal strut model. Table 4.4 gives a summary of the results for the applied load and how it was resisted by the elements of the infilled wall. It gives: the value of external load, F_{fr} , which caused maximum shear stress in the panel equal to 0.3 MPa; the portion of the load resisted by the wall alone, $F_{wall} = F_{fr}-(F_{left\ col} + F_{right\ col})$, at this level of shear stress; the displacements of the top right hand corner of the wall, Δ_{wall} , and the effective stiffness of the wall, $k_{wall} = F_{wall}/\Delta_{wall}$, for the case of no gap between the frame and the wall and for a non-zero gap. Also in this table $F_{left\ col}$ is the force in the left column below the contact region and $F_{right\ col}$ is the force in the right column above the contact region. The size of the gap (provided it is empty - no elastomers or shear connectors in the gap) was varied through the analyses from 4 mm to 16 mm. From this series of analyses it was observed that the strength and stiffness of the infill wall remained constant for all non-zero gap sizes. The positive directions of the forces are shown in fig. 4.12.

Table 4.4. Stiffness and strength of the infill wall

model	NO GAP						GAP		
	F_{fr} , kN	$F_{left\ col}$, kN	$F_{right\ col}$, kN	F_{wall} , kN	Δ_{wall} , mm	k_{wall} x10^6 , N/m	F_{wall} , kN	Δ_{wall} , mm	k_{wall} x10^6 , N/m
M1	19.00	-0.21	0.12	19.10	0.17	111.5	13.23	0.23	57.70
M2	61.50	-1.31	0.98	61.83	0.17	368.5	40.97	0.21	196.12
M3	77.45	-1.54	1.56	77.43	0.18	432.1	40.83	0.18	231.79
M4	96.00	-1.80	4.36	93.44	0.20	458.9	40.94	0.18	231.82
M5	153.00	3.51	17.33	132.20	0.26	499.3	41.00	0.18	231.75
M6	78.70	-1.72	1.63	78.79	0.14	566.4	41.09	0.12	336.30
M7	79.10	-1.78	1.76	79.12	0.11	725.2	40.93	0.09	471.50
M8	86.70	-3.07	5.11	84.66	0.14	587.5	38.60	0.12	314.40

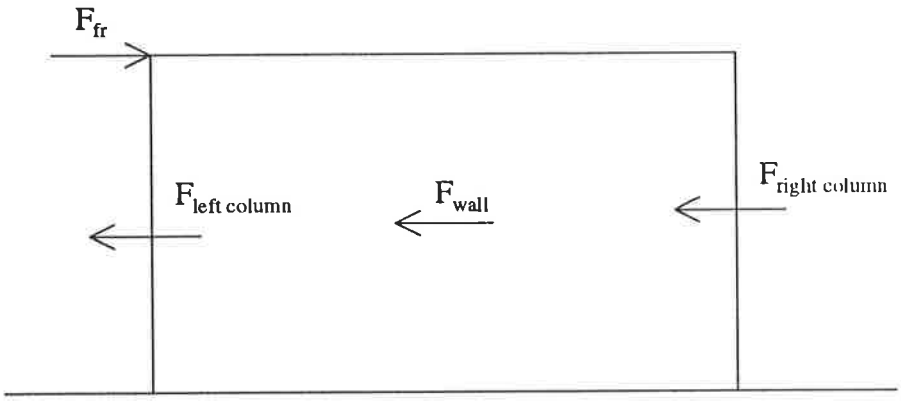

Fig. 4.12. Positive force sign convention in the static model

In some of the models the force in the wall was greater than the applied force which is a result of the very small flexural stiffness of the frame columns compared to the very large stiffness of the infill wall in this statically indeterminate system.

Table 4.5 gives a summary of the results of the percentage of the ratio of the total load to the load resisted by the infill wall. The percentage varied considerably with variations in the stiffness of the frame while changes in the l/h ratio did not affect the load resisted by the wall. Model M5 had the stiffest frame and the frame's contribution to the lateral load resistance was the biggest. For the infilled frames with varying l/h ratio, the lateral load was mainly resisted by the wall which can be explained with the fact that the frame was not stiff enough to resist that load by itself.

With the introduction of a gap between the frame and the wall, the strength and stiffness of the infill dropped considerably. In the static analysis the size of the gap was not of primary importance. It should be noted again that for the infilled frames (models M3, M4 and M5) the stiffness and strength of the infill wall were almost constant. This highlights the fact that the confinement of the wall was inadequate due to the presence of a gap and the wall's strength and stiffness corresponded to that of a free standing wall irrespective of the frame stiffness.

Table 4.5. Strength and stiffness changes depending on h/ℓ, λh and presence of a gap

model	h/ℓ infill	λh	NO GAP	GAP	
			F_{fr}/F_{wall}	decrease of strength of the wall	decrease of stiffness of the wall
M1	3m/3m	6.36	99.48%	30.73%	48.27%
M2	3m/4m	4.63	99.47%	33.74%	46.78%
M3	3m/4.5m	4.20	100.03%	47.27%	46.36%
M4	3m/4.5m	3.34	102.74%	56.18%	49.48%
M5	3m/4.5m	2.52	115.73%	68.99%	53.59%
M6	3m/6m	4.05	99.89%	47.85%	40.63%
M7	3m/8m	3.86	99.97%	48.27%	34.98%
M8	3.15m/5.6	3.36	102.41%	54.41%	46.49%

To clarify the effect of the relative stiffness, λh, and the length to height ratio, ℓ/h, on the load distribution and the wall strength and stiffness the results from the above table were plotted in fig. 4.13. Models M2, M3, M6 and M7 had varying ℓ/h ratios and constant moment of inertia of the frame while models M3, M4 and M5 had constant ℓ/h ratios but changing moments of inertias of the frame.

The results can be summarised as follows:

- for the same geometry, changes in the stiffness of the frame influence considerably the strength and stiffness of the infills;
- changes in the ℓ/h ratio, unless accompanied by changing moment of inertia of the frame, do not influence the strength and stiffness of the infilled wall; and
- the strength and stiffness of the wall panel drops considerably with the introduction of a gap. The relative stiffness parameter then loses its primary importance in determining the behaviour of the wall.

Load resisted by the wall

Models M2, M3, M6 and 7M

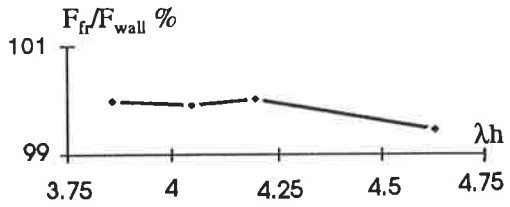

Models M3, M4 and M5

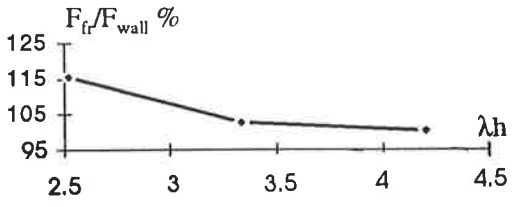

Strength decrease of the wall after introducing the gap

Models M2, M3, M6 and M7

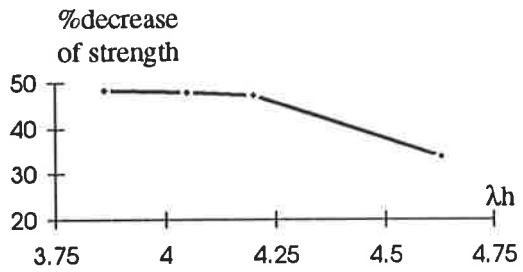

Models M3, M4 and M5

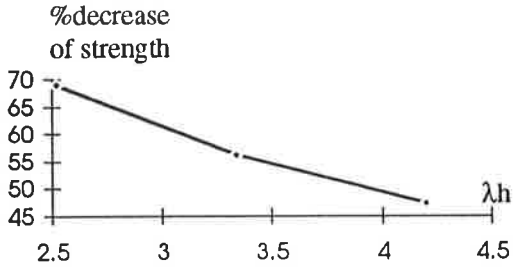

Stiffness decrease of the wall after introducing the gap

Models M2, M3, M6 and M7

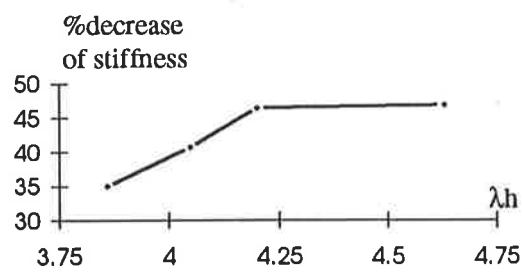

Models M3, M4 and M5

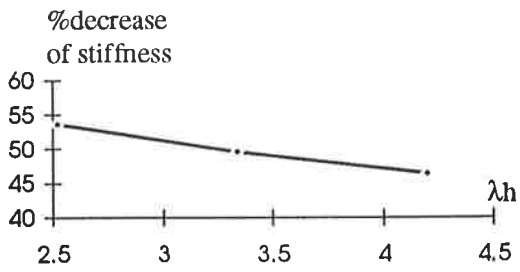

Fig. 4.13. Summary of the static results

4.6. Comparison with results from previous investigations

The results presented in fig. 4.14 were used to compare the results of the strength of the infill. The diagram is based on the theoretical investigation by B.S. Smith [5] on diagonally loaded square infilled frames (steel frame and mortar infill). In his research the contact between the frame and the wall was considered to be analogous to that of a beam on an elastic foundation. A triangularly distributed reaction was assumed to act over the contact length. It was found that for $\lambda h \leq 5$, the frame stiffness contributes to the overall response. The results obtainet by Smith [5] are consistent with the results for model M1, the square infill frame. For the other models the increasing l/h ratio adds more to the wall stiffness and even for values of λh=3.86 (M7) the infill has primary importance in the resisting the lateral load due to the increased length.

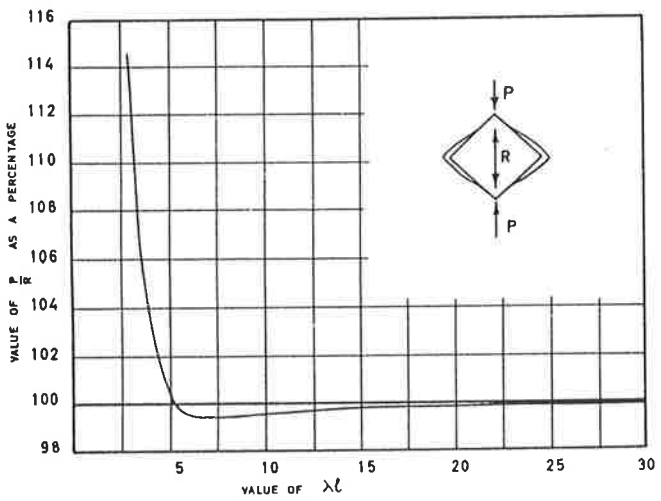

Fig. 4.14. P/R as a function of λh (after B.S. Smith [5])

Test observations by Zarnic [50] showed that nearly all the initial load was carried by the masonry wall in reinforced concrete infilled frames in the elastic range of the response and only about 2% were carried by the frame. This result is consistent with predictions for the high percentage of the load resisted by the wall obtained from the theoretical analysis of the present study.

Absence of transfer of vertical forces from the beam into the wall for the case of a construction gap was confirmed by the theoretical and experimental investigation of Dawson and Ward [31].

4.7. Conclusion

The finite element method was used to develop a model with linear elastic material properties and non-linear spring elements to represent the interaction between the frame and the infill wall. The behaviour of the infilled frames with varying relative stiffness ratio (λh) and length to height ratio (l/h) was investigated. The influence of a construction gap on the lateral response was also evaluated. The results from the static analysis are consistent with results reported by previous researchers. The effective elastic stiffness and strength of the infill walls were obtained from the static analysis for use in the next stage of the research, non-linear modelling of the infilled frames using an equivalent diagonal strut analogy and dynamic loading.

CHAPTER 5 - DYNAMIC ANALYSIS - MODEL

5.1. Introduction

The dynamic analysis reported in this chapter was carried out using the program "Ruaumoko" [69]. This is a non-linear analysis computer program which allows various rules for representation of the non-linearity in the elements of two-dimensional structures. It also allows the following options for elastic or inelastic analysis: static (only elastic), dynamic due to ground acceleration and dynamic due to time varying force excitation.

The model developed for this study in "Ruaumoko" was a single storey single bay diagonally braced frame with two diagonals. The node and element numbering is shown in fig. 5.1. The two diagonals were used to model the infill masonry wall in the reinforced concrete frame. The diagonals were modelled to represent as close as possible: (1) - the stiffening and strengthening effect of the infill on the frame; (2) - the process of cracking of the wall; and (3) - the infill's strength and stiffness reduction. This model was able to evaluate the overall response of infilled frames due to dynamic loading.

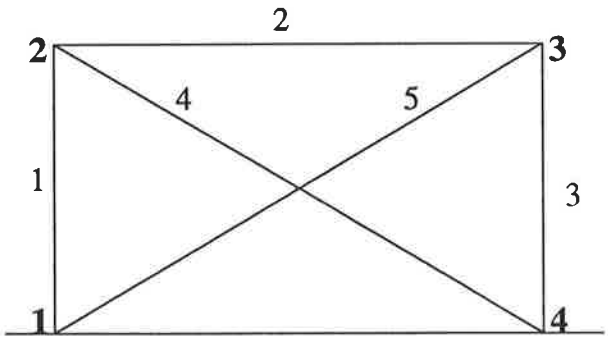

Fig. 5.1. Diagonal model of an infilled frame

5.2. Development of the dynamic model

5.2.1. Parameters governing the solution

The dynamic analysis was an inelastic time-history analysis and used Newmark's beta method of constant average acceleration [70]. The diagonal mass matrix which was used was a result from the consistent masses of the frame and the diagonals (the infill wall mass included as self weight of the diagonals) and the concentrated masses at nodes 2 and 3. These lumped masses represented the approximately evaluated dead load from beams and slabs from an adjacent level and imaginary second storey above the investigated frames. The values of the lumped masses varied from model to model depending on the geometry. Damping was introduced in the structure using linear variation of damping with frequency which was an alternative to Rayleigh damping model [70] that could also be used in the analysis. The percentage of damping for the first and the second mode of vibration was assumed to be 3% and it was the same for all models for the bare frame, for the infilled frame without a gap and for the infilled frame with a gap. This assumption was made for simplicity of the model, however, in reality the percentage of damping would be different for bare frames and infilled frames with varying relative stiffness and length to height ratio. For reinforced concrete with considerable cracking and working stress no more than about 0.5 of the yield point recommended values are in the range from 3% to 5% [71]. For steel infilled frames without shear connectors recommended values ranged from 6% to 8.5% [53]. For numerical stability of the solution the iteration time step should be less than 0.1 of the period of the highest mode of vibration.

5.2.2. Member type

The program allowed different types members for modelling the structure. For the diagonally braced frame, the type of members used were frame members for the reinforced concrete frame and spring type members for the two diagonals. Several options could be considered for the diagonals in the braced frame following models from other researchers as discussed in the literature review (chapter 2), such as one loaded diagonal in each direction or multiple diagonals in each direction for the small deformation range. Another option was to introduce elements which would cause shear

as well as flexural type of failure on the frame for the large deformation range. A model with one diagonal strut in each direction was chosen for this research. This offered a simpler definition of the problem and excluded uncertainties associated with parameters which require experimental evaluation.

5.2.3. The reinforced concrete frame

Concrete beam-column type members were used to model the reinforced concrete frame(members 1, 2 and 3, fig. 5.1). Various hysteresis rules were available in the program to describe the non-linearity and plastic hinge formation in the frame. The program required calculation of the strength interaction diagram for a reinforced concrete section. The values which were needed in the input file were the axial force and bending moment at balanced failure (PB, MB), the yield moments at 2/3 PB and 1/3 PB, the yield moment in pure bending MO and the axial compression and tension yield forces (PYC, PYT) as shown in fig. 5.3. The influence of a slab was not included in the calculations of moment of inertia.

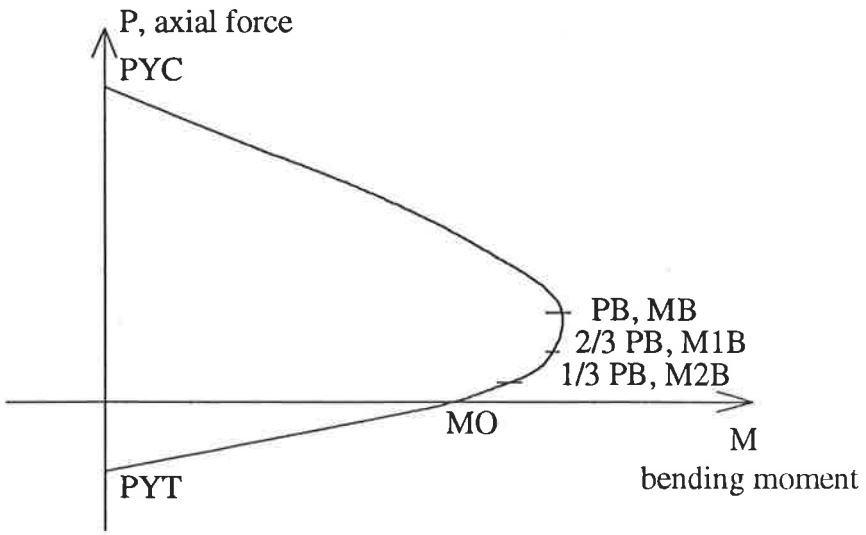

Fig. 5.3. Strength interaction diagram for concrete bean-column member

The moment of inertia for the initial stiffness of the frame members was taken as 25%I_g for a frame without infill and 30%I_g for a frame with infill wall irrespective of the gap presence or its size. The value for the bare frame members was assumed on the basis of

comparison with the modelling of a reinforced concrete joint and frame by other researchers [64]. The increase of the moment of inertia for the infilled frame was made assuming that the infill's stiffening effect on the frame would cause less cracking in the frame members. The experimental hysteresis rules of tested infilled frames [72] are consistent with this assumption. Although the stiffness in the hysteresis rule used for the frame elements was degrading, this rule was a relatively simple representation of the complex behaviour of the reinforced concrete members.

5.2.4. The diagonals

As discussed previously, the diagonal strut action of the brick infill was modelled using spring type members. The properties of the spring elements were chosen to represent the behaviour of the masonry infill with reasonable simplicity and accuracy. Generally, a spring type element in "Ruaumoko" can have stiffness in the longitudinal and transverse directions and rotational stiffness as shown in fig. 5.4. The model with the spring elements would probably perfectly match the brick infill action if these three stiffnesses were used.

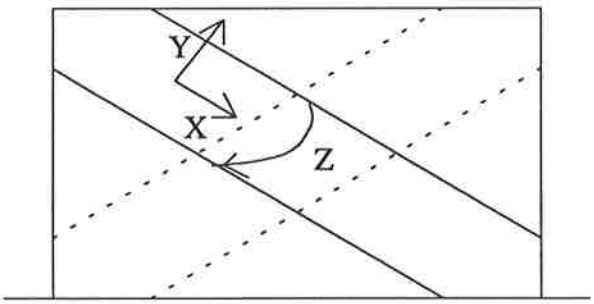

Fig. 5.4. Spring member stiffness

In this research, only the axial effect of the spring members was used. The stiffness in rotation could be used to develop a more precise model, which would represent the rocking of the infill wall within the frame. However, this idea was abandoned due to insufficient data to define the parameters for rotational stiffness and rotational yield moment. Similar difficulties existed with the yield and ultimate force values for the transverse direction. Thus the simplified action of the diagonals was axial tension and axial compression or only compression. It should be noted that the diagonals work only

in compression for the case of no gap between the frame and the wall and in compression and tension for the cases of existing gap as it is explained in detail later in section 5.2.10. The failure surface for the spring elements ignored interaction of the X, Y or Z components (fig. 5.5). The notation for the spring member interaction surface (fig. 5.5) follows the notation from "Ruaumoko"'s manual. The values of interest from this failure surface were the yield forces in axial tension and compression. The cracking force in compression (PX^-) was calculated (as shown in the following section 5.2.5) from the results of the finite element analysis with elastic material properties (chapter 4) for the force which caused shear stresses in the panel equal to assumed mean shear bond strength of masonry of 0.3 MPa (chapter 4).

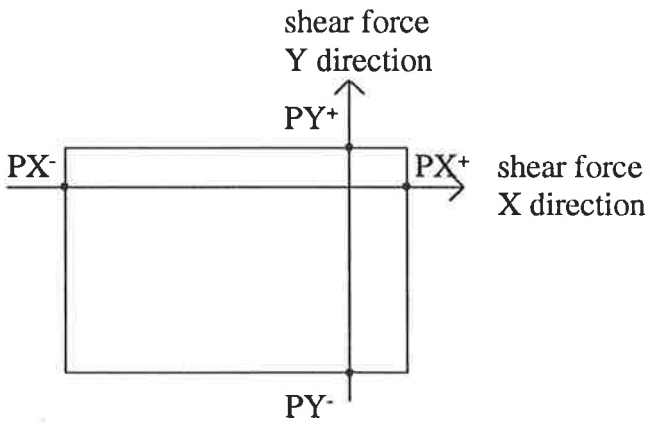

Fig. 5.5. Failure surface of a spring type element without interaction of X and Y components (notation follows manual [69])

5.2.5. Relation between the static finite element model and the dynamic diagonal strut model

Considering only the strut action of the wall panel, the forces transferred into the wall at the loaded corner can be represented as shown in fig. 5.6. The horizontal force F^h_{wall} was taken to be equal to the sum of the forces in the loaded springs along the column and the vertical force F^v_{wall} was set equal to the sum of the forces in the loaded springs along the beam. The resultant of these two forces is F^d_{wall} which forms angle θ with the horizontal as shown in fig. 5.6. The angle θ is usually different from the angle α which the diagonal forms with the base of the wall (fig. 5.7). All the calculations from "Images - 3D"

(chapter 4) showed that with a gap between the frame and the wall there was no vertical force transfer in the springs connecting the beam and the frame. This result from the static analysis required two cases to be considered separately: case 1 - presence of a gap and case 2 - no gap between the frame and the wall.

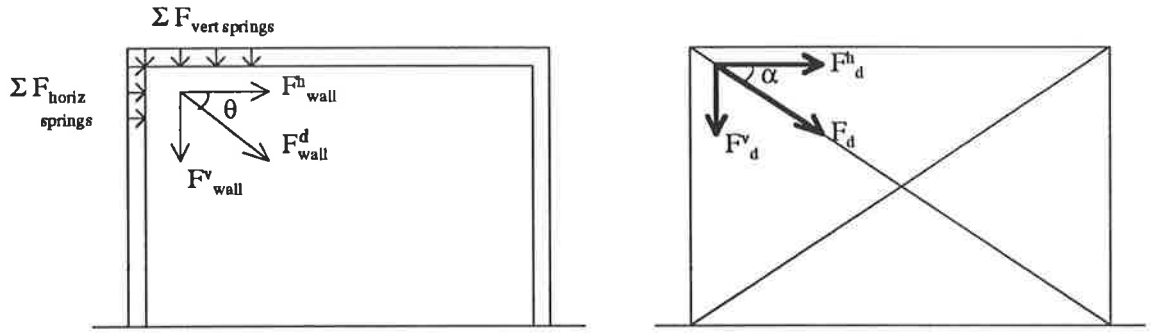

Fig. 5.6. Relation between the forces in the wall for the static and dynamic models

Results from the calculations for no gap between the frame and the are summarised in Table 5.1. For models M1 to M3, θ approaches α with increasing frame stiffness and θ=α for model M3. After λh=4.2 (M3) θ becomes larger than α and approaches a 45 degree angle. With increasing *l*/h ratio (models M3, M6, M7, M8) θ approaches a 45 degree angle and is much bigger than the angle of the diagonal with the base of the wall. In summary: the angle of the maximum force transferred by the wall approaches a 45 degree angle with increasing frame stiffness and *l*/h ratio.

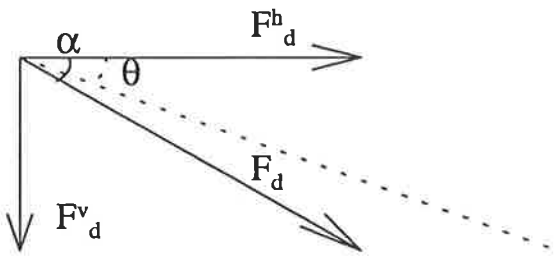

Fig. 5.7. Relationship between the angle of the diagonal and the angle of the maximum force in the wall

Table 5.1. Forces in the wall panel from the finite element analysis

model	F^h_{wall}, kN	F^v_{wall}, kN	F^d_{wall},kN	cos θ	θ	α	λh
M1	19.098	13.614	23.454	0.814	35.48	45.00	6.36
M2	61.831	42.150	74.831	0.826	34.28	36.87	4.63
M3	77.431	51.600	93.049	0.832	33.68	33.69	4.20
M4	93.435	63.784	113.130	0.826	34.32	33.69	3.34
M5	123.200	94.836	155.474	0.792	37.59	33.69	2.52
M6	78.792	54.572	95.845	0.822	34.71	26.57	4.05
M7	79.121	59.505	98.999	0.799	36.95	20.52	3.86
M8	84.660	77.849	115.012	0.736	42.60	26.57	3.36

For the case of no gap, it was assumed that the horizontal component of the force in the diagonal from the dynamic model, F^h_d , is equal to the horizontal force in the wall from the static analysis, F^h_{wall} , (fig. 5.6). Obviously this assumption affects the calculated values of the vertical forces in the wall and the normal forces in the columns of the frame. For a single storey frame these changes in the magnitude of the normal forces were not of primary importance to the lateral response of the infilled frame. This assumption allowed a simple and adequate representation of the horizontal forces in the system due to lateral loading. Table 5.2 shows the comparison between the forces in the wall and in the diagonal at yield for the case without a construction gap.

Based on the results from chapter 4 there was no vertical force transfer into the wall from the beam for the case of an existing construction gap. For this case it was assumed that the horizontal component of the force in the diagonals was equal to half of the horizontal component of the force in the wall from the finite element analysis (the total horizontal component of the forces in the two diagonals was equal to the total force in the wall). As described later in section 5.2.10 each diagonal carried half of the horizontal force - one in tension and one in compression. As a result the axial forces in the columns of the diagonal model for a construction gap did not correspond exactly to the realistic situation. Since only the horizontal component of the wall force from the static analysis was used in the dynamic analysis it is subsequently referred to as F_{wall} everywhere in the text and is the same as F_{wall} in chapter 4).

Table 5.2. Comparison between the forces in the wall and in the diagonal

model	F^h_{wall} , kN	F_{wall} , kN	F_d , kN	F^v_{wall} , kN	F^v_d , kN	λh
M1	19.098	23.454	27.009	13.614	19.098	6.36
M2	61.831	74.831	77.288	42.150	46.372	4.63
M3	77.431	93.049	93.061	51.600	51.620	4.20
M4	93.435	113.130	112.295	63.784	62.290	3.34
M5	123.200	155.474	148.068	94.836	82.133	2.52
M6	78.792	95.845	88.096	54.572	39.405	4.05
M7	79.121	98.999	84.504	59.505	29.678	3.86
M8	84.660	115.012	94.657	77.849	43.339	3.36

Note: $F^h_{wall} = F^h_d = F_{wall}$

On the basis of the above assumptions and fig. 5.8 the stiffness of the diagonals was calculated as follows:

$$\Delta_d = \Delta_{wall} \cos\alpha \tag{5.1}$$

$$F_d = \frac{F_{wall}}{\cos\alpha} \tag{5.2}$$

$$k_d = \frac{F_d}{\Delta_d} = \frac{k_{wall}}{\cos^2\alpha} \tag{5.3}$$

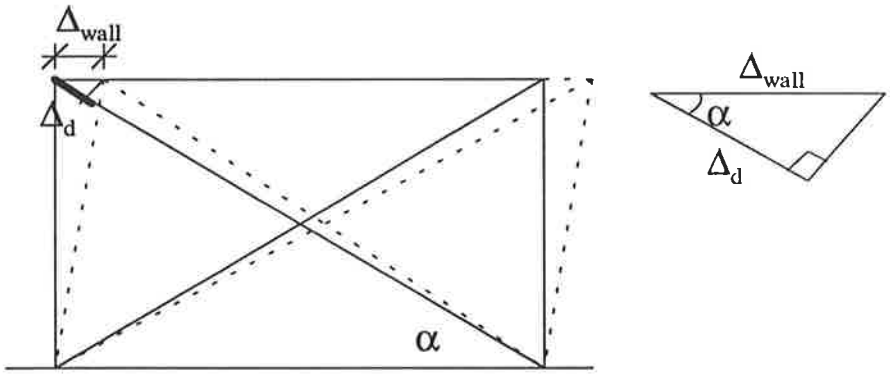

Fig. 5.8. Relation between the displacements of the wall and shortening of the diagonal

In the above equations α was the angle between the diagonal and the horizontal in the dynamic model. Frame center line distances were used in the dynamic model. This value was slightly different from α in the static model because the nodes from the edge of the wall did not coincide with the nodes from the centre line of the frame in the finite element model.

5.2.6. Hysteresis rules

There are thirty hysteresis rule available in the "Ruaumoko" program. Two of the hysteresis rules were considered for the frame members. The selection of the best hysteresis rule for the spring members was of main importance in this analysis. All the options were investigated to establish which rule best represented the infill wall behaviour. Two main cases were considered: overall behaviour for the case of no gap and for the case of gap between the frame and the wall. The behaviour for the case of no gap was represented by appropriate hysteresis rules for the frame members and hysteresis rule for the diagonals which allowed diagonal action only in compression. For the case of construction gap between the frame and the wall both diagonals were working - one in tension and one in compression each loaded with half of the total lateral force expected in the infill wall panel. The theoretical model in this case was trying to simulate the overall response hysteresis behaviour of the frame-wall system rather than the behaviour of its individual components.

5.2.7. Hysteresis rules used for the frame members

A bi-linear inelastic hysteresis rule (like the hysteresis rule in fig. 5.9 but $k_u=k_0$) was used for the reinforced concrete members in the preliminary analyses for evaluation of the response of the system while developing the model and defining values for different parameters. A degrading bi-linear hysteresis rule (fig. 5.9) was used in the final analyses. It modelled the degradation of the stiffness of the frame elements. The Mehran Keshavarzian hysteresis rule (fig. 5.10) was used by Wong [64] in a detailed model for a reinforced concrete joint and a frame. It has degrading stiffness at unloading and reloading. In this analysis it was used only in model M8 to evaluate the sensitivity of the results to the type of hysteresis rule for the frame members. The three hysteresis rules also allowed for strength degradation.

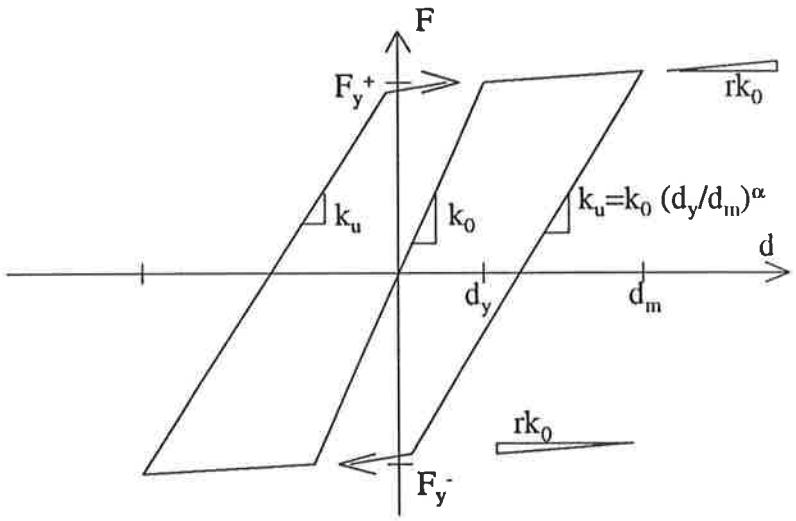

Fig. 5.9. Degrading bi-linear hysteresis

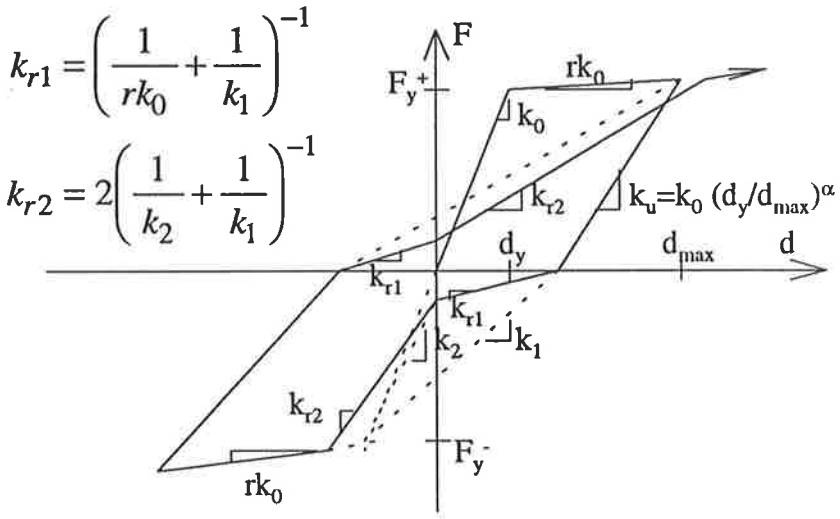

Fig. 5.10. Mehran Keshavarzian hysteresis

5.2.8. Hysteresis rules used for the spring members

As was found by other researchers, the hysteresis rule of an infilled frame can be defined by a three-linear envelope and it also has a pinched region (fig. 2.8 and fig. 2.9, chapter 2). The presence of a construction gap should also be accounted for when specifying the input parameters for the hysteresis rule. Two hysteretic models were considered for the spring members which allowed with different degree of accuracy representation of the infill wall behaviour.

Bi-linear with slackness hysteresis (fig. 5.11) - This rule was used in the preliminary investigation of the problem. The unwanted action of the diagonals in tension with this hysteresis rule was avoided by introducing a very large gap in tension which would not close at any stage of the analysis (fig. 5.12). Thus, the diagonals were loaded only in compression. The value of the yield force in tension was not important in this case and the stiffness did not degrade with increase of the load. This hysteresis rule worked well for loads which caused forces in the diagonal in the vicinity of the compression yield force. When forces in the diagonal were much bigger than the compression yield force, the model was inaccurate because as shown in fig. 5.12 the accumulated inelastic deformation caused the effective gap to become very large.

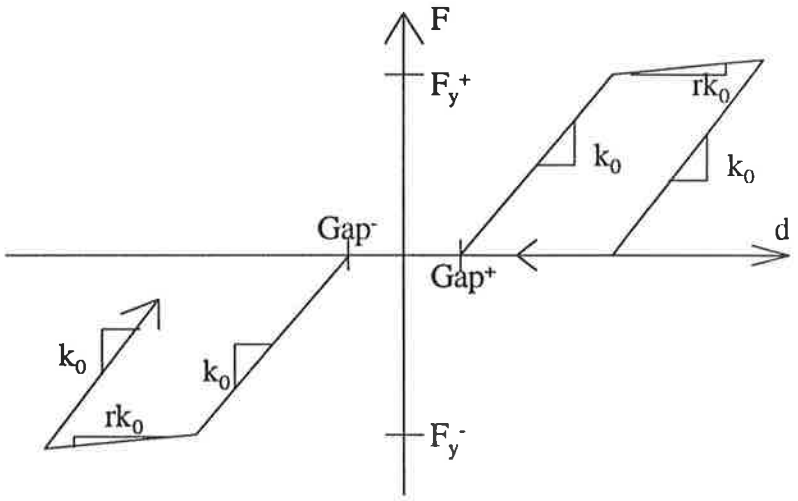

Fig. 5.11. Bi-linear with slackness hysteresis

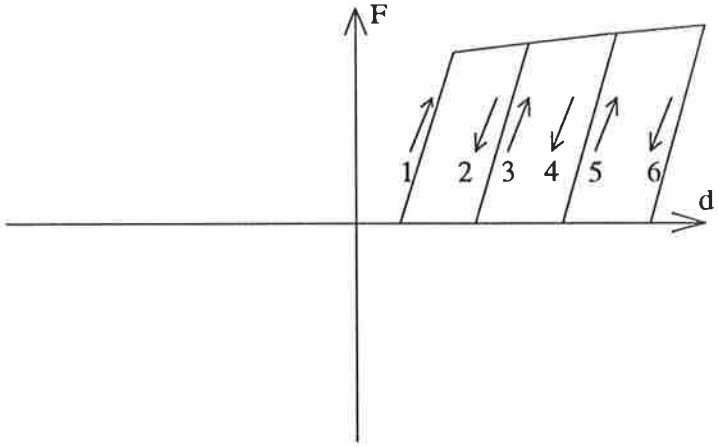

Fig. 5.12. Force/displacement diagram for a diagonal element

Wayne Stewart Degrading Stiffness hysteresis (fig. 5.13) - This model was developed by previous researchers [73] to represent the behaviour of timber framed structural walls sheathed in plywood nailed to the framework. This hysteresis rule was used in this study for evaluating the response of the infilled frames because of the similarity of the mechanism which develops under lateral loading. It has been observed from many experimental results that the strength and stiffness of masonry degrades after cracking. The rate of degradation depends on the stressed condition - the normal stresses as well as the shear stresses. The different confinement of the wall defines the parameters for degrading strength and stiffness.

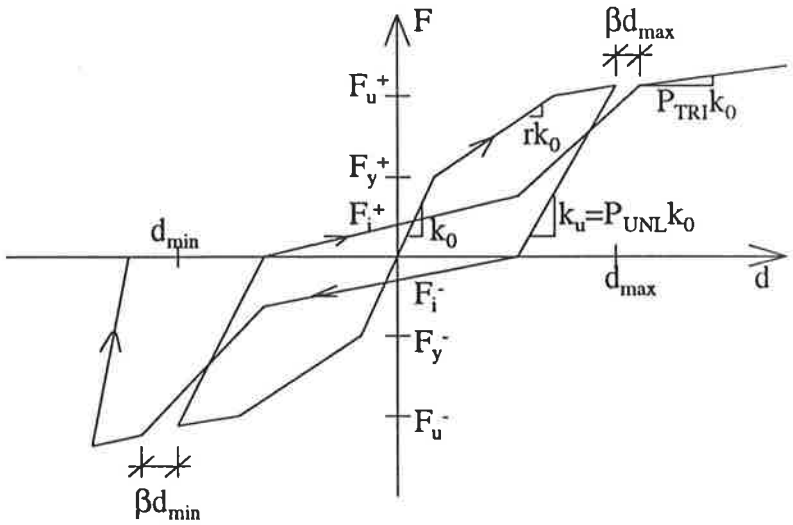

Fig. 5.13. Wayne Stewart Degrading Stiffness Hysteresis

In order to define this hysteresis model the following parameters are used:

k_0 - initial stiffness

r - bi-linear factor

F_u - ultimate force or moment

F_i - intercept force or moment

P_{tri} - tri-linear factor beyond ultimate force or moment

P_{unl} - unloading stiffness factor

Gap^+ - initial slackness along positive axis

Gap^- - initial slackness along negative axis

β - beta or softening factor

α - reloading or pinch power factor

This hysteresis model appeared in two versions throughout the analysis - one for the case of no gap and one for the case of a gap between the frame and the wall. It should be emphasised that the case of no gap in reality corresponds to a very small gap between the frame and the wall which is closed by the thickness of shear connectors and mortar particles trapped in the process of construction. Theoretically the limit value of this "small" gap was assumed to be 5 mm. This case corresponded to contact between the frame and the wall from the very first stages of loading. The case of a construction gap (assumed gap bigger than 5 mm) between the frame and the wall was investigated using a generalised model. This allowed development of a region with lower contact rate in the hysteresis which, in practice, is due to the transfer of forces through the shear connectors between the frame and the wall. Table 5.3 gives the values of the parameters used to define the hysteresis model for the case of no gap and for the case of a construction gap. The next two sections of this thesis explain how the values of the parameters were obtained for these two cases.

Table 5.3. Values of the parameters for Wayne Stewart degrading hysteresis rule

Parameter	Requirement of the program	Value used by Wayne Stewart	Value in the case of no gap	Value in the case of a gap
r	--	--	equation (5.7)	equation (5.7)
F_u	>0.0	1.5 F_y	equation (5.4)	equation (5.4)
F_i	>0.0	0.25 F_y	10N<<F_y	0.5 F_y
P_{tri}	--	0.0	0.0	0.0
P_{unl}	>1.0	1.45	1.001	1.001
Gap^+	>0.0	--	0.2 (0.3) m	0.0001 m
Gap^-	<0.0	--	- 0.0001 m	-0.0001 m
β	$\geq$1.0	1.09	1.02	1.02
α	$\leq$1.0	0.38	0.6	0.4

5.2.9. Values of the parameters for Wayne Stewart degrading hysteresis for the case of no gap

Some of the parameters used to define the hysteresis rule were calculated using equations defined later in the text and some were found using a trial and error approach. The hysteresis response of the masonry wall in this case was based on compression only diagonal action. The aim was to produce theoretical hysteresis loops of a similar shape to the experimental loops reported by other researchers. The hysteresis loop in fig. 5.14 is a typical result for a vertically confined masonry wall under quasistatic cyclic loading [74] when confinement of the wall with a vertical load was equal to 16.6% of the ultimate compressive load on the wall. These experiments were carried out on masonry wall specimens (950x970x110) from cored extruded clay bricks. The shape of the hysteresis rule for the wall for the case of no gap was developed similar to the loop from this experimental result because of the strong confinement from the frame. In the first cycles of this test (fig 5.14) before yield the wall was very stiff and produced very narrow loops. As the load increased and pushed the wall into the inelastic region the stiffness dropped slowly and the loops gradually opened but the overall hysteresis showed very stiff response of the brick wall.

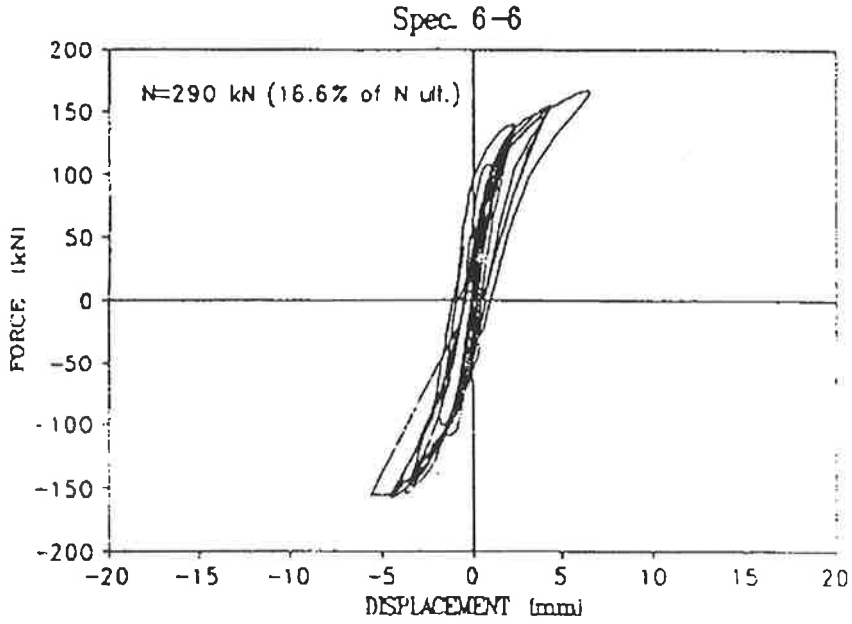

Fig. 5.14. Experimental hysteresis for a masonry wall
(after E. Jankulovski et al. [74])

The ultimate strength of the wall panel F_u could be roughly calculated as a shear failure force

$$F_u = tl\tau \tag{5.4},$$

where t and l are the thickness and length of the wall and τ is the maximum shear stress. On the other hand, the value of the ultimate force is dependant on the confinement of the panel from vertical forces coming from the vertical springs. The failure mechanism develops along the main diagonal with a length l_{dw1} confined by normal stresses developed by the composite action of the frame and the wall (fig. 5.15). This length is equal to the contact length along the beam in the calculations from the static analysis. Knowing the vertical forces from the same analyses, the compressive stresses along the diagonal can be calculated:

$$f_d = \frac{\Sigma F_{vertsprings}}{A_{dw1}} \tag{5.5}.$$

where $A_{dw1} = tl_{dw1}$

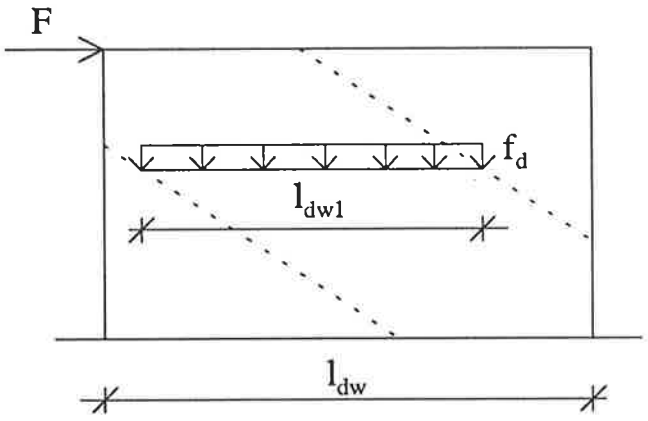

Fig. 5.15. Ultimate strength of the diagonal

The formula for the calculation of the ultimate strength of the wall in shear (SAA Masonry code [75]) is:

$$V_d \leq C_m f_{ms}' A_{dw} + k_v f_d A_{dw} \qquad (5.6),$$

$$\text{where } A_{dw} = t l_{dw}$$

and the characteristic shear strength of masonry is f_{ms}'=0.25 MPa. The following Table 5.4 gives the results from the calculations for the ultimate strength of the masonry walls for each of the eight models considered in this study.

Table 5.4. Calculations for the ultimate strength of the masonry wall

model	$\Sigma F_{vertspring}$ kN	l_{dw1} , mm	A_{dw1} , mm^2	f_d , MPa	V_1 , kN	V_2 , kN	φ
M1	13.614	273	30030	0.4533	94.377	99.000	0.9533
M2	42.150	500	110000	0.3832	233.165	264.000	0.8832
M3	51.600	500	110000	0.4691	287.823	297.000	0.9691
M4	63.784	750	165000	0.3866	263.320	297.000	0.8866
M5	94.836	750	165000	0.5748	319.216	297.000	1.0748
M6	54.572	500	110000	0.4961	394.456	396.000	0.9961
M7	59.505	500	110000	0.5410	549.648	528.000	1.0410
M8	77.849	600	132000	0.5898	402.790	369.600	1.0898

The value of the ultimate shear force $V_1=V_d$ was calculated using the formula from AS 3700 (equation (5.6)) while V_2 was calculated using the approximate equation (5.4) $V_2=tl\tau$. The value of the shear stress τ was assumed to be 0.3 MPa. The calculation of V_1 was a little conservative because the self weight of the panel and the normal forces from dead load and live load of the slab were not included in f_d. The two values of the ultimate shear force in the table were related with a coefficient $\varphi = \frac{V_1}{V_2}$. For the calculations of the ultimate strength of the wall F_u in the dynamic analysis for infilled frames without a gap the approximate equation and the values of V_2 were used and these were multiplied by an approximate value of the factor φ. The value used for models M1 to M4 was 1.0 and 1.1 for models M5 to M8. For the longer frames the limiting value after which the ultimate shear force should be multiplied by a factor of 1.1 was considered to be l/h=2.

The bi-linear factor r was calculated from the equation:

$$r = \frac{\frac{F_{ult} - F_y}{\Delta_{ult} - \Delta_y}}{k_0} \qquad (5.7),$$

where the value of the maximum elastic displacement was obtained from the results from the static analysis and the displacement at ultimate load Δ_{ult} was 0.5% of the height of the wall - an experimental result obtained by other researchers [74]. This was an approximate value for compressive load on the wall larger than 10% of the ultimate compressive strength.

The intercept force F_i was assumed to be a very small number due to requirements of the hysteresis rule when the action in tension of the diagonals is excluded through the introduction of a very large gap. The tri-linear factor P_{tri}, the unloading stiffness factor P_{unl}, β and α were selected to achieve similarity with experimental results within the restrictions of the hysteretic model. The gap size in the tensile direction was set to a relatively big value (300 mm) to ensure that the diagonals were never loaded in tension and the gap size along the negative axis was set to a very small number (0.1 mm) to ensure immediate contact with the diagonals in compression.

As a result of the above settings for the parameters, each diagonal had a hysteresis rule similar to the one shown in fig. 5.16. Note that each diagonal works only in compression in each direction. Thus, the cross-braced system was able to represent the overall hysteretic response of an infilled frame under lateral loading.

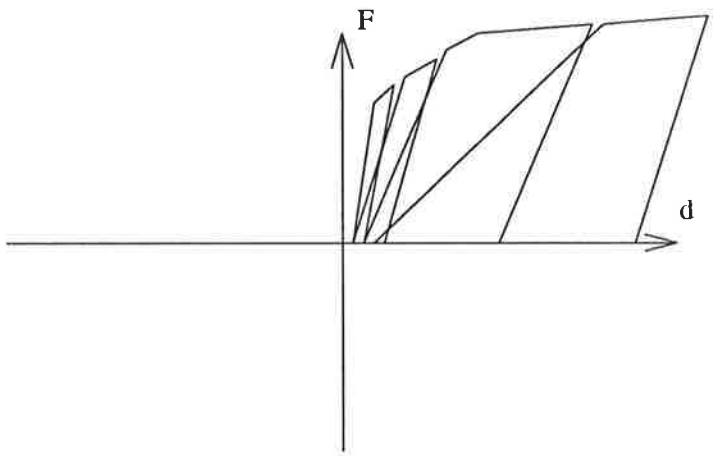

Fig. 5.16. Force/displacement diagram for a diagonal member
for no gap between the frame and the wall

5.2.10. Values of the parameters for Wayne Stewart Degrading hysteresis for the case of a gap between the frame and the wall

For the case of an existing gap the same hysteresis rule was used for the diagonals and represented behaviour of tension and compression since both diagonals were simultaneously carrying the lateral load in the infill wall. The aim was to choose the parameters for this hysteresis so that the overall frame-wall response was represented adequately. A second experimental hysteresis model (fig. 5.17) from the same series of tests performed by Jankulovski et al. [74] was used as a guide for the case of an infill frame with a gap. The vertical load of the wall specimen was 5.5% of the ultimate load. The stiffness of the wall was large in the very initial cycles but the wall was not very strong due to the low compressive load. Hence, the wall response quickly went into the inelastic region where the stiffness degraded quickly and the force/displacement loops opened considerably in comparison to those for the first cycles. In the infilled frame model, the normal forces coming from shear connectors and self weight provided

insufficient confinement of the wall so the theoretical hysteresis was similar to the one in fig. 5.17.

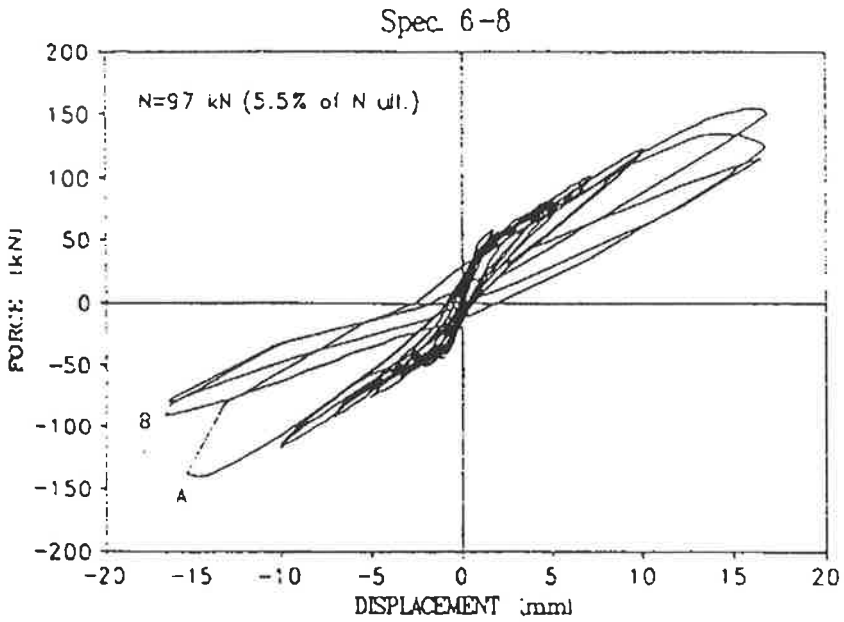

Fig. 5.17. Experimental hysteresis for a masonry wall
(after E. Jankulovski et al. [74])

For the case of a construction gap between the frame and wall the ultimate shear strength of the masonry wall F_u was calculated with equation (5.4). The shear strength was assumed to be 0.3 MPa. This value of F_u was multiplied by a factor of 0.6 (SAA Masonry code [75]) to account for variability of conditions, workmanship and poor confinement of the wall panel. The influence of the self weight on the shear strength was ignored here as well.

The value of the intercept force F_i was assumed to be 50% of the value of the yield force F_y for each diagonal. This assumption was not based on any experimental or theoretical findings because of the uncertainty of the conditions. It was simply a parameter which was used to adjust the hysteresis loop to take account of the forces transferred through the shear connectors between the frame and the wall before the gap completely closed. The gap size along the positive and the negative axis was a very small number. As a result, both diagonals came in contact and resisted forces immediately after loading.

The bi-linear factor "r" was calculated from the same equation (5.7) as in the model without a gap. As before, the maximum elastic displacement was obtained from the results of the static analysis (chapter 4) but the displacement at ultimate load Δ_{ult} was 1.0% of the height of the wall. This was an approximate value based on the results from tests by Jankulovski et al. [74] where the compressive load on the wall was smaller than 10% of the ultimate compressive strength.

The theoretical hysteresis loop for the case of a gap between the frame and the wall was similar to the one shown in fig. 5.18. Each of the diagonals was working in both directions - one in tension and one in compression. The diagonally braced system was symmetric and the vertical components of the diagonal forces were in equilibrium with each other. Hence, the normal forces in both columns were equal in magnitude in the diagonally braced model.

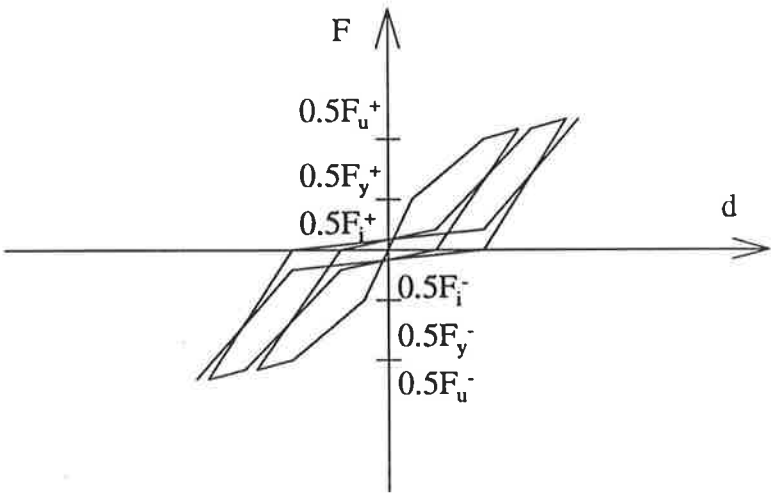

Fig. 5.18. Hysteresis for each diagonal of the braced frame
for a gap between the frame and the wall

5.2.11. Overall hysteresis rule for an infilled frame

The system hysteretic behaviour was a superposition of two hysteresis rules - that of the frame and that of the diagonal. The shape of the idealised hysteresis loop is shown in fig. 5.19.

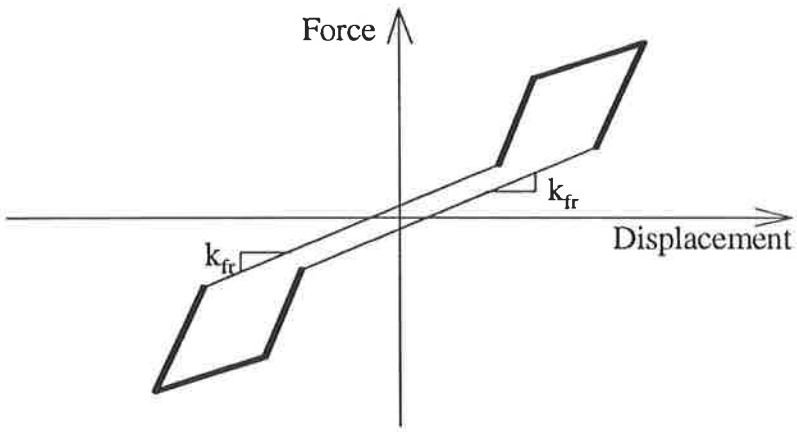

Fig. 5.19. Idealised hysteresis rule for infilled frames

The initial pinched region was the response of the frame before it contacted the wall. Due to the presence of the shear connectors and particles trapped in the gap, the wall would actually be expected to resist some part of the horizontal load from the very start. For the case of perfect fit between the frame and the wall, the pinched region would not be present. However, the main role of the wall came when there was transfer of forces along a contact length between the frame and the wall. The stiffness and strength of the combined system was increased considerably over that of the individual components. The response of the frame and the wall acting together corresponded to the region with the thicker line in fig. 5.19. The stiffening effect of the infill wall consisted of increasing the stiffness of the frame itself k_{fr} and increasing the stiffness of the whole system. The wall also increased the strength and improved the energy dissipating capacity of the whole system.

5.2.12. Applied loads and lumped weights

The theoretical loading history applied to the frame was a sine wave with increasing amplitude which started with a 40 kN amplitude and increased by 40 kN every cycle. For model M5, the amplitude started and increased with 50 kN (60 kN for the model without a gap). The horizontal displacement of node 3 was coupled to that of node 2 to exclude the effect of axial deformations in the beam. Lumped weights were applied at nodes 2 and 3 to account for dead load coming from upper storeys. The plot of loading/time history applied to the models is shown in fig. 5.20.

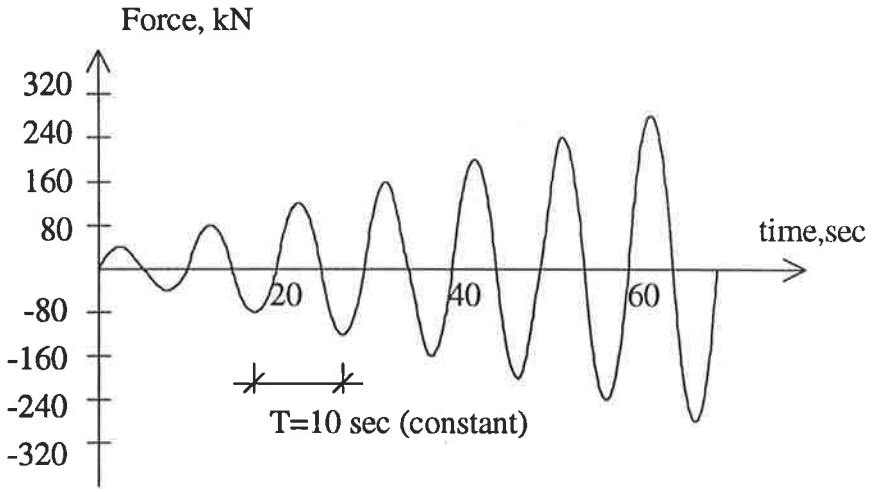

Fig. 5.20 Dynamic loading

5.3. Improvement of the model and comparison with experimental results of infilled frames tests

Experimental tests were carried out by R. Alaia [72] at the University of Adelaide to evaluate the lateral load resistance of infilled frames in respect to the gap size between the frame and the wall. In this section comparisons are made between some of the results from these experimental tests and the final hysteresis loops for the theoretical models. Disadvantages of the theoretical model are discussed as well as its adequacy to represent the behaviour of infilled frames under lateral loading with the presence of construction gaps.

Alaia [72] tested four 1/2-scale frames. One of the frames was without infill and the other three had infill panels with construction gaps between the frame and the wall of 5, 10 and 15 mm respectively. The frame dimensions were 5000 mm - length and 1800 mm - height. The infill thickness was 50 mm. These frames were first investigated using the finite element method. The results from the static analysis were then processed to be used in a dynamic model developed using the Wayne Stewart degrading stiffness hysteresis rule for the diagonals. The parameters describing this hysteresis rule were chosen as described in section 5.2 for the two cases - an infilled frame with a gap and an infilled frame without a gap. Minor adjustments were made to some of the values to improve the correlation with the shape of the hysteresis from the experiment. Comparisons were also made between the results of the frame hysteresis from the theoretical model and the experimental test.

5.3.1. Lateral resistance of a single storey single bay frame

A single storey single bay reinforced concrete frame without masonry infill wall was tested under cyclic loading. Figure 5.21. gives a comparison between the hysteretic behaviour from the experimental results and the theoretical results. The moment of inertia was chosen to be equal to $25\%I_g$. This value was used to calculate the initial stiffness of the frame and the hysteresis rule taking into account the stiffness degradation due to cracking.

The load applied at the frame in the theoretical model was a sine wave with 20 kN amplitude and increasing by 20 kN at each subsequent cycle. The maximum number of cycles was 5 where four hinges were formed in the frame. The loading history of the experimental model was a monotonously increasing cyclic loading by 10 kN at each cycle.

Comparison of the two hysteresis loops indicated a modest correlation between the results from the test and the theoretical model (fig. 5.21). The load at which complete failure of the frame occurred was approximately 83 kN from the analysis and the maximum load of the last cycle of the test was about 82 kN. The stiffness of the frame from the analysis was 5.19×10^6 N/m while the test hysteresis had stiffness approximately equal to 8×10^6 N/m in the positive direction and 5×10^6 N/m in the other direction.

It should be noted that the analytical hysteresis rule used for the frame was very simple and did not produce loops to account for the energy dissipation by the frame. That is why the theoretical hysteresis loops were very tight. However, the stiffness and strength were reasonably consistent with the test results using even this simple rule.

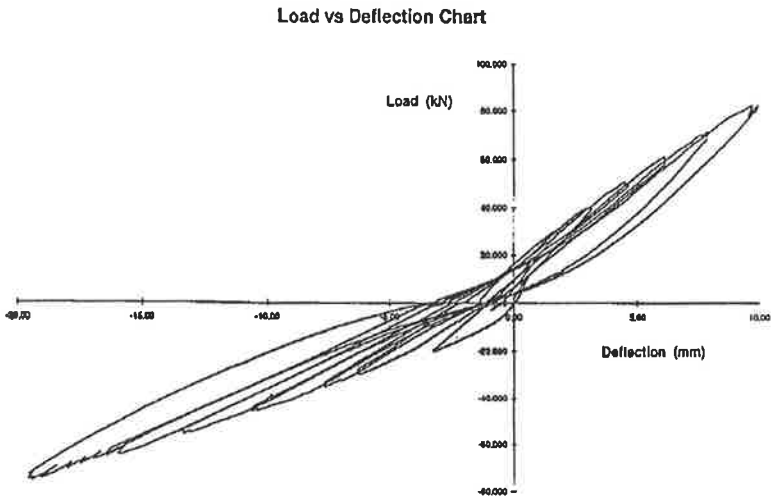

EXPERIMENTAL HYSTERESIS (after Alaia [72])

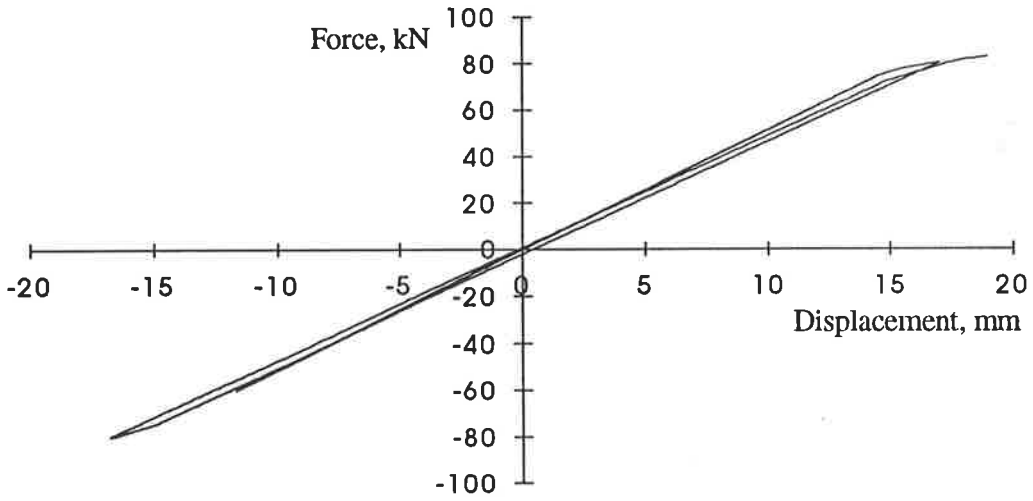

THEORETICAL HYSTERESIS

Fig. 5.21. Comparison of the frame hysteresis

5.3.2. Lateral resistance of an infilled frame with 5 mm gap between the frame and the wall

The theoretical model for this frame was developed as described in section 5.2 for a model with no gap. The ultimate shear force capacity for the brick wall was found using formula (5.4) without multiplying the value by a coefficient of 1.1. The loading history of the theoretical model was a sine wave with an amplitude increasing by 20 kN in each cycle starting with 20 kN in the first cycle. The load applied to the experimental frame differed from the analytical sine wave and looked as shown in fig. 5.22. The load in the experiment was increased to a maximum of 140 kN and each cycle after the first one was repeated three times with a certain magnitude of the force.

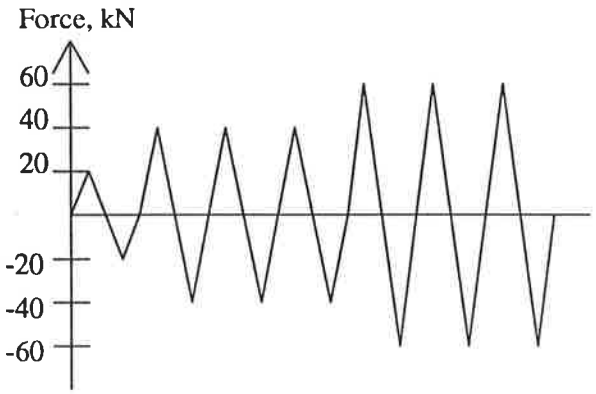

Fig. 5.22. Loading history of the test infilled frame

Figure 5.23 shows the force/displacement hysteresis loops for the theoretical and experimental results tested for the first cycles at four different amplitudes. The values of the displacements are in Table 5.3. The experimental displacements are from the first of the three cycles with the same amplitude.

As can be seen from Table 5.3, the results for the displacements show reasonable agreement for loads of 80 kN and less. The theoretical predictions are not so accurate for loads of 100 kN and more. The shape of the first four to five cycles were also reasonably similar although the loops of the theoretical model were bigger - a result of the large stiffness at unloading of the diagonals. The energy dissipation was mainly due to the hysteresis of the diagonals rather than the hysteretic behaviour of the frame elements.

Table 5.5. Comparison of the displacements for the infilled frame with 5 mm gap

Force, kN	20	40	60	80	100	120	140	-
experim. Δ, mm	+0.2/ -0.6	+1.5/ -2.3	+3.6/ -3.4	±4.8	+8.5/ -6.0	+13.3/ -13.0	+23.0/ -20.5	max 58.0
theory Δ, mm	±0.4	±1.3	±2.9	±4.2	±5.7	±7.2	±10.5	max 22.6

For the largest loads (120 kN and 140 kN) the inelastic displacements of the experimental results were much larger than those predicted by the theoretical model. This can be seen clearly in fig. 5.24 (see also Table 5.5). After the 140 kN loading cycle, the frame in the test was loaded to failure with control on the displacements. The frame in the theoretical analysis was loaded with one more cycle at which complete failure of the frame occurred. The loading history of the experiment was different from the one in the theoretical model (three cycles of one and the same amplitude in the experiment corresponded to only one cycle of this amplitude in the theoretical analysis). This was the reason the experimental frame in the very last cycles of loading to develop larger inelastic deformations.

The analytical model failed to develop large inelastic deformations. It was also stiffer than the experimental frame due to the very stiff diagonals. The stiffness of the diagonals was slightly larger because it corresponded to the results from the static analysis for no gap and the theoretical model was a general one for the case of perfect fit or a gap smaller than 5 mm. Nevertheless, the envelope of the experimental hysteresis data had a similar shape to the envelope of the hysteresis data for the theoretical model. It was concluded that despite the above mentioned disadvantages, the overall response of the infilled frame with a gap of 5 mm or less was adequately described by this model.

There was shear failure in the columns of the test specimen as well as joint failure. These phenomena could not be represented by the theoretical model. The program accounts only for flexural failure in the members, not for shear failure.

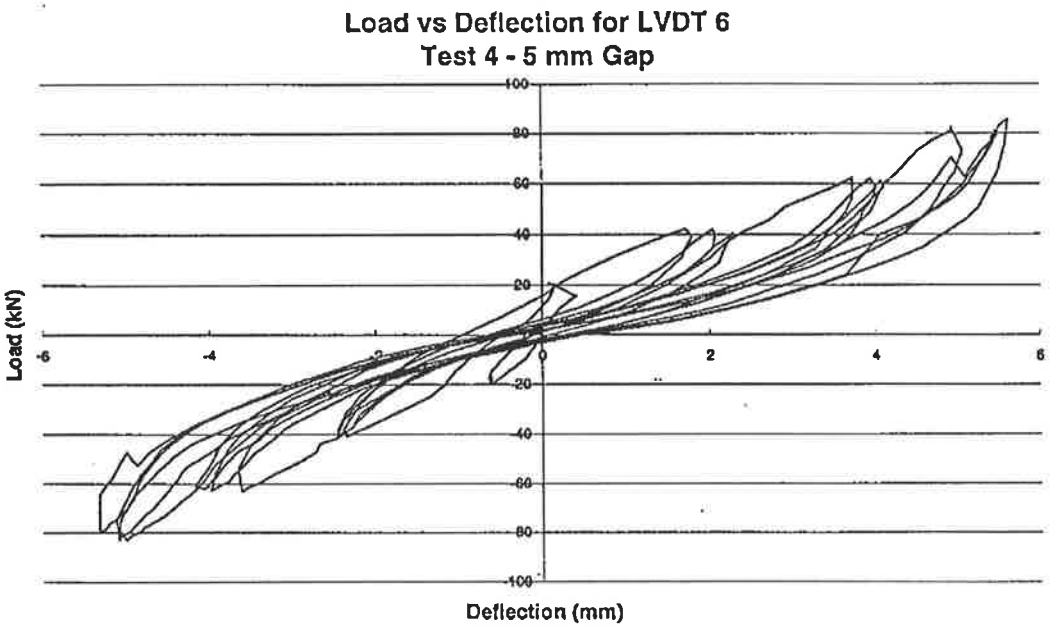

EXPERIMENTAL HYSTERESIS (after Alaia [72])

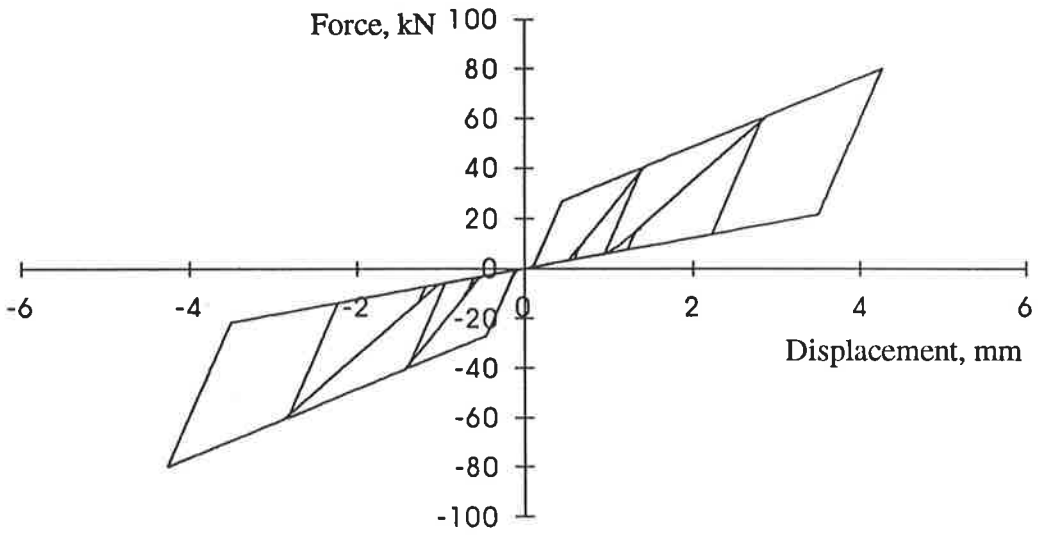

THEORETICAL HYSTERESIS

Fig. 2.23. Comparison for infilled frame with 5 mm gap
(first four increasing amplitudes of the loading)

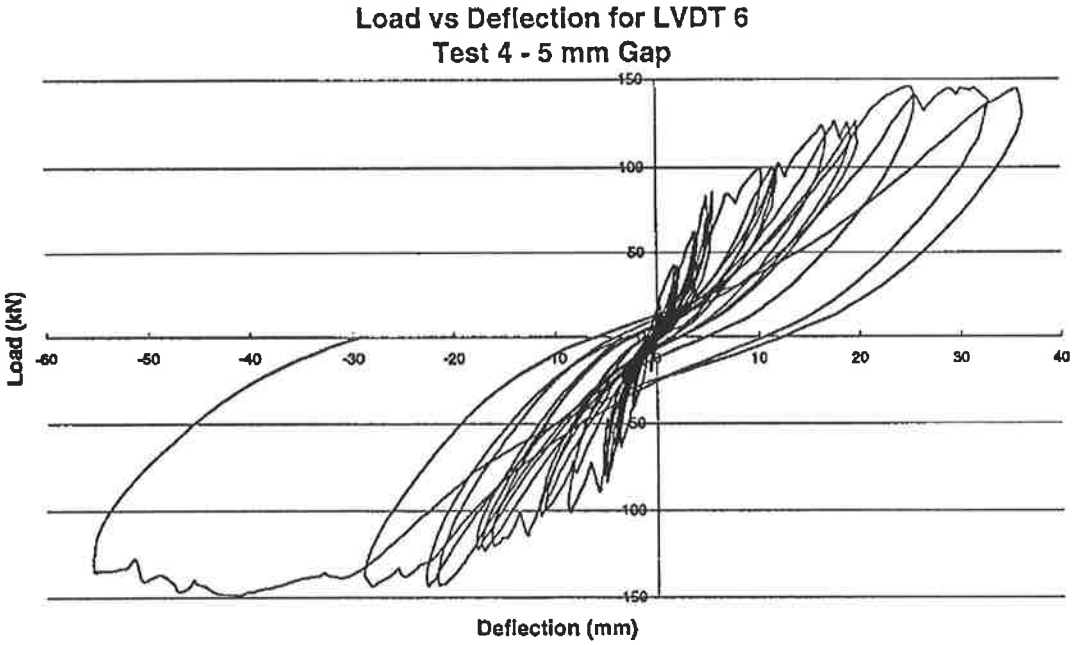

EXPERIMENTAL HYSTERESIS (after Alaia [72])

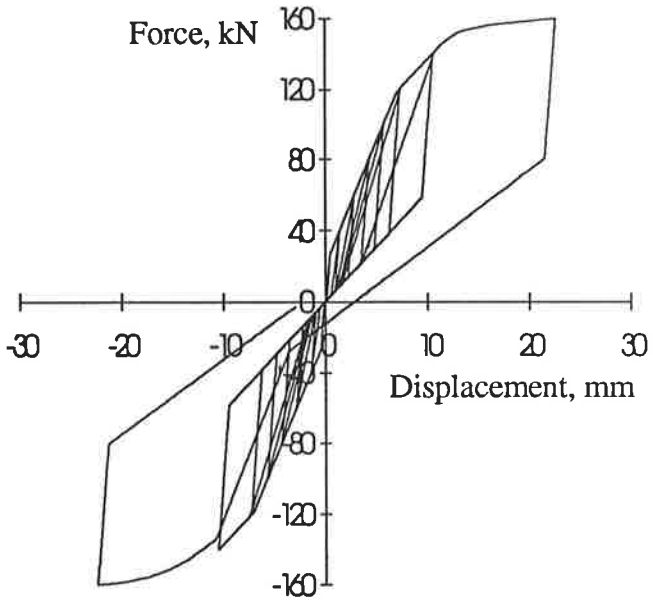

THEORETICAL HYSTERESIS

Fig. 5.24 Comparison for infilled frame with 5 mm gap
(complete loading history)

5.3.3. Lateral resistance of an infilled frame with 15 mm gap between the frame and the wall

The theoretical model was developed following the assumptions for the general model of an infilled frame with a gap. The theoretical loading was an increasing sine wave by 20 kN. The load on the test specimen was monotonously increasing with the same amplitudes and number of cycles as in the analysis. As a result, each cycle of the test corresponded to a cycle of the theoretical analysis.

Figure 5.25 is a comparison between the experimental results for an infilled frame with 15 mm gap and the corresponding analytical results for the first four cycles. The maximum theoretical displacements are listed in Table 5.6 along with the experimental results (Alaia [72]). As before, there was good correlation between the displacements of the experimental and the analytical model for the first four cycles. The shape of the hysteresis was also similar. The stiffness of the frame from the experiment (the closing line of the hysteresis loop) was about 6.6×10^6 N/m while for the theoretical model it was about 5.8×10^6 N/m. The moment of inertia of the frame was taken as $30\% I_g$. The opening of the loop at higher loads due to the interaction of the infill and the frame was also in good agreement. For instance, the height of the loop for the fourth cycle for the experimental result was about 20 kN while for the theoretical model it was about 25 kN.

Table 5.6. Comparison of the maximum displacements for 15 mm gap

Force, kN	20	40	60	80	100	120	140
experim. Δ, mm	+1.3	+4.3/ -3.5	+6.4/ -6.0	+8.9/ -8.0	+11.0/ -15.0	+17.0/ -21.0	+30.0/ -35.5
theory Δ, mm	±1.6	±3.8	±6.0	±8.2	±10.6	±13.1	±40.0

The complete force/displacement plots of the tested and analysed frames are given in fig. 5.26. After the fourth cycle when the frame went well into the inelastic region and the wall slipped and started to slide along its base. At that point, the experimental and theoretical hysteresis loops also became different. The theoretical model did not

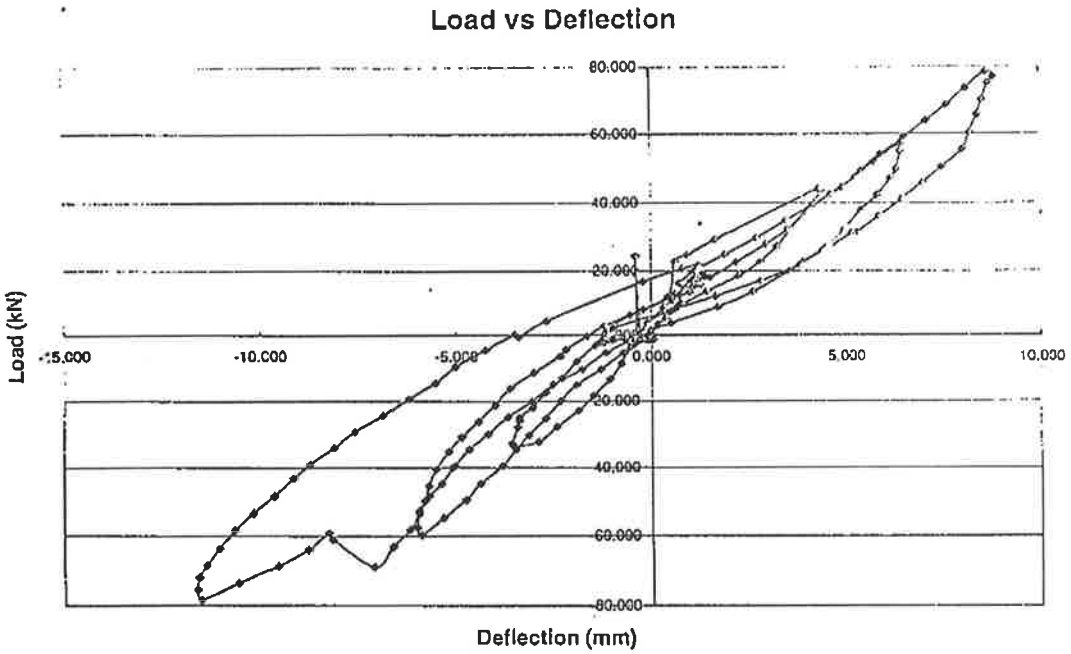

EXPERIMENTAL HYSTERESIS (after Alaia [72])

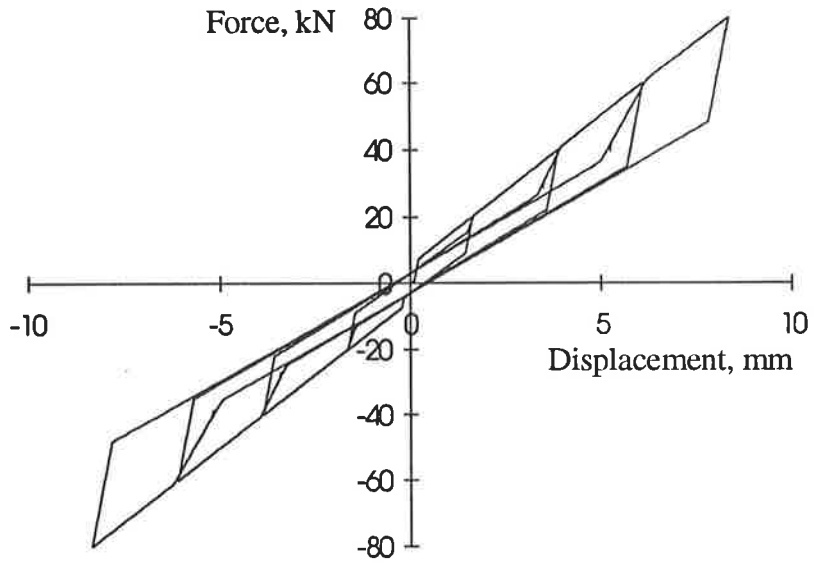

THEORETICAL HYSTERESIS

Fig. 5.25. Comparison for infilled frame with 15 mm gap
(first four cycles of loading)

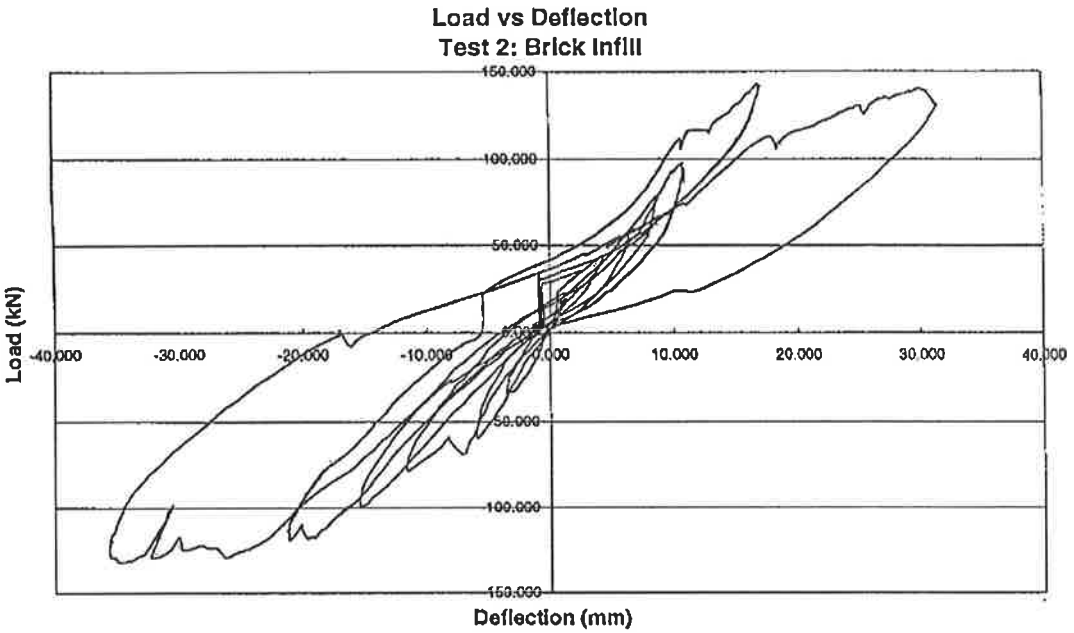

EXPERIMENTAL HYSTERESIS (after Alaia [72[)

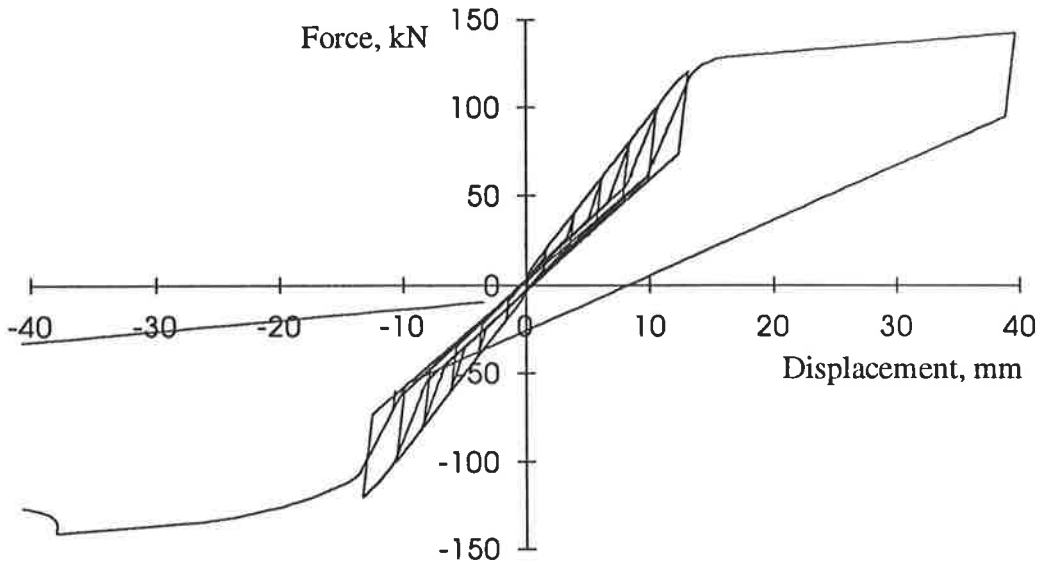

THEORETICAL HYSTERESIS

Fig. 5.26. Comparison for infilled frame with 15 mm gap
(complete loading history)

adequately represent the non-linearity of the frame in the last cycles. As before, the energy dissipation was mainly due to the inelastic response of the diagonals. The smooth changes of stiffness observed with the experimental data after contact with the wall and movement of the wall did not appear in the theoretical force/displacement hysteresis loops. The theoretical unloading slope was steeper than the experimental slope and the loops of the theoretical model were much more rectangular. The ability of the frame to develop large inelastic deformations was not represented adequately as well.

5.3.4. Adequacy of the analytical models

Figure 5.27 shows the results from the fourth test - the infilled frame with 10 mm construction gap (Alaia [72]). The overall effective stiffness of the hysteresis data is an intermediate value between the stiffness value form the tests specimen with a 5 mm gap and a 15 mm gap. The shape of the loops in the first few cycles is similar to the shape of the loops for the specimen with 15 mm gap. The general model for the case of a construction gap includes gap sizes larger than 5 mm. The differences in the data for the test result for a 10 mm gap can be accounted for by adjustment of the theoretical parameters which affect the pinched region. However, insufficient data exists to allow better specification of the parameters so the general model was accepted as a reasonable solution for the investigated models. Most of the theoretical infilled frames have relatively stiff masonry infill wall in comparison to the stiffness value for the experimental test specimens.

As a result of the comparison of the two theoretical models to the experimental results in section 5.3 the following points should be emphasised:

- the non-linearity and energy dissipation in the theoretical models was mainly due to inelastic response of the diagonal struts;
- the hysteretic model used for the frame elements was very simple. For the regions with large inelastic deformations the loops did not open and the hysteresis rule did not adequately represent the behaviour of the frame elements;
- the "Ruaumuko" solution did not account for shear failure or joint failure in the reinforced concrete frame;

- the loops in the region where the frame and the wall resist the lateral load together were wider in the theoretical model than in the experimental results due to the very large unloading stiffness associated with the hysteresis rule for the diagonals; and
- the overall response of the system, with and without gaps, was represented adequately by the theoretical models. This was especially true for the small deformation range. These were general models which were used for the evaluation of the influence of the presence of a construction gap in infilled frames with different relative stiffness and *l*/h ratio.

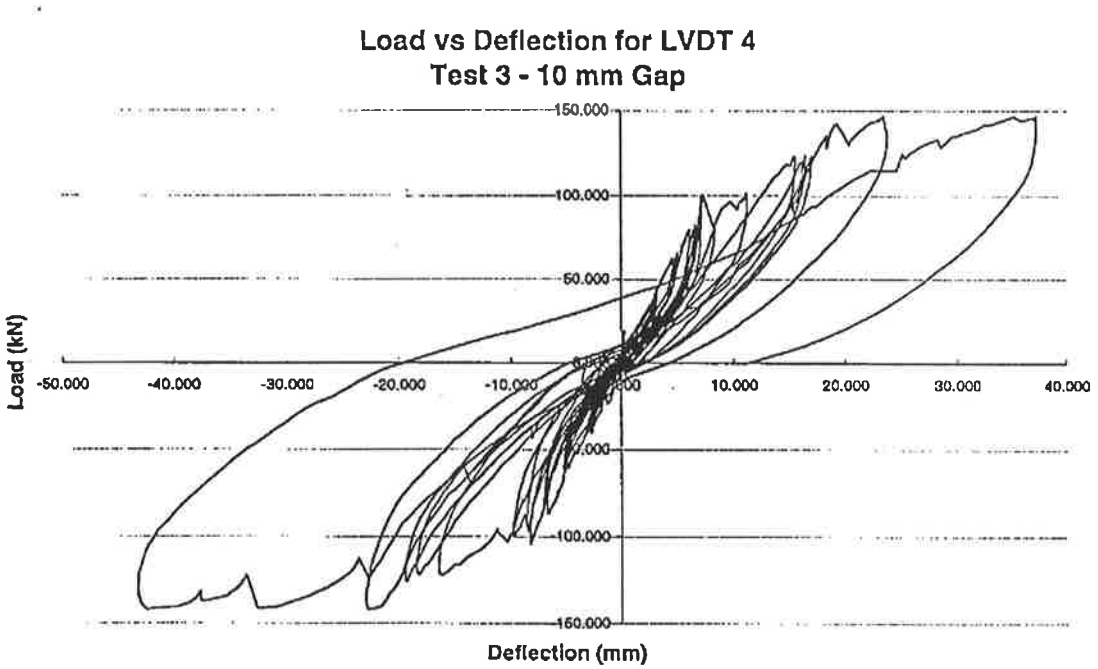

Fig. 5.27. Test result from infilled frame with 10 mm gap
(after Alaia [72])

CHAPTER 6 - DYNAMIC ANALYSIS - RESULTS

In this section the results from the dynamic analysis are presented and the influence of a gap on models with varying relative stiffness λh and length to height ratio is investigated. The time/displacement graphs and the force/displacement hysteretic behaviour of the eight models are presented and differences in the response discussed. For all eight models, the time/displacement graphs consist of three lines. The light colour line corresponds to the lateral resistance of a bare frame (line 1); the line with normal thickness (line 2) represents the response of an infilled frame without a construction gap; and the thickest line (line 3) represents the response of an infilled frame with a construction gap. The analysis was stopped once a collapse mechanism formed in the frame. For each model the hysteresis for a bare frame and infilled frame with a gap and without a gap are also compared. The hysteresis plots and the time/displacement plots finish at the point where four hinges formed in the frame. Hence, the complete last cycle is not shown.

6.1. Model M1

This is the model with the most flexible frame. The bare frame failed at a very low load. The presence of an infill wall changed the overall response by drawing most of the lateral load towards it. The composite system was able to resist 2 to 3 cycles of loading more than the bare frame (fig. 6.1). The model with a construction gap was able to develop larger deformations than the model without a gap but the system collapsed at a lower load than the system with perfect fit between the frame and wall (fig. 6.2). This was characteristic for most of the models with a flexible frame and a stiff infill wall. The large stiffness of the infilled frame without a gap from the very start of the loading history was due to the relatively large stiffness of the infill wall. The overall hysteresis (fig. 6.2) showed that the load was resisted mainly by the infill wall helped by the confinement provided by the frame.

The sequence of hinging in the infilled frame was identical to that for the bare frame (Table 6.2, section 6.6). It started with hinges in the beam then a hinge was formed at the base of the directly loaded column and then at the base of the other column. The hinges formed first in the beam because the beam in this model had a relatively low stiffness and the bracing increased even more the stiffness of the column in comparison to that of the beam. It should be noted again that "Ruaumoko" does not account for shear failure in the frame members. All hinges were a result of flexural actions and the possibility of joint or shear failure in the frame could not be captured by this theoretical model.

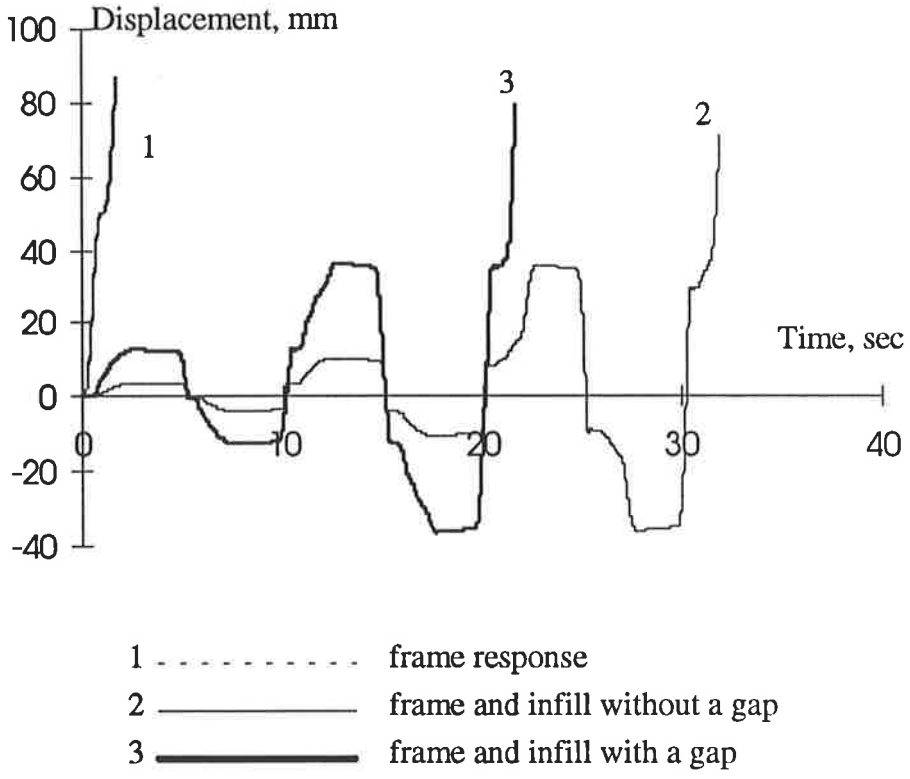

Fig. 6.1. Model M1 - time/ displacement plot

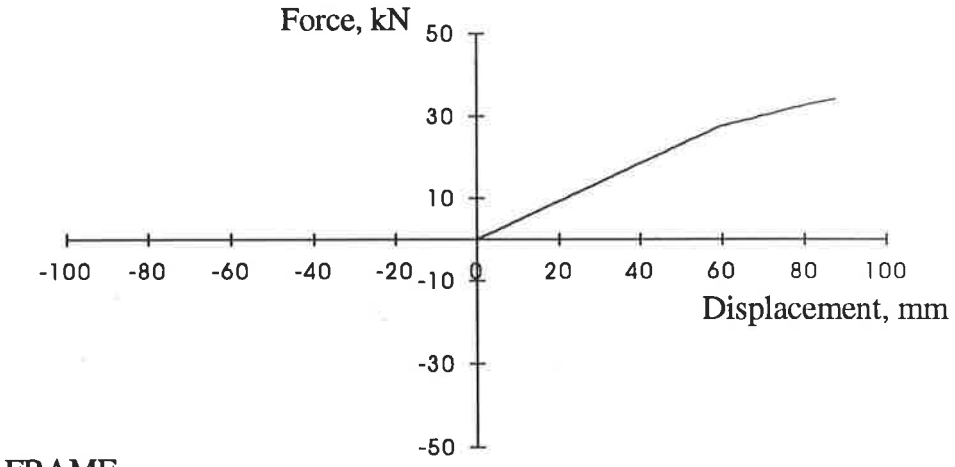

FRAME

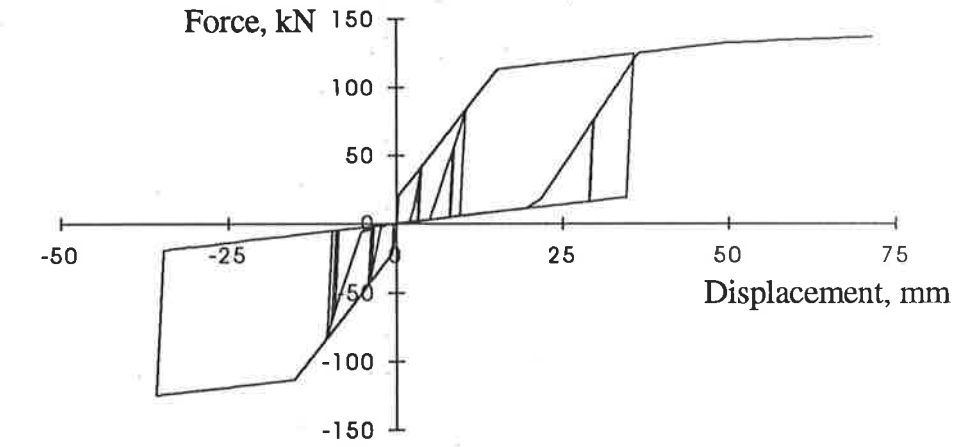

INFILLED FRAME - NO GAP

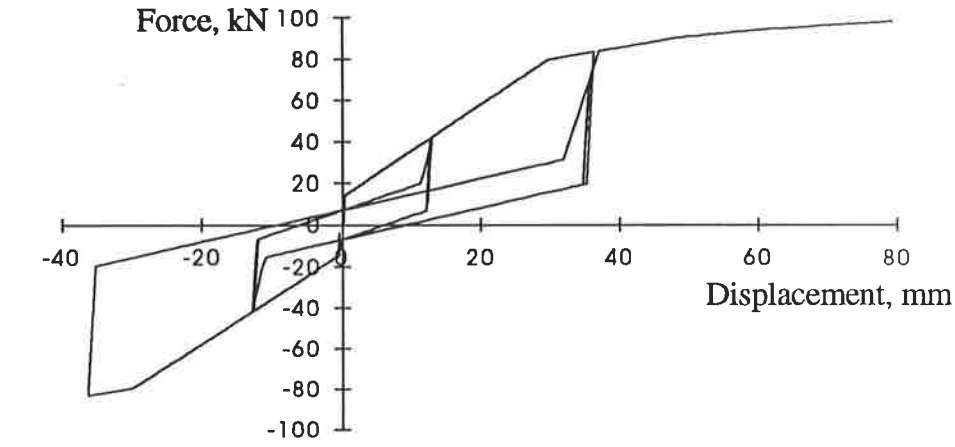

INFILLED FRAME - GAP

Fig. 6.2. Model M1 - hysteresis plots

6.2. Models M2, M3, M6 and M7 - constant I_g and varying l/h ratio

6.2.1. Model M2

This model had a relatively stiff infill wall which changed the response of the frame not only by increasing its load bearing capacity but also by changing the sequence of the hinge formation. The frame without a gap (line 2 on fig. 6.3) had smaller deformations in the initial cycles due to the very large combined stiffness of the frame and the wall. The hysteresis loops shown in fig. 6.7 show that the emphasis of the load resistance was on the wall for the infilled frame without a gap while for the model with a gap the stiffness and strength of both frame and wall participated in the response and the hysteresis was much more flat. The first hinge in the infilled frame without a gap appeared at the base of the loaded column unlike the models of the bare frame and the infilled frame with a gap where the first hinges appeared in the beam (Table 6.2, section 6.6). The wall for the case of no gap increased the stiffness considerably without significantly affecting the strength of the frame.

6.2.2. Model M3

In comparison to model 2, model 3 has a slightly longer frame (l/h=1.5 compared to 1.33 for M2 and f_c'=40 MPa compared to f_c'=20 MPa for M2). This was enough to change the sequence of appearing of hinges (Table 6.2, section 6.6). For both infilled frames of model M3 (with and without a gap) the first hinge appeared at the base of the loaded column whereas this happened only for the case of no gap for model M2. Comparison of the time displacement plots for model M2 and model M3 showed great similarity between the behaviour of model M2 and M3 (the cross sectional properties were the same for the two frames but f_c' was different) but the strength of the frame with a gap for M3 (line 3 fig. 6.4) was greater. Both the frame and the wall were stronger than model M2 (fig. 6.8) due to larger value of f_c' and slightly longer infill.

6.2.3. Model M6

The frame of this model differed only from model M3 in that it was longer (l/h=2.0). The bare frame was able to resist the same load as the frame from model M3 but the sequence of hinging was different. When infilled, this frame resisted considerably more

load than the infilled frame from model M3 because of the greater length of the wall (fig. 6.5). The presence of a gap in such a long model also changed the hysteretic behaviour noticeably. The infilled frame without a gap was very stiff in the initial cycles of loading in comparison to the frame with a gap (fig. 6.9). The overall shape of the hysteresis was different for the two cases of infilled frames. For the case of a construction gap the load was obviously resisted by the combined action of the frame and the wall while for no gap the wall was the main component resisting the lateral load. The sequence of hinging in the bare frame and the infilled frames without and with a gap was the same for the three cases of model M6 (Table 6.2, section 6.6).

6.2.4. Model M7

This was the longest frame modelled (l/h=2.66). It had the same material and cross-sectional properties as model M6 but the span of the frame was longer. The bare frame failed in a similar way to model M6. The infilled frame was able to withstand larger loading than the infilled frame of model M6 (fig. 6.6). The analytical displacements of the infilled frame with and without a gap were considerably different from each other. The shape of the force/displacement hysteresis plots for the two cases was also very different. The presence of the strong infill in the frame without a gap made the system very stiff and able to resist very high loads (fig. 6.10) due to confinement of the wall by the frame. The hysteretic response of the infilled frame with a gap showed that the overall system was not that stiff and the noise which appeared in the regions of sharp change of stiffness was a result from the contact of the frame with a relatively stiff infill at higher load levels and smaller frequency. The hysteretic behaviour of the infilled frames for model M7 show a significant sensitivity to the presence of a construction gap between the frame and the wall for longer infilled frames.

The following points should be emphasised.

- Bare frame - the changes in the behaviour of the bare frame with respect to l/h ratio were mainly in the sequence of hinge formation (section 6.6). For the shorter models hinges formed first in the beam while for the longer model in the columns. There were no noticeable changes in strength or stiffness with increase of l/h.

- Infilled frame without a gap - the increase in strength and stiffness of the infilled frames without a gap was mainly due to the increased length of the infill wall panel. The hinge formation sequence (Table 6.2, section 6.6) was nearly the same in the case of no gap for models M2, M3, M6 and M7 starting with a hinge in the columns. The shape of the hysteresis was very similar as well.
- Infilled frames with a gap - the increase in strength with increase of *l*/h ratio was more noticeable for the case of existing gap rather than increase in stiffness. The shape of the hysteresis was similar in this case as well. The hinge formation sequence for the shorter models was more like the sequence of the corresponding bare frames.

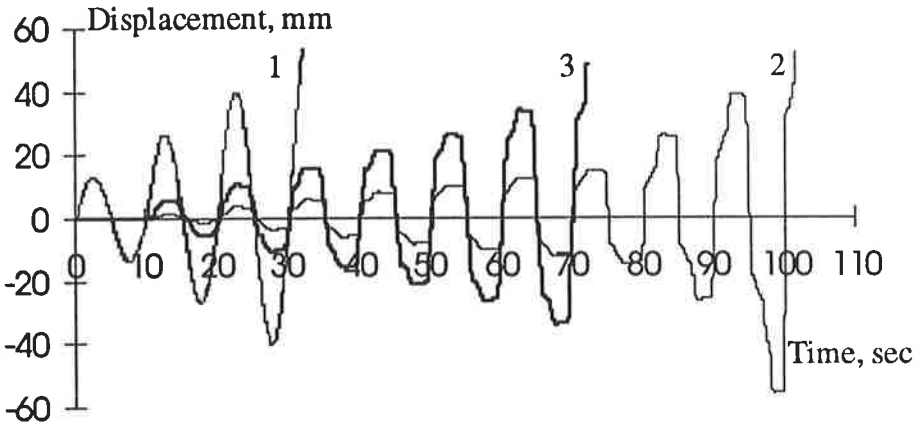

Fig. 6.3. Model M2 - time/displacement plot

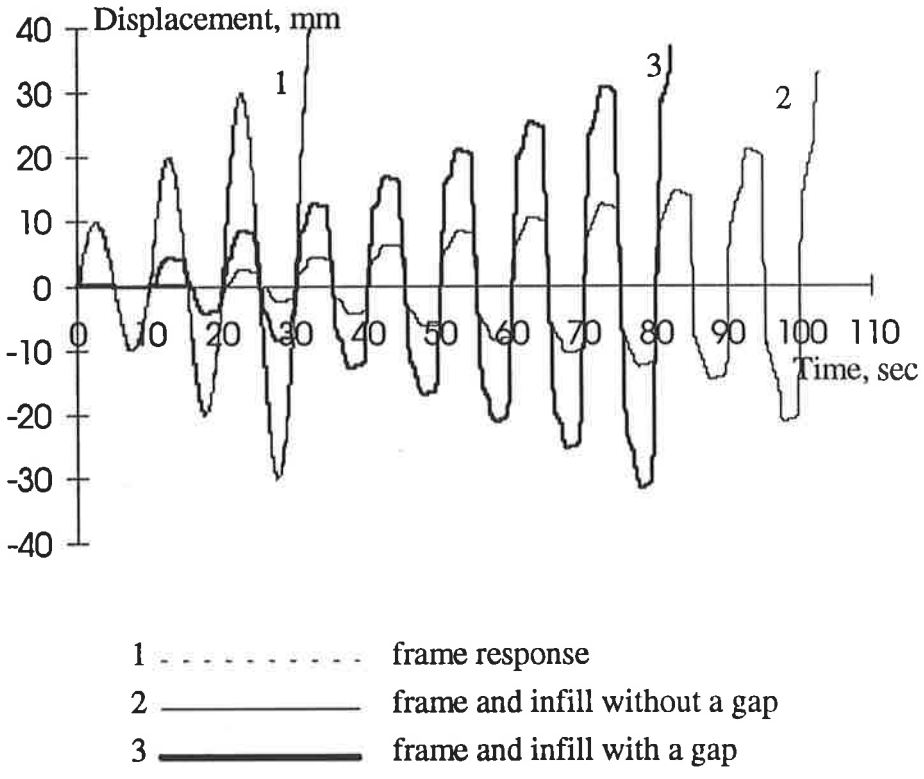

Fig 6.4. Model M3 - time/displacement plot

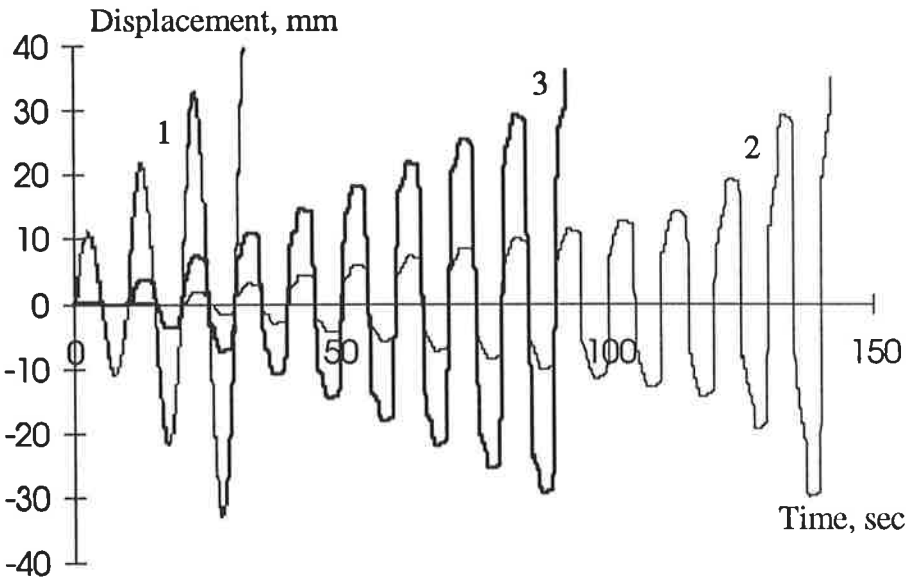

Fig. 6.5. Model M6 - time/displacement plot

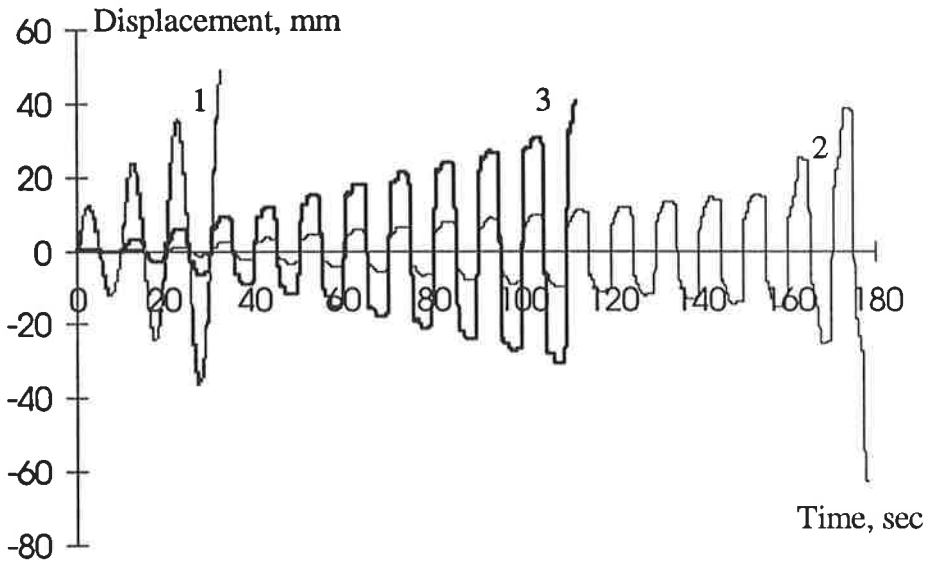

1 . . . . . frame response

2 _____ frame and infill without a gap

3 ▬▬▬▬ frame and infill with a gap

Fig. 6.6. Model M7 - time/displacement plot

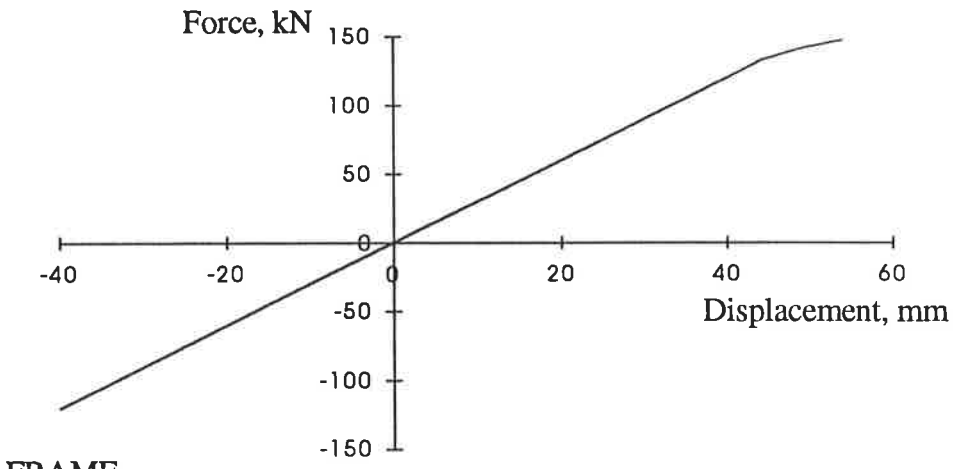

FRAME

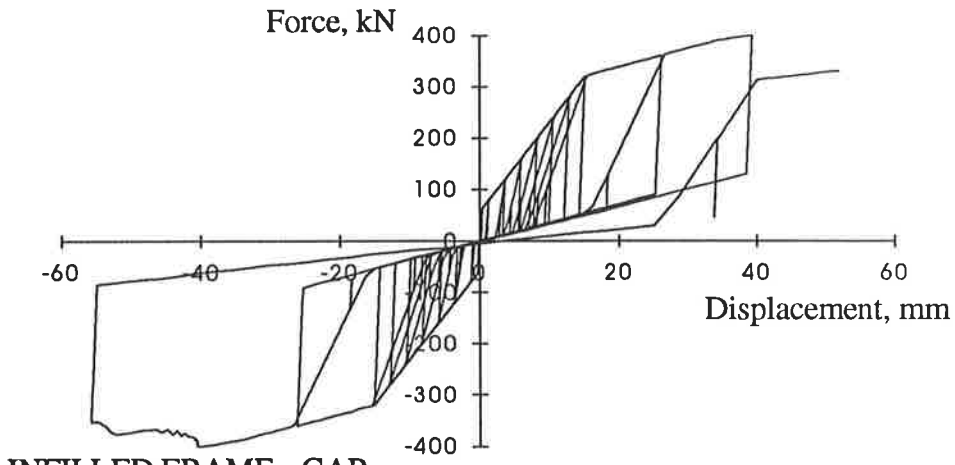

INFILLED FRAME - GAP

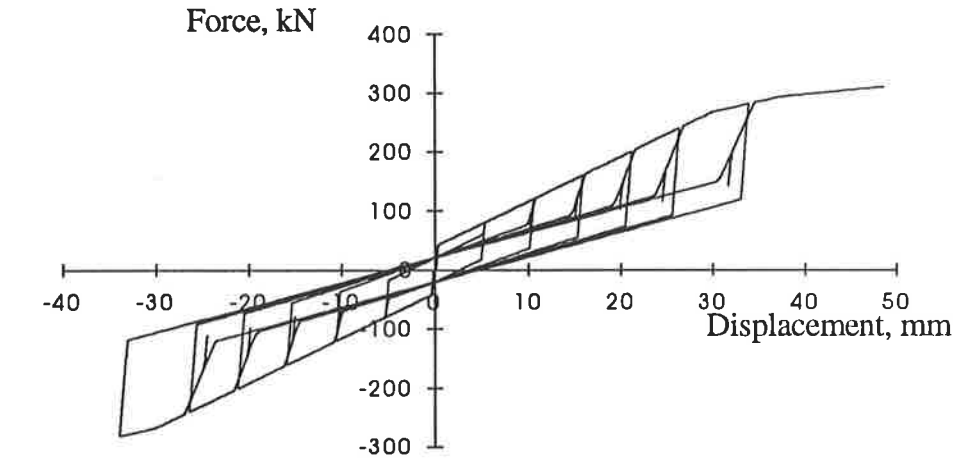

INFILLED FRAME - NO GAP

Fig. 6.7. Model M2 - hysteresis plots

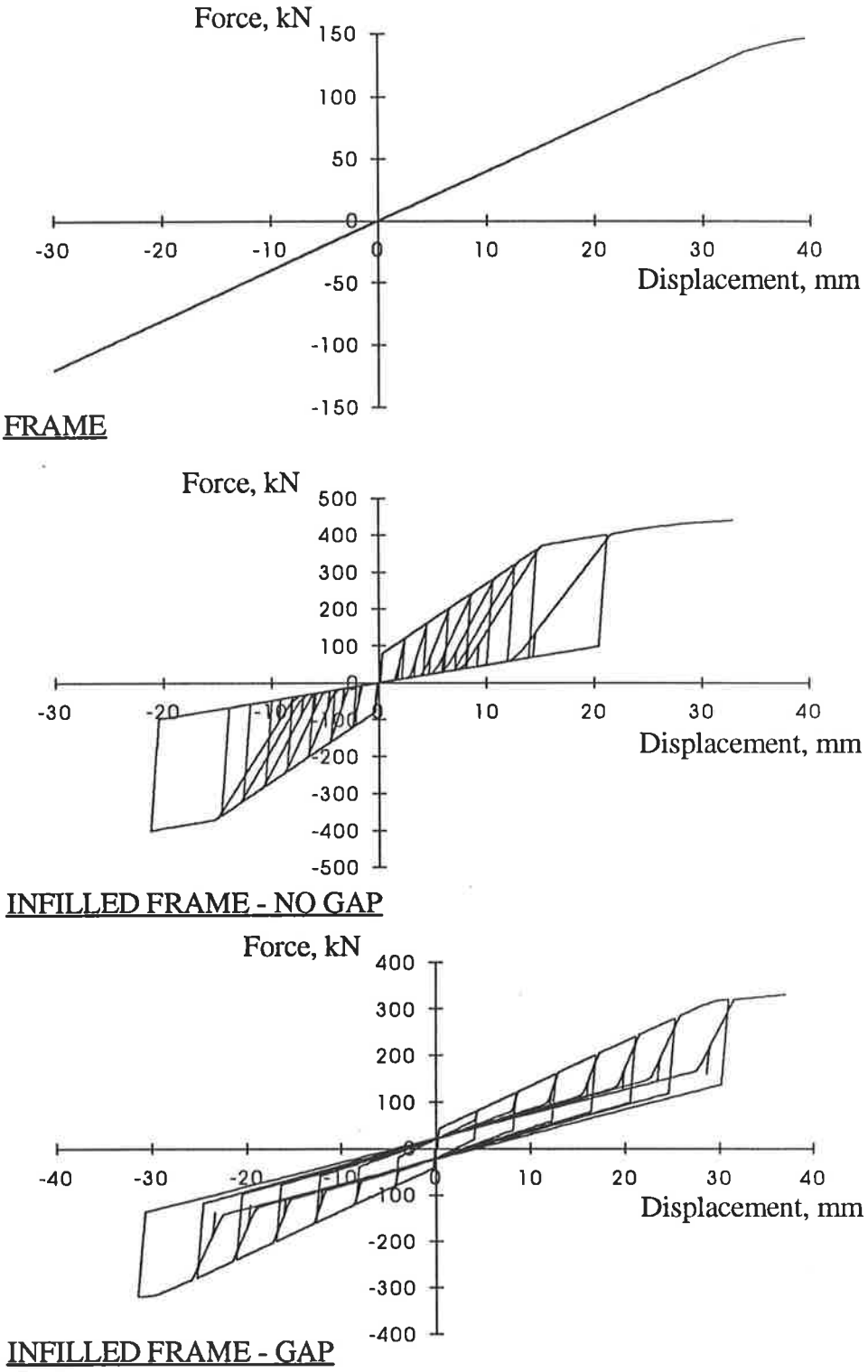

Fig. 6.8. Model M3 - hysteresis plots

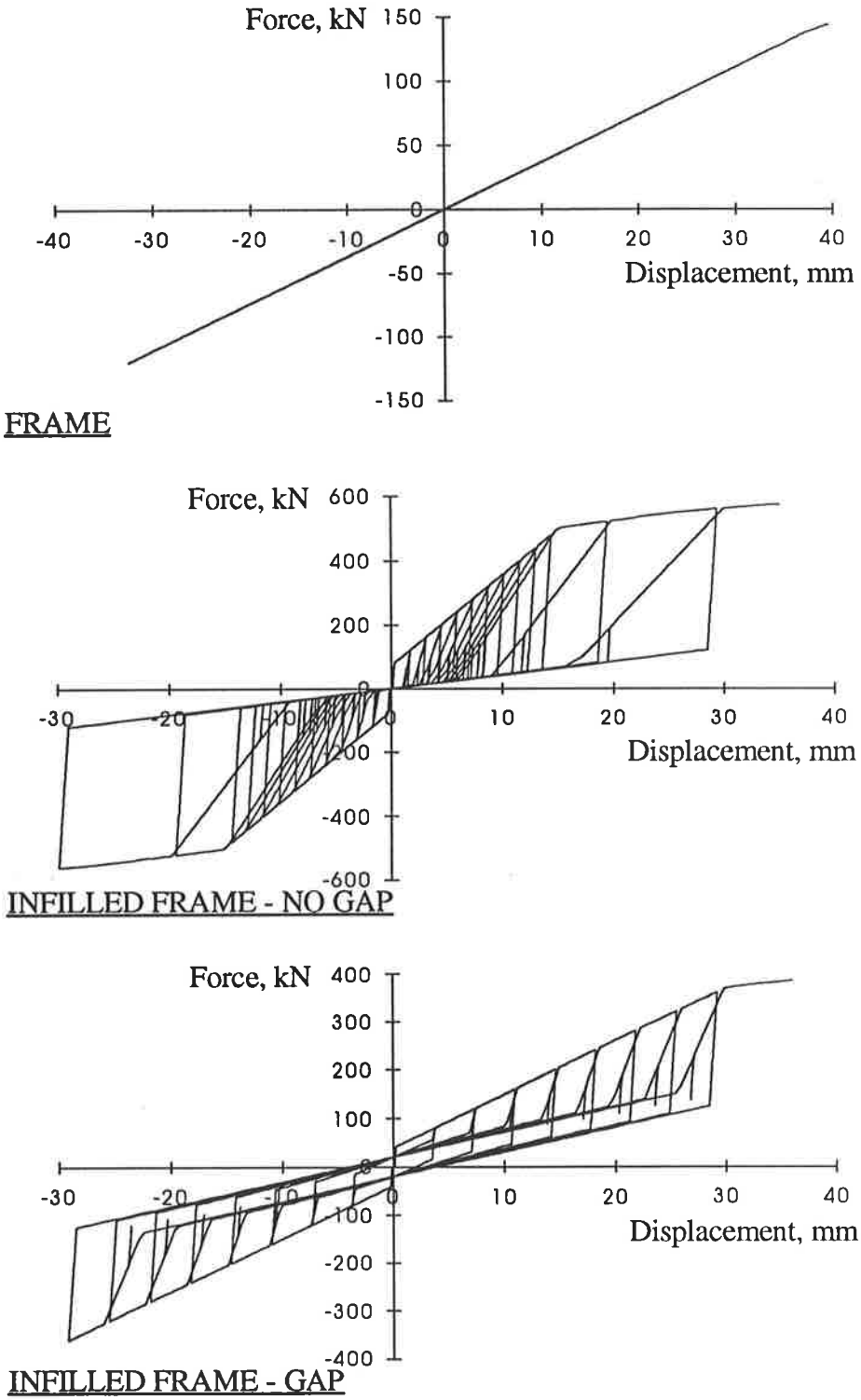

Fig. 6.9. Model M6 - hysteresis plots

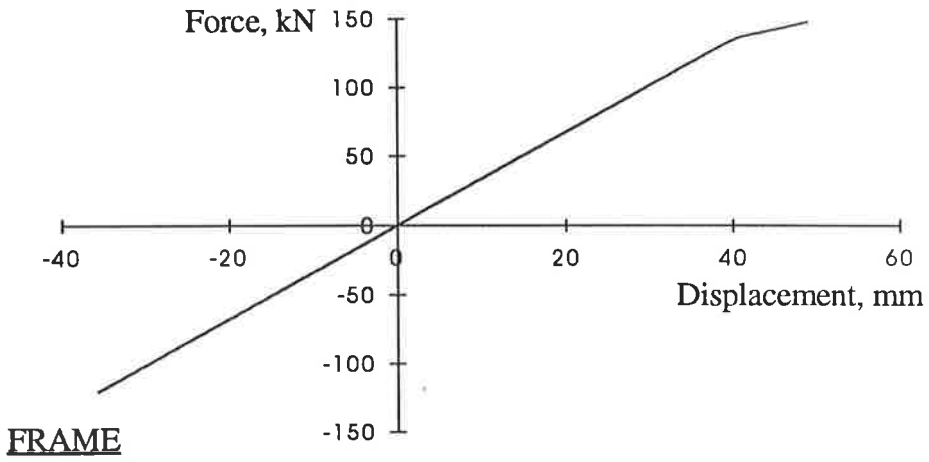

FRAME

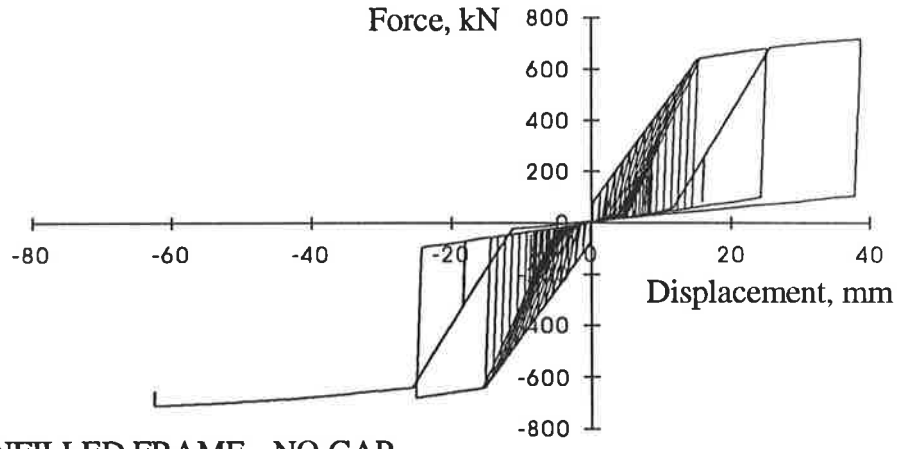

INFILLED FRAME - NO GAP

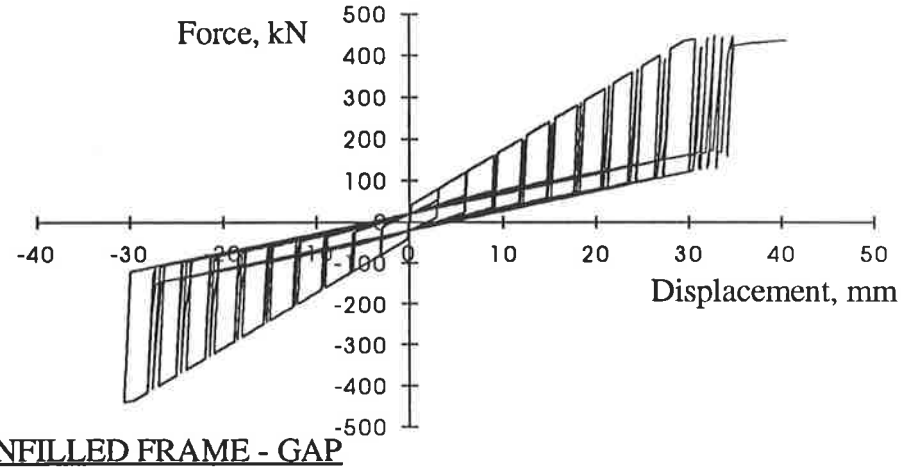

INFILLED FRAME - GAP

Fig. 6.10. Model M7 - hysteresis plots

6.3. Models M3, M4 and M5 - varying I_g and constant l/h ratio

6.3.1. Model M4

This model had a bigger cross section for the frame members than those in model M3. Although the frame in model M4 was more stiff than that in model M3, the frame displacements and the infilled frames' displacements were still considerably different from one another (fig. 6.4 and fig. 6.11). Comparison of the force/displacement hysteresis plots for each case (fig. 6.8 and fig. 6.13) shows increased similarity over that in the previous model between the hysteretic behaviour for the case of gap and no gap. They had similar heights and shape - a consequence of the increased frame stiffness.

The sequence of hinge formation was similar for the bare frame and the two cases of infilled frame, starting with hinges in the beam and then in the columns (Table 6.2, section 6.6). The sequence of hinge formation for model M1 was the same for the frame and the infilled frame and the four hinges formed on the last loading cycle. In contrast, model M4 had two or three hinges formed in the cycle proceeding the cycle of complete failure. This was probably due to the stiffer frame which resisted a large percentage of the load.

6.3.2. Model M5

This model had the stiffest frame. The displacement versus time plot (fig. 6.12) shows the importance of frame stiffness to the overall response. The displacements throughout the analysis for the three cases (lines 1 to 3) were almost the same (the infilled frame without a gap was loaded with 60 kN increasing amplitude and the one with a gap with 50 kN increasing amplitude). The shape of the hysteresis rules of the two infilled frames was much more similar than seen for model M4: the loops were very similar and the behaviour governed largely by the stiffness and strength of the frame (fig. 6.14). The appearance of hinges started with the base of the loaded column and was the same for the three cases (Table 6.2, section 6.6). As for model M4, some hinges in the frame occurred a couple of cycles before the cycle of complete failure.

The following points should be emphasised.

- Bare frame - as the frame gets stiffer the sequence of hinging changed from first hinges forming in the beam to first hinges forming in the columns.
- Infilled frame without a gap - the increase in frame strength and stiffness with decreasing λh is due to the combined effect of the frame and the wall and the strong confinement provided by the stiffer frames. The stiffer the frame the narrower the hysteresis loops become. For the models with weak frames the sequence of hinging was different for the bare frame and the infilled frame.
- Infilled frame with a gap - the stiffness of the frame-wall system was governed by the stiffness of the frame. Increased frame stiffness made the hysteresis loops become narrow leading to the frame resisting most of the load.

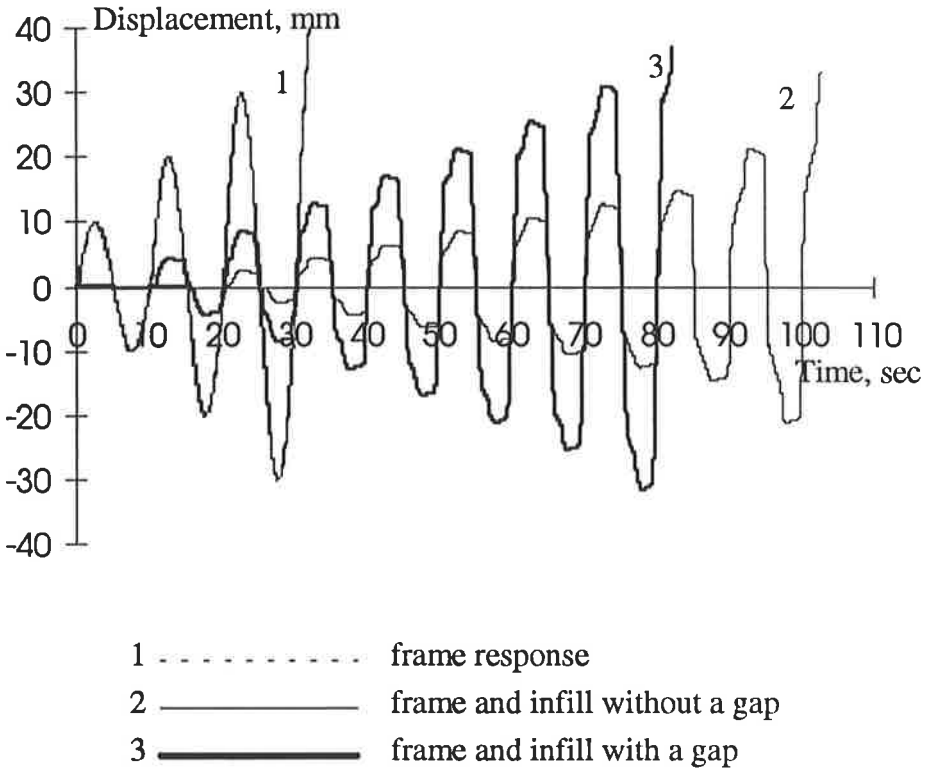

Fig 6.4. Model M3 - time/displacement plot

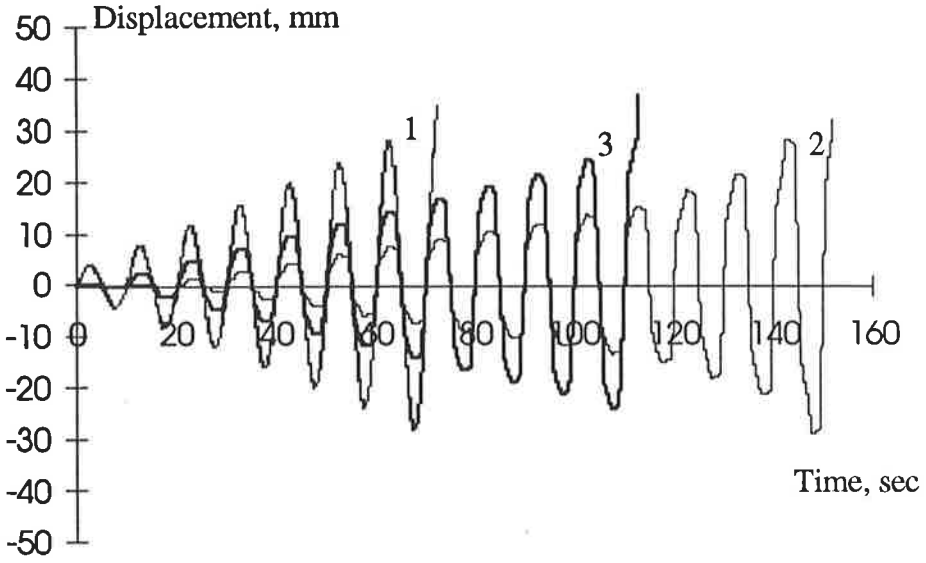

Fig. 6.11. Model M4 - time/displacement plot

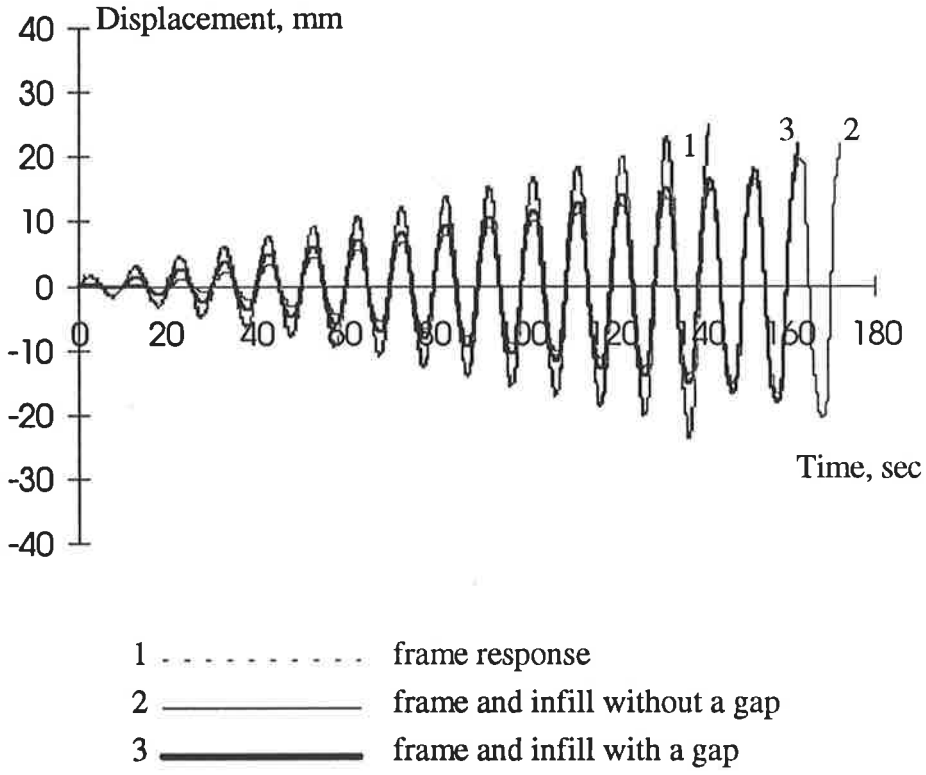

Fig. 6.12. Model M5 - time/displacement plot

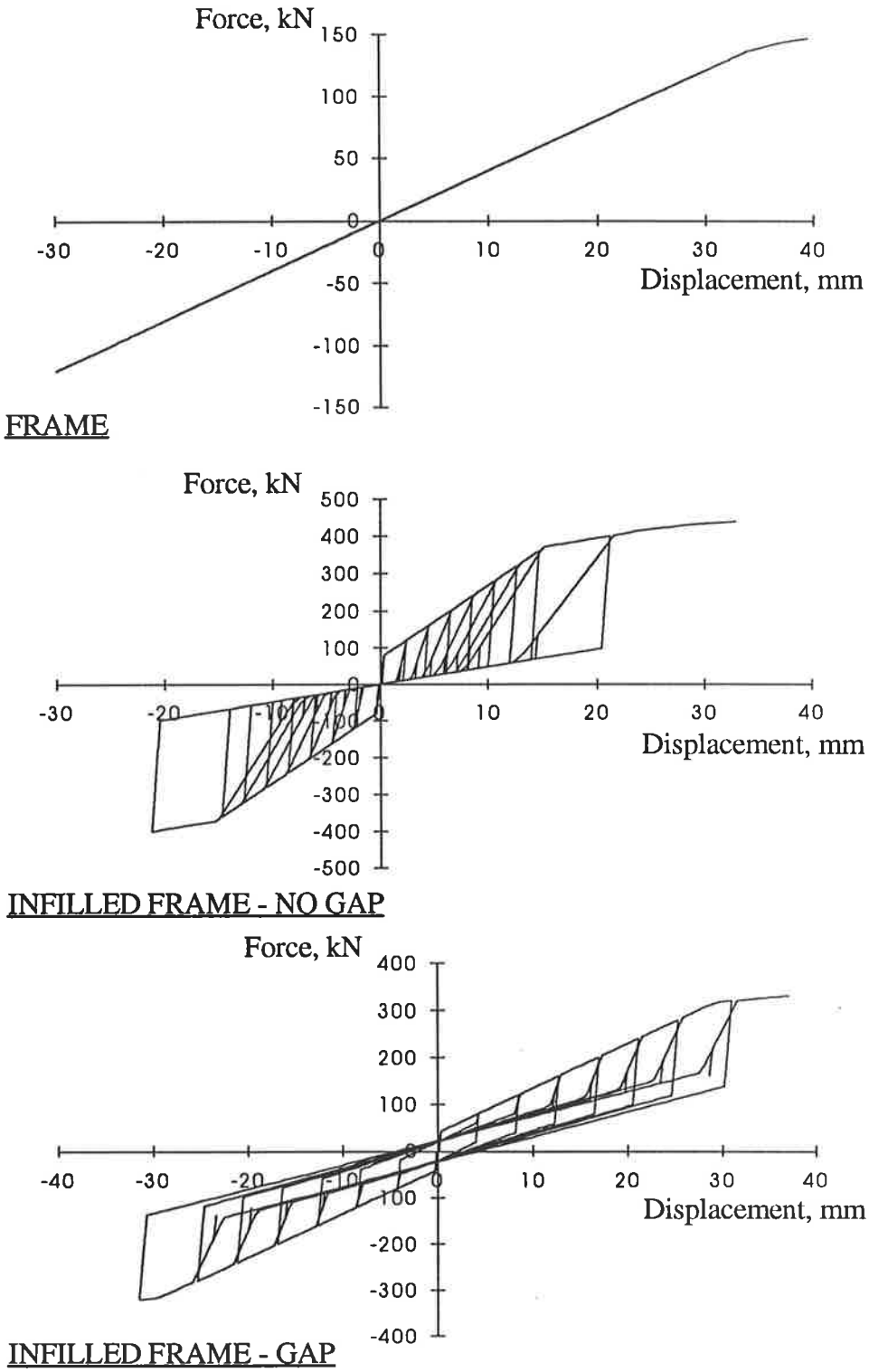

Fig. 6.8. Model M3 - hysteresis plots

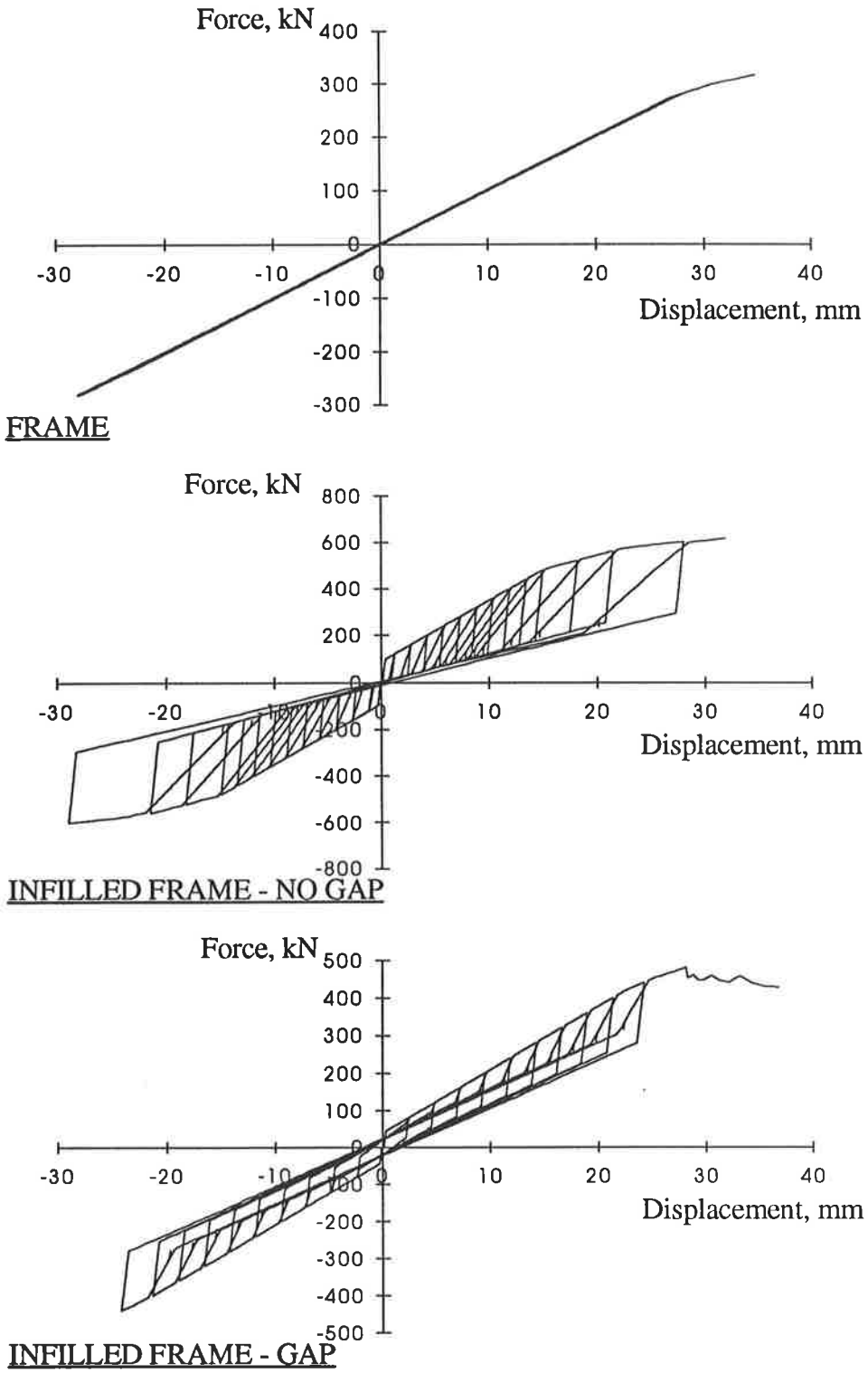

Fig. 6.13. Model M4 - hysteresis plots

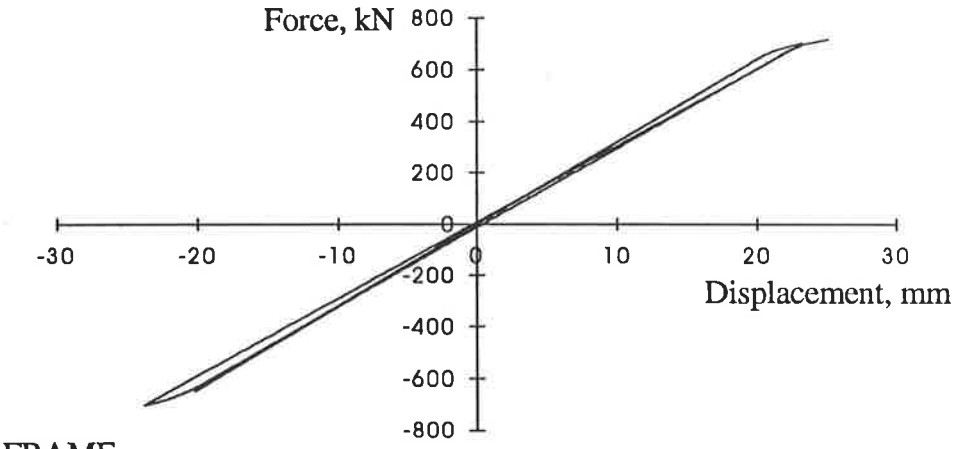

FRAME

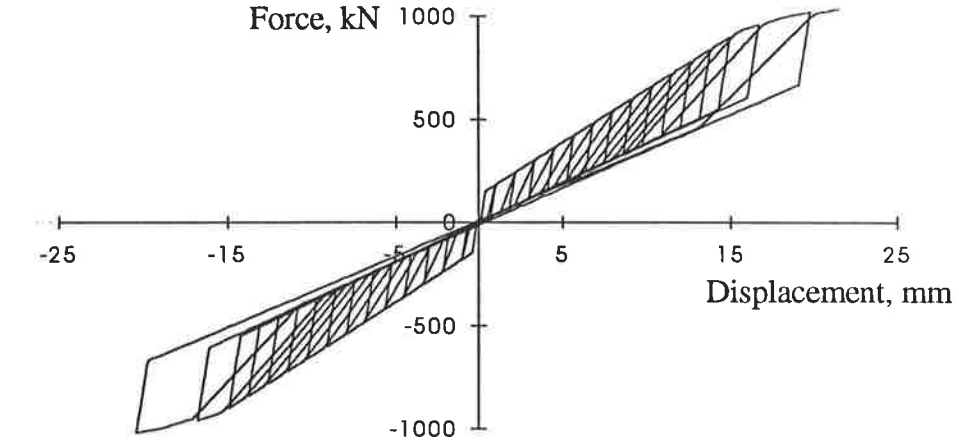

INFILLED FRAME - NO GAP

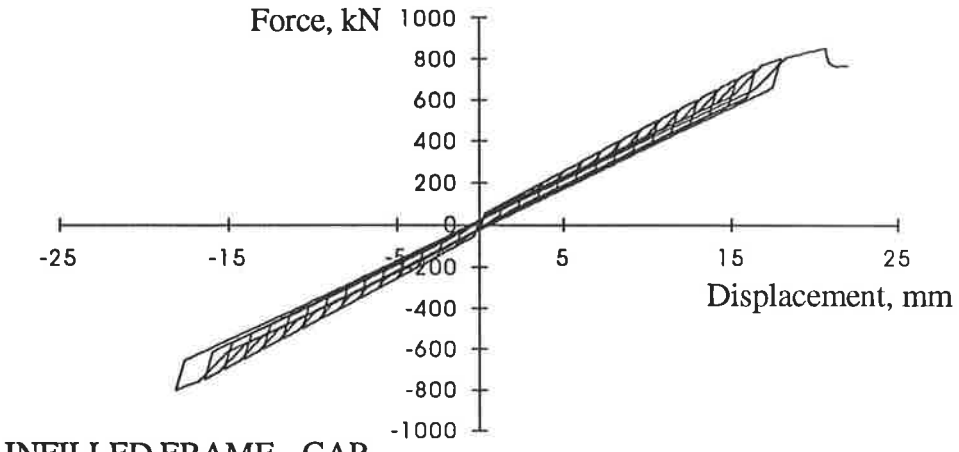

INFILLED FRAME - GAP

Fig. 6.14. Model M5 - hysteresis plots

6.4. Model M8a

Model M8a was created to match a theoretical model investigated by Wong [64] and to test the effect of the simple hysteresis rule used for the frame members on the overall response of the infilled frame. This frame had a stiffer and stronger beam in comparison to the frames of models M1 to M7. Therefore, the hinges in the bare frame formed only in the columns starting with hinges at the column base (Table 6.2, section 6.6). The very stiff beam confined the wall in the infilled frame model and increased the stiffness of the whole system, particularly for the case of no gap between the frame and the wall (fig. 6.16). The influence of the stiff beam on the overall response of the frame-wall system was not taken into account in this research. The results from the analysis of this model, M8a, were used only for comparison with the results of model M8 which had more detailed hysteresis rule for the frame members as investigated by Wong [64].

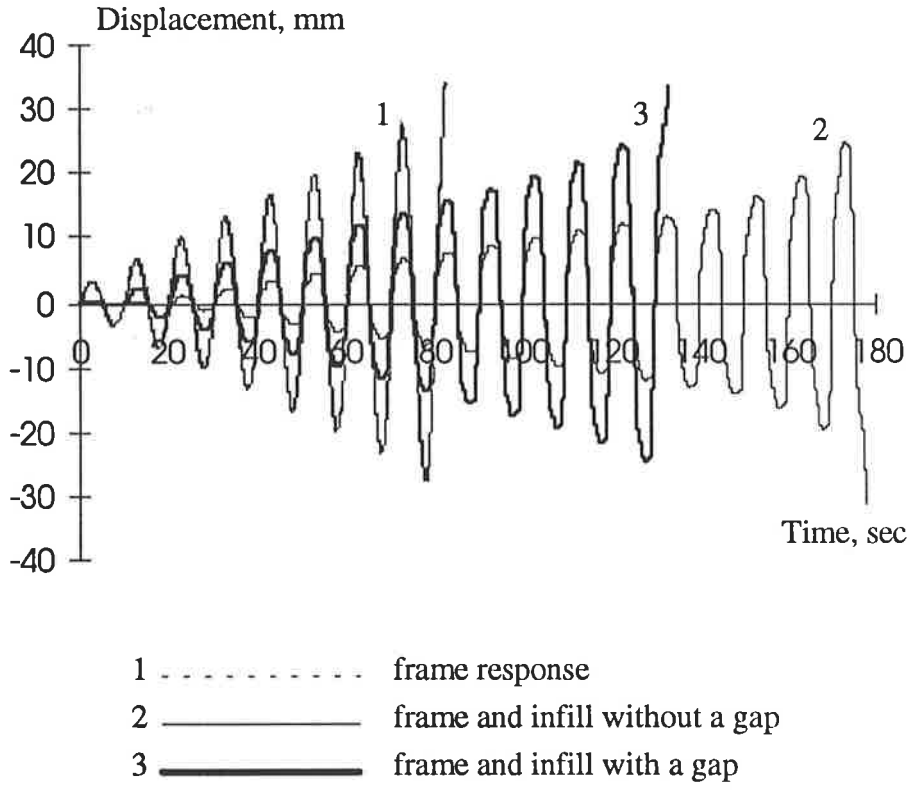

Fig. 6.15. Model M8a - time/displacement plot

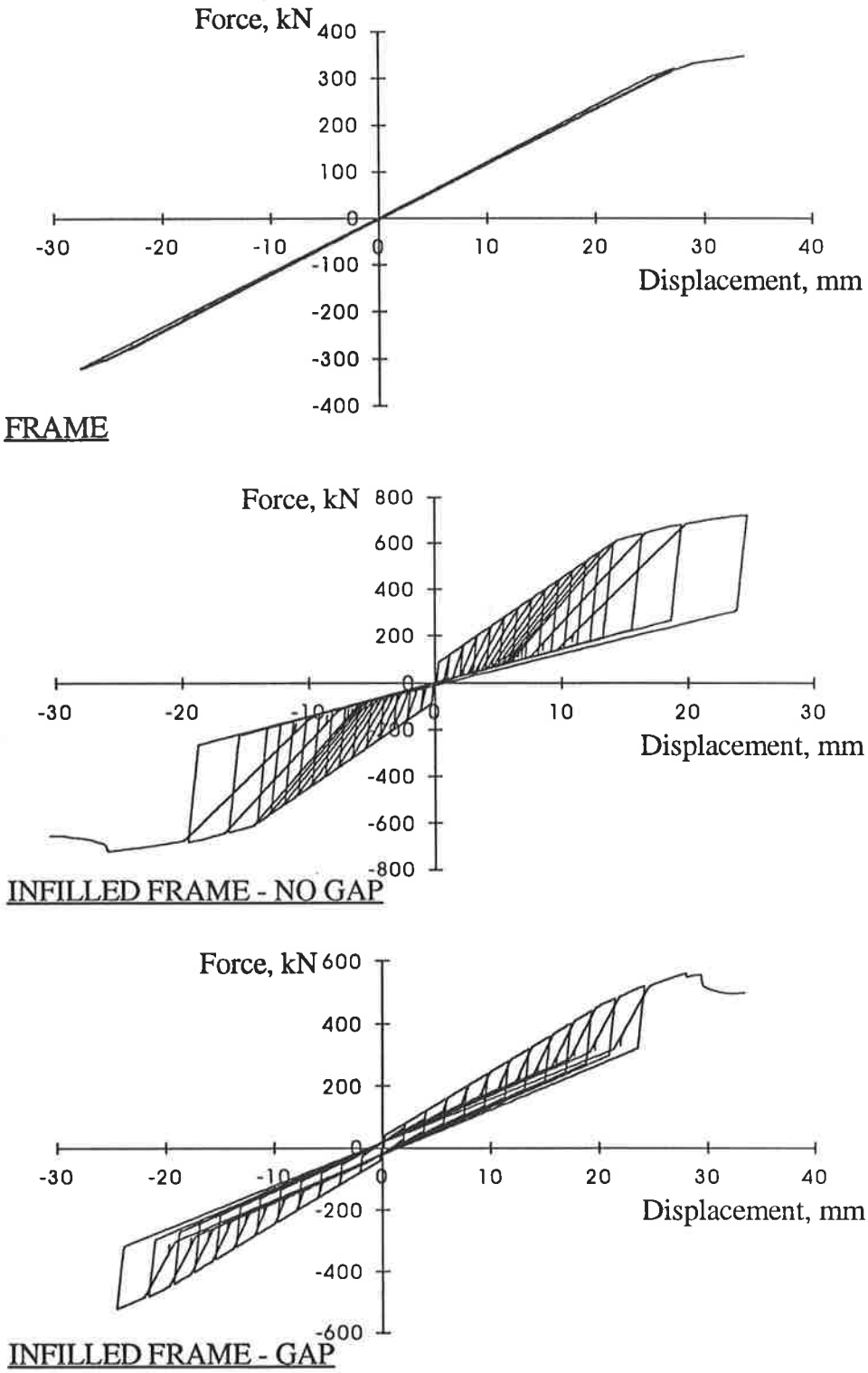

Fig. 6.16. Model M8a - hysteresis plots

6.5. Comparison of model M8a with model M8

The results given in this section are for a model with the same geometry of the frame and the infilled wall as model M8a. This model is referred to as model M8. The properties of the concrete cross section of model M8 were adjusted to match experimental results [64]. The frame members were modelled using a scaled strength interaction diagram which corresponded to the test results. In addition, the hysteresis rule used for the concrete cross section was much more complicated. A Mehran Keshavarzian degrading and pinching hysteresis rule was used for the frame members [69]. In this analysis for the models with brick infill the moment of inertia of the beam and the columns was assumed to be 30% of I_g. For the model of the bare frame, it was set equal to the value corresponding to the experiment results [64].

Comparison of the results for the calibrated model (M8) and the general model of this research (M8a) showed that the bare frame of the general model was stronger (fig. 6.15 and fig. 6.17 line 1). The infilled frames of the calibrated model resisted less load than the infilled frames of the general model (fig. 6.15 and fig. 6.17 lines 2 and 3). However, the shape of the overall hysteresis was similar in both cases (fig. 6.16 and fig. 6.18). It should be noted that the calibrated infilled frame model exhibited more inelastic deformation and opened the loops towards the x-axis. This disadvantage of the general model in the research was also seen in the comparison of the theoretical and experimental hysteresis loops for the infilled frames discussed in section 5.3. This disadvantage could be overcome by first investigating the behaviour of a bare frame and adjusting the hysteresis rule for the frame to best match the experimental results.

The sequence of hinging in model M8 was very much similar to the sequence seen for the general model M8a (Table 6.2, section 6.6). It started with a hinge at the base of the loaded column and then followed hinging only in the columns. For the model without a gap, noise due to the vertical vibration in the beam appeared in the eleventh cycle (fig. 6.18). The infilled frame model with a construction gap was actually predicted to fail due to beam vibrations in the vertical direction. When analysing the changes of the internal forces in the frame it was found that the loading in the case of an infilled frame with a

construction gap which went into the beam was not sinusoidal. There was a very short time interval during which very large loads were resisted by the frame itself (especially for the last cycles of loading). After the gap closed, the frame suddenly hit the infill and the most of load went into the diagonals, causing large sudden changes to the loads in the frame and the beam (both diagonals were working in tension and compression). Since the horizontal displacements of the end nodes of the beam were set to be equal and the stiffness of the beam was larger than the stiffness of the columns these vibrations were possible to occur in a model like this one. This disadvantage of the model, especially for frames with stiffer and heavier beams, could be excluded if only one of the diagonal was working in each direction for the case of a construction gap or by developing a model with three diagonal braces. This "noise" was most obvious for model M8 although it also appeared at different stages in some of the other models. It could also be excluded by increasing the percentage of critical damping of the structure for second mode of vibration.

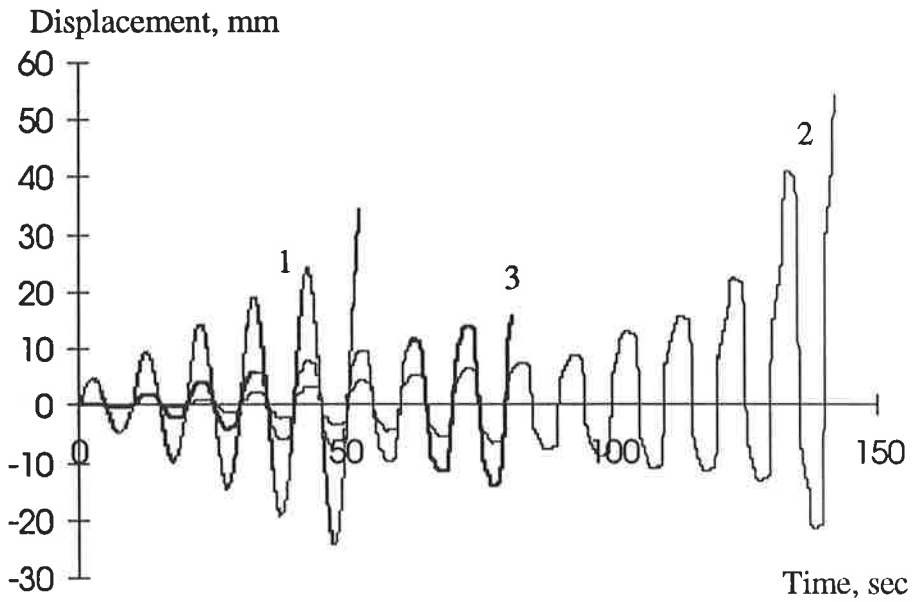

Fig. 6.17. Theoretical model with improved properties for frame members (time/displacement plot)

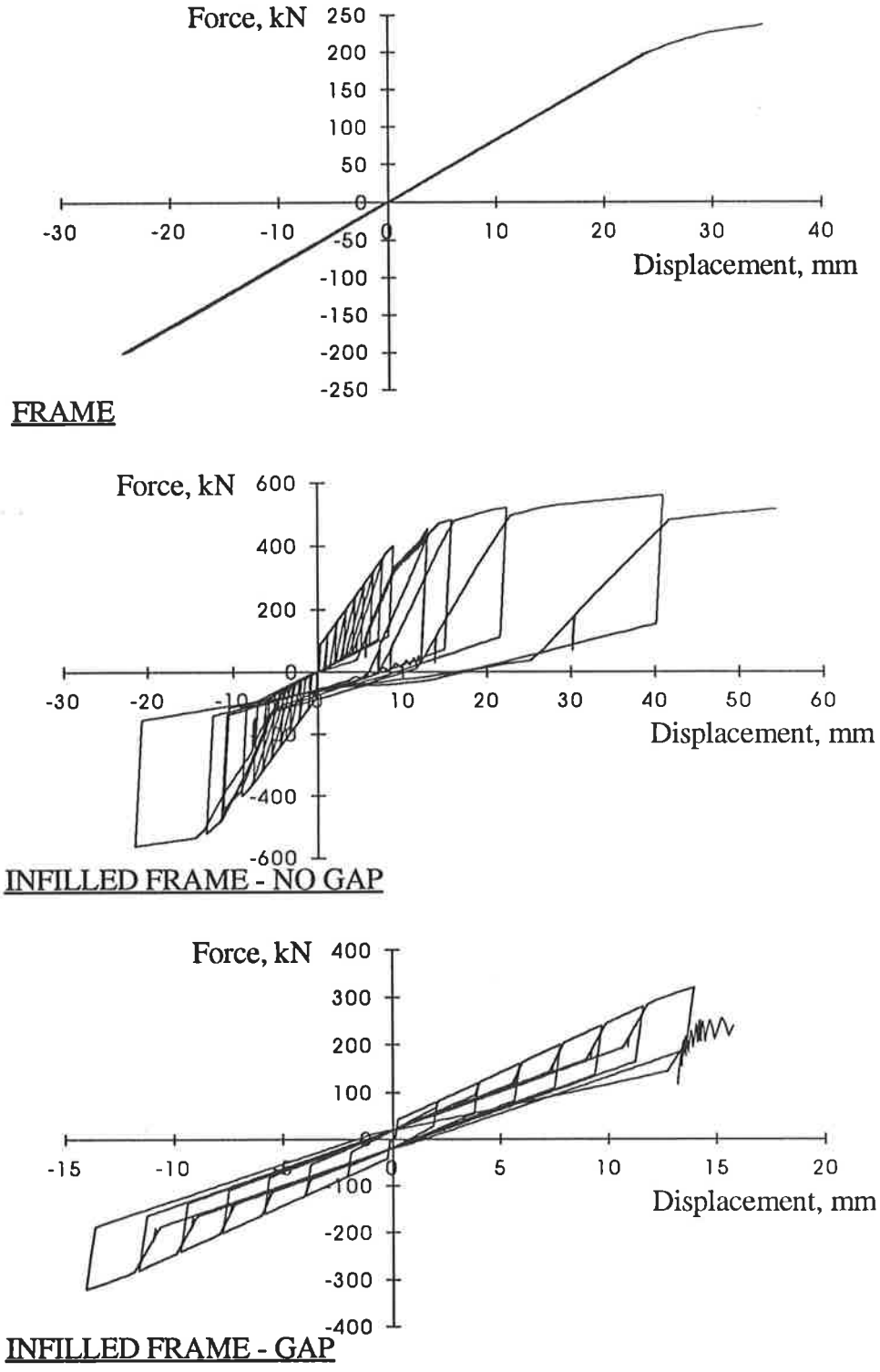

Fig. 6.18. Theoretical model with improved properties for frame members (hysteresis plots)

6.6. Comparison of parameters used in the analysis and results from the analysis

Table 6.1 shows the values of the bi-linear factors for the axial spring forces and the ratio between the yield force and the ultimate force for the diagonals for the case of perfect fit and an existing gap between the frame and the infill wall. For the case of no gap, the bi-linear factor increased with increasing λh (M5 to M3) and l/h ratio (M3, M6, M7). This was a result of the increasing influence of the wall on the overall response of the infilled frames. For the case of a gap the bi-linear factor was almost constant for all the models. This indicated that the response of the wall was very similar to that of a "free-standing" wall. The ratio of the ultimate load to the yield load for the diagonals for the case of no gap decreased with decreasing λh. For model M5 (the model with the stiffest frame) this ratio was 2.47. When the infill wall became relatively stiff or the frame became longer this ratio of the ultimate load to the yield load increased which meant that more inelastic deformations would occur in the diagonals.

Table 6.1. Comparison of input parameters

model	λh	NO GAP			GAP		
		F_{ult}/F_y	r	F_{ult} , kN	r	F_{ult}/F_y	F_{ult} , kN
M1	6.36	5.18	0.0480	140.028	0.0269	4.49	84.017
M2	4.63	4.27	0.0370	330.000	0.0200	3.87	198.000
M3	4.20	3.84	0.0340	356.928	0.0200	4.36	214.157
M4	3.34	3.18	0.0300	356.928	0.0200	4.36	214.157
M5	2.52	2.47	0.0264	392.621	0.0200	4.36	214.157
M6	4.05	5.53	0.0424	487.030	0.0196	5.78	265.653
M7	3.86	7.34	0.0460	620.314	0.0196	7.74	338.353
M8	3.36	4.80	0.0440	454.562	0.0209	5.75	247.943

Table 6.2 shows the sequence of hinge formation leading to collapse for each of the frame models (M1 to M8). Letters separated by commas indicate simultaneous appearance of hinges. Each sequence in the brackets corresponds to a cycle of loading. Figure 6.19 shows the location of the hinges. For most of the models, the first hinges

appeared in the beams since the beam stiffness was the same as the column stiffness and the influence of slabs was not taken into account. For the stiffest and the longest frame (M5 and M7), the hinging sequence for the bare frame case was almost the same as the sequence for the infilled frame with or without a gap.

Table 6.2. Sequence of frame hinging (see fig. 6.19 below the table)

model	bare frame	infilled frame-no gap	infilled frame - gap
M1	(c,d - a - f)	(c,d - a - f)	(c,d - a - f)
M2	(c,d - a - f)	(a - d - c); (c,d - a - f)	(c,d - a - f)
M3	(c,d - a - f)	(a - d - c - f)	(a,c,d); (d - c - a - f)
M4	(c,d); (c,d - a - f)	(c,d - a); (d - c - a - f)	(c,d); (c,d - a - f)
M5	(a - d - c); (d - c - a - f)	(a); (a - d - c); (d - c - a - f)	(a - d); (a - d - c - f)
M6	(a - d - c,f)	(a); (a - d - c,f)	(a - d - c - f)
M7	(a - f - d - c)	(a - f); (a - c - f - d)	(a - f - d - c)
M8a	(a - f - b - e)	(a); (a - b - e); (f - e - a - b)	(a); (a - b); (a - b - e - f)
M8	(a); (a - b - f - e)	(a - b); (b - e - a - f)	vibrations of the beam

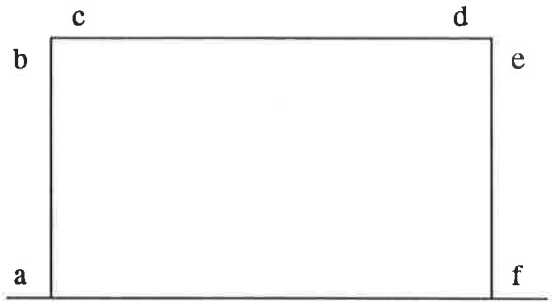

Fig. 6.19. Location of the hinges

6.7. Summary and conclusion

The behaviour of infilled frames under lateral loading can be described by analysing:

- the ratio of the frame stiffness and the infill wall, λh;
- the length to height ratio, l/h; and
- the presence of a construction gap between the frame and the wall.

The results can be summarised as follows:

1. The gap reduced the confinement of the panel and, irrespective of the relative stiffness of the two components, the wall resisted the load very much like a free standing wall.
2. The presence of the gap was crucial for the models with weaker and longer frames (longer infill walls) since it dramatically changed the behaviour and the shape of the force/displacement hysteresis plots from the case of no gap.
3. For the models with a relatively strong frame, the influence of the gap was not the main factor determining the response. The hysteresis rules looked similar for the case of a gap and no gap which meant that the most important factor for these frames was the relative stiffness λh of the frame and the wall.
4. The influence of the presence of a gap on the sequence of hinging was more obvious for the models with weaker and shorter frames.

Although the dynamic model was a very simple one it was seen to be adequate for investigating the behaviour of infilled frames and the influence of λh, the l/h ratio and the presence of a construction gap. This model matched experimental and theoretical results from other researchers reasonably well and was useful for the evaluation of the response of infilled frames for the case with a gap and without a gap between the frame and the wall. For a more detailed prediction of the failure mechanism of the infilled frames, this model is not adequate as shear and joint failure in the frame cannot be simulated with the described model.

CHAPTER 7 - CONCLUSION

7.1. Summary

This research investigated the behaviour of a number of reinforced concrete frames infilled with brick masonry walls with respect to:

- the varying relative stiffness of the frame and the wall, λh;
- the varying length to height ratio of the wall, l/h; and
- the presence of a construction gap between the frame and the wall.

The analysis was carried out in two stages - static analysis for the linear-elastic range of the materials and dynamic analysis for inelastic behaviour of the frame-wall system. The static analysis was conducted using the finite element method to predict the strength and stiffness of the wall at yield. The model developed for the dynamic analysis was a braced frame with two diagonals. This simple model was able to predict the behaviour of the infilled frames with reasonable accuracy.

It has been found that the presence of a construction gap between the frame and the wall is one of the most important factors which determine the overall response. For no gap between the frame and the wall, the relative stiffness parameter and the length to height ratio are convenient parameters for predicting the behaviour of an infilled wall. For this case the strength and stiffness in the initial elastic range were primarily influenced by changes in the relative stiffness and less by changes in the length of the panel. When a gap was introduced between the frame and the wall the behaviour changed noticeably and in the elastic range of response for the materials the infill panel behaved essentially as a free standing wall.

Assessment of the overall inelastic dynamic response also confirmed the major influence of the presence of a construction gap. For no gap the overall behaviour was governed by

the relative stiffness of the frame and the wall. When a construction gap was present, the difference in the response was more dramatic for weaker and longer frames. Changes in the sequence of hinging in such models for the cases of no gap and a gap would be expected to result in different failure modes in practice.

7.2. Recommendations

The diagonal strut model developed in this analysis for the analytical investigation of infilled frames with and without gaps was a simple representation of the problem of infilled frames. Despite many disadvantages this model is preferred because of its simplicity and reasonable accuracy. The diagonal strut model is an approximation and as such its accuracy depends on the initial assumptions. The model developed in this research was not able to adequately simulate the behaviour at a higher loading range where shear failure in columns or joint failure are expected to occur. It also did not model "rocking" of the infill wall (especially for shorter walls). Therefore, other investigators of the problem have suggested numerous mechanical models of braced frames which are able to cope with some of the disadvantages of the single diagonal strut analogy. In most cases for infilled frames without a gap, multiple struts would give a more accurate solution. For the case of a construction gap, because of the pure shear failure of the wall, greater probability of shear failure in the columns exists. Infilled frame models which simulate shear failure in the columns are needed. A model with multiple struts bracing the wall in a special manner would better represent the failure mechanism it this situation .

REFERENCES

1. Polyakov, S.V., "On the Interaction between Masonry Filler Walls and Enclosing Frame when Loaded in the Plane of the Wall", Translations in Earthquake Engineering, Earthquake Engineering Research Institute 1960, pp 36-42

2. Polyakov, S.V., "Some Investigations of the Problem of the Strength of Elements of Buildings Subjected to Horizontal Loads", Symposium on Tall Buildings, Univ. of South-Hampton, April 1966, pp 465-480

3. Holmes, M., "Steel Frames with Brickwork and Concrete Infilling", Proc. of the Institution of Civil Engineers, Vol. 19, August 1961, pp 473-478

4. Smith, B.S., "Lateral Stiffness of Infilled Frames", Journal of the Structural Division, ASCE, ST 6 (1962), pp 183-199

5. Smith, B.S., "Behaviour of Square Infilled Frames", Journal of the Structural Division, ASCE, ST 1 (1966), pp 381-403

6. Smith, B.S., "The Composite Behaviour of Infilled Frames", Symposium on Tall Buildings, Univ. Of South-Hampton, April 1966, pp 481-495

7. Smith, B.S., Carter, C., "A Method of Analysis for Infilled Frames", Proc. of the Institution of Civil Engineers, Vol. 44, Sept. 1969, pp 31-48

8. Benjamin, J.R., Williams, H.A., "The Behavior of One -storey Brick Shear Walls", Journal of the Structural Division, ASCE, ST 4 (1959), pp (1723-1) - (1723-29)

9. Discussion Mallick, D.V., Severn, R.T., "The Behaviour of Infilled Frames under Static Loading", Proc. of the Institution of Civil Engineers, Vol. 41 (1968), Sept., pp 205-222

10. Dukuze, A., Dawe, J.L., "In-plane Behaviour of Three-storey Three-bay RC Frames Infilled with URM Panels: Qualitative Assessment", 4th Australian Masonry Conference, Univ. of Technology, Sydney, 23-24 Nov. 1995, pp 208-217

11. Mainstone, R.J., "On the Stiffnesses and Strengths of Infilled Frames", Proc. of the Institution of Civil Engineers, Supplement 4 (1971), pp 57-90

12. Liauw, T.C. and Kwan, K.H., "Plastic Theory of Non-integral Infilled Frames", Proc. of the Institution of Civil Engineers, Part 2, 1983, Vol. 75, Sept., pp 379-396

13. Liauw, T.C. and Kwan, K.H., "Plastic Theory of Infilled Frames with Finite Interface Shear Strength", Proc. of the Institution of Civil Engineers, Part 2, 1983, Vol. 75, Dec., pp 707-723

14. Liauw, T.C., Kwan, K.H., "New Development in Research of Infilled Frames", 8th World Conference on Earthquake Engineering, San Francisco 1984, Vol. 4, pp 623-630

15. Liauw, T.C., Kwan, K.H., "Non-linear Analysis of Multistorey Infilled Frames", Proc. of the Institution of Civil Engineers, Part 2, 1982, Vol. 73, June, pp 441-454

16. Smolira, M., "Analysis of Infilled Shear Walls", Proc. of the Institution of Civil Engineers, Part 2, Vol. 55, Dec. 1973, pp 895-912

17. Islam, M.S., Kim, H.I., Maniar, F., "Seismic Retrofit of Two Historic Steel Buildings with Unreinforced Masonry Infill Walls", 5th National Conference on Earthquake Engineering, July 1994, Chicago, Illinois, Vol. 3, pp 891-900

18. Zarnic, R., Tomazevic, M., "An Experimentally Obtained Method for Evaluation of the Behaviour of Masonry Infilled R/C Frames", Proc. of the 9th World Conference on Earthquake Engineering, Tokyo-Japan 1988, Vol. 6, pp 163-168

19. Leuchars, J.M., Scrivener, J.C., "Masonry Infill Panels Subjected to Cyclic Inplane Loading", Bulletin of the New Zealand National Society for Earthquake Engineering, Vol. 9, No. 2, June 1976, pp 122-131

20. Mander, J.B., Aycardi, L.E., Kim, D.-K., "Physical and Analytical Modeling of Brick Infilled Steel Frames", Proceedings from the NCEER Workshop on Seismic Response of Masonry Infills, San Francisco, California, February 4-5, 1994, Technical Report NCEER-94-0004, pp (1-21) - (1-26)

21. Thiruvengadam, V., "On the Natural Frequencies of Infilled Frames", Earthquake Engineering and Structural Dynamics, Vol. 13, 1985, pp 401-419

22. Chrysostomou, C.Z., Gergely, P., Abel, J.F., "Non-linear Seismic Response of Infilled Steel Frames", 10th World Conference, Spain, 19-24 July 1992, pp 4435-4437

23. Gergely, P., White, R, Mosalam, k., "Evaluation and Modeling of Infilled Frames", Proceedings from the NCEER Workshop on Seismic Response of Masonry Infills, San Francisco, California, February 4-5, 1994, Technical Report NCEER-94-0004, pp (1-51) -(1-56)

24. Gergely, P., White, R., Zawilinski, D., Mosalam, K., "The Interaction of Masonry Infill and Steel or Concrete Frames", Proc. of 1993 National Earthquake Conference, pp 183-191

25. Hamburger, R.O., Chakradeo, A.S., "Methodology for Seismic Evaluation of Steel Frame Buildings with Infill Unreinfored Masonry", Proc. of 1993 National Earthquake Conference, pp 173-182

26. Durrani, A.J., Luo, Y.H., "Seismic Retrofit of Flat-Slab Building with Masonry Infills", Proceedings from the NCEER Workshop on Seismic Response of Masonry Infills, San Francisco, California, February 4-5, 1994, Technical Report NCEER-94-0004, pp (1-3) - (1-8)

27. Lourenco, P.B., Rots, J.G., Blaauwendraad, J., "Two Approaches for the Analysis of Masonry Structures: Micro- and Macro-modeling", HERON, Vol. 40, No. 4 (1995) ISSN 0046-7316, pp 313-340

28. Page, A.W., "Finite Element Model for Masonry", Journal of the Structural Division, ASCE, ST 8 (1978), pp 1267-1285

29. Zhuge, Y., Yang, Y., Thanbiratham, D., Corderoy, H.J.B., "On the Behaviour of Brick Masonry Structures under Lateral Loads", 13th Australian Conference on the Mechanics of Structures and Materials, Univ. of Wollongong 1993, pp 1025-1032

30. Crisafulli, F.J., Carr, A.J., Park, R., "Shear Strength of Unreinforced Masonry Panels", Pacific Conference on Earthquake Engineering, Melbourne, 20-22 Nov. 1995, Vol. 3, pp 77-86

31. Dawson, R.V., Ward, M.A., "Dynamic Response of Framed Structures with Infill Panels", 5th World Conference on Earthquake Engineering, Rome 1973

32. Riddington, J.R., Smith, B.S., "Analysis of Infilled Frames Subject to Racking with Design Recommendations", The Structural Engineer, June, 1977, No 6, Vol. 55, pp 263-268

33. El Haddad, M.H., "Finite Element Analysis of Infilled Frames Considering Cracking and Separation Phenomena", Computers and Structures, Vol. 41, No 3, 1991, pp 439-477

34. Mallick, D.V., Severn, R.T., "The Behaviour of Infilled Frames under Static Loading", Proc. of the Institution of Civil Engineers, Vol. 38 (1967), Dec., pp 639-656

35. Discussion Liauw, T.C., Kwan, K.H., "Non-linear Analysis of Multistorey Infilled Frames", Proc. of the Institution of Civil Engineers, Part 2, 1983, Vol. 75, March, pp 139-140

36. Kost, G., Weaver, W., Barber, R.B., "Nonlinear Dynamic Analysis of Frames with Filler Panels", Journal of the Structural Division, ASCE, ST 4 (1974), pp 743-757

37. Rivero, C.E., Walker, W.H., "An Analytical Study of the Interaction of Frames and Infill Masonry Walls", 8th World Conference on Earthquake Engineering, San Francisco, 1984, Vol. 4, pp 591-598

38. Shing, P.B., Lofti, H.R., Barzegarmehrabi, A., Brunner, J., "Finite Element Analysis of Shear Resistance of Masonry Wall Panels with and without Confining frames", 10th World Conference on Earthquake Engineering, Spain 1992, 19-24 July 1992, pp 2581-2586

39. Hart, G.C., Elhassan, R.M., Srinivasan, M., "Earthquake Response Records of Masonry Infill Buildings", 5th National Conference on Earthquake Engineering, July 1994, Chicago, Illinois, Vol. 2, pp 681-690

40. Karamanski, T., "Calculating Infilled Frames by the Method of Finite Elements", Symposium on Tall Buildings, Univ. of South-Hampton, April 1966, pp 455-461

41. Discussion on Karamanski, T., "Calculating Infilled Frames by the Method of Finite Elements", Symposium on Tall Buildings, Univ. of South-Hampton, April 1966, pp 462-463

42. Youssef, N., "The influence of Modeling Assumptions on the Predicted Behaviour of Unreinforced Masonry Infill Structures", Proceeding from the NCEER Workshop on

Seismic Response of Masonry Infills, San Francisco, California, February 4-5, 1994, Technical Report NCEER-94-0004, pp (1-39) - (1-44)

43. King, G.J.W., Pandey, P.C., "The Analysis of Infilled Frames Using Finite Elements", Proc. of the Institution of Civil Engineers, Part 2, 1978, 65, Dec., pp 749-760

44. Mehrabi, A.B., Shing, P.B., "Performance of Masonry-Infilled R/C Frames under In-plane Loads: Analytical Modeling", Proceedings from the NCEER Workshop on Seismic Response of Masonry Infills, San Francisco, California, February 4-5, 1994, Technical Report NCEER-94-0004, pp (1-45) - (1-50)

45. Jankulovski, E., Parsanejad, S., "Analytical Evaluation of In-plane Resistance of Unreinforced Masonry Walls", 4th Australian Masonry Conference, Univ. of Technology, Sydney, 23-24 Nov. 1995, pp 65-70

46. Scaletti, H., Chariarse, V., Cuadra, C., Cuadros, G., Tsugawa, T., "Pseudo Dynamic Tests of Confined Masonry Buildings", 10th World Conference on Earthquake Engineering, Spain 1992, 19-24 July 1992, pp 3493-3497

47. Ravara, A., Mayorga, A., Carvalho, C., "Seismic Tests of Infilled Reinforced Concrete Frames", 6th World Conference on Earthquake Engineering, India, 1977, Vol. 3, pp 2772-2777

48. San Bartolome, A., Quiun, D., Torrealva, D., "Seismic Behaviour of a Three-storey Half Scale Confined Masonry Structure", 10th World Conference on earthquake Engineering, Spain 1992, 19-24 July 1992, pp 3527-3531

49. Manos, G.C., Yasin, B., Triamataki, M., "Experimental and Numerical Simulation of the Influence of Masonry Infills on the Seismic Response of Reinforced Concrete Framed Structures", 5th National Conference on Earthquake Engineering, July 1994, Chicago, Illinois, Vol. 2, pp 817-826

50. Zarnic, R., "Experimentally Based Inelastic Models of Masonry Infilled R.C. Frames", 5th National Conference on Earthquake Engineering, July 1994, Chicago, Illinois, Vol. 2, pp 161-170

51. El-Gazairly, L.F., Goodno, B., Craig, J., "Nonlinear Dynamic Response of Unreinforced Masonry Walls in RC Structures", 5th National Conference on Earthquake Engineering, July 1994, Chicago, Illinois, Vol. 4, pp 735-744

52. Schuller, M., Mehrabi, A.B., Noland, J.L., Shing, P.B., "Performance of Masonry-Infilled R/C Frames under In-plane Lateral Loads: Experiments", Proceedings from the NCEER Workshop on Seismic Response of Masonry Infills, San Francisco, California, February 4-5, 1994, Technical Report NCEER-94-0004, pp (1-27) - (1-32)

53. Mallick, D.V. and Severn, R.T., "Dynamic Characteristics of Infilled Frames", Proc. of the Institution of Civil Engineers, Vol. 39 (1968), pp 261-287

54. Base, G.D., Baker, L.R., "Fundamental Properties of Structural Brickwork", Journal of the Australian Ceramic Society, Vol. 9, No. 1, May 1973, pp 1-5

64. Booth, E., "Concrete Structures in Earthquake Regions: Design and Analysis", pp 181-182

55. Dhanasekar, M., Kleeman, P.W., Page, A.W., "Biaxial Stress Strain Relations for Brick Masonry", Journal of the Structural Division, ASCE, ST May 1985, pp 1085-1100

56. Dhanasekar, M., Kleeman, P.W., Page, A.W., "The Failure of Brick Masonry under Biaxial Stresses", Proc. of the Institution of Civil Engineers, Part 2 1985, Vol. 79, June, pp 295-313

56. Samarasinghe, W., Page, A.W, Hendry, A.W., "A Finite Element Model for the In-plane Behaviour of Brickwork", Proc. of the Institution of Civil Engineers, Part 2, 1981, Vol. 71, Sept., 1882, Vol. 73, Mar., pp 171-178

58. Klopp, G.M., Griffith, M.C., "The Design of Unreinforced Masonry Buildings for Earthquake Induced Forces", Pacific Conference on Earthquake Engineering, Melbourne, 20-22 Nov. 1995, Vol. 3, pp 87-96

59. Calvi, G.M., Magenes, G., Pavese, A., Abrams, D.P., "Large Scale Seismic Testing of an Unreinforced Brick Masonry Building", 5th National Conference on Earthquake Engineering, July 1994, Chicago, Illinois, Vol. 1, pp 137-146

60. Priestley, M.J.N., 1980, Masonry in "Design of Earthquake Resistant Structures", Rosenbleuth, E. (ed), Rentech Press, Plymouth, Chapter 6

61. Kato, H., Goto, T., Mizuno, H., Iiba, M., "Cyclic Loading Tests of Confined Masonry Wall Elements for Structural Design Development of Apartment Houses in the Third World", 10th World Conference on Earthquake Engineering, Spain 1992, 19-24 July, pp 3539-3544

62. Haskell, G.O., ""Seismic Retrofit of a Seven-Story Non-Ductile Concrete Frame Building with URM Infill Using Viscous Dampers", 5th National Conference on Earthquake Engineering, July 1994, Chicago, Illinois, Vol. 3, pp 677-686

63. Comartin, C.D., Bendimerad, F.M., Jones, H., "Practical Aspects of the Seismic Rehabilitation of Unreinforced Masonry Buildings", 5th National Conference on Earthquake Engineering, July 1994, Chicago, Illinois, Vol. 3, pp 861-870

64. Wong, A., "Theoretical Investigation of Australian Designed Reinforced Concrete Frames Subjected to Earthquake Loading", Thesis to be submitted for Master of Engineering Science Degree, The Department of Civil and Environmental Engineering, The University of Adelaide

65. Page, A.W., Kleeman, P.W., Dhanasekar, M., "An In-plane Finite Element Model for Brick Masonry", Proc of a session held in conjunction with Structures Congress '85 Chicago, Illinios, Sept 18, 1985, ed. by Subhash C. Anand, pp 1-18

66. Standards Association of Australia: SAA Concrete Structures Code: AS3600 - 1988

67. IMAGES - 3D User's Manual, Celestian Software, Berkeley, California (1993)

68. Rockey, K.C., Evans, H.R., Griffiths, D.W., Nethercot, D.A., "The Finite Element Method - A Basic Introduction for Engineers", BSP Professional Books, Second Edition, 1983, Chapter 6

69. Carr, A., "RUAUMOKO", User's manual, University of Canterbury, 1996

70. Clough, R.W., Penzien, J., "Dynamics of Structures", McGraw-Hill, Inc., Second Edition, 1993

71. Newmark, N.M., Hall, W.J., "Earthquake Spectra and Design", Published by the Earthquake Engineering Research Institute, Library of Congress catalogue card number 82-71183

72. Alaia, R., "An Investigation into the Seismic Behaviour of Reinforced Concrete Frames with Brick Infill Panels", Thesis to be submitted for Master of Engineering Science Degree, The Department of Civil and Environmental Engineering, The University of Adelaide

73. Dean, J.A., Stewart, W.G., Carr, A.J., "The Seismic Behaviour of Plywood Sheathed Shearwalls", Bulletin of the New Zealand National Society for Earthquake Engineering, Vol. 19, No. 1, March 1986, pp 48-63

74. Jankulovski, E., Parsanejad, S., "Hysteresis Behaviour of Plain Brick Masonry Walls: an Experimental Investigation", Australian Structural Engineering Conference, Sydney, 21-23 Sept. 1994, pp 679-683

75. Standards Association of Australia: SAA Masonry Code AS3700 - 1988